CUKUROVA UNIVERSITY
INSTITUTE OF NATURAL AND APPLIED SCIENCES

PhD THESIS

Automated Detection of Autism Based on the Electrical Signals of the Brain (EEG)

BASHAR SAAD FALIH AL-SAFFAR

Electrical and Electronic Engineering Department

May, 2025

CUKUROVA UNIVERSITY
INSTITUTE OF NATURAL AND APPLIED SCIENCES

PhD THESIS APPROVAL

Automated Detection of Autism Based on the Electrical Signals of the Brain (EEG)

BASHAR SAAD FALIH AL-SAFFAR

Electrical and Electronic Engineering Department

This Doctorate Thesis was evaluated by the following Jury Members on 26/05/2025 and was approved by unanimity of votes.

Jury	: Assoc. Prof. Dr. Ahmet AYDIN (Advisor)	…………
	: Prof. Dr. Mustafa Kerem ÜN	…………
	: Prof. Dr. Umut ORHAN	…………
	: Assoc. Prof. Dr. Gökay DİŞKEN	…………
	: Assist. Prof. Dr. Kasım ZOR	…………

This Thesis was written in the Department of Electrical and Electronic Engineering, Institute of Natural and Applied Sciences.

Thesis Number:

Prof. Dr. Sadık DİNÇER
Director
Institute of Natural and Applied Sciences

CONTENTS

CUKUROVA UNIVERSITY
INSTITUTE OF NATURAL AND APPLIED SCIENCES

PhD THESIS

Automated Detection of Autism Based on the Electrical Signals of the Brain (EEG)

BASHAR SAAD FALIH AL-SAFFAR

Advisor: Assoc. Prof. Dr. Ahmet AYDIN

Second -advisor: Assist. Prof. Dr. Mohannad Kadhim SABIR

Electrical and Electronic Engineering Department

ABSTRACT

Early screening is essential for effective intervention and rehabilitation in children with Autism Spectrum Disorder (ASD). EEG signals, offering real-time and sensitive monitoring, were used in this study to develop two proposed methods for ASD diagnosis. A dataset of 52 samples (22 with ASD and 30 controls) was collected using 19-channel sleep EEG recordings. Method 1: This method utilized energy differences between the left and right brain hemispheres. Preprocessing steps included decimation, involved noise removal FIR-BPF (< 0.5 Hz and > 49 Hz to reject unwanted frequencies) and artifact subspace reconstruction, and amplitude normalization. EEG signals were decomposed into five frequency bands, and peak channel envelopes were calculated for each hemisphere. Features—maximum, mean, and minimum energy values—were extracted using a sliding window approach with varying overlap ratios (12.5%–87.5%). The SVM classifiers with Linear (L), RBF, and Quadratic kernels were used and, the highest performance was achieved in the theta band: accuracy 91.7%, sensitivity 91.4%, and F1 measure 91.6%, with SVM-L using maximum energy features. Method 2:This approach analyzed two EEG dataset from Iraq and Poland. Preprocessing involved noise removal (< 0.5 Hz and > 49 Hz to reject unwanted frequencies) and artifact subspace reconstruction. EEG channel power spectral density features and brain topography maps were processed using deep feature extractors (e.g., AlexNet, GoogLeNet). ANOVA was applied for feature selection, followed by classification using SVM and Linear Discriminant Analysis (LDA). The alpha band demonstrated the best performance. The mean accuracy reached 98% with an standard deviation (SD) of 2.3% (Iraq, GoogLeNet + ANOVA + SVM-L) and 96.5% with an SD of 3.6% (Poland, AlexNet-FC6 + ANOVA + SVM-L). Both methods highlight the potential of EEG-based systems as cost-effective and accurate diagnostic tools, providing valuable decision-support for healthcare professionals in ASD diagnosis.

Keywords: Autism Spectrum Disorder (ASD), Electroencephalography (EEG), Automated Detection, Support Vector Machine (SVM), Feature Selection (ANOVA).

ÇUKUROVA ÜNİVERSİTESİ
FEN BİLİMLERİ ENSTİTÜSÜ

DOKTORA TEZİ

Beynin Elektrik Sinyallerine (EEG) Dayalı Otizmin Otomatik Tespiti

BASHAR SAAD FALIH AL-SAFFAR

Danışman: Doç. Dr. Ahmet AYDIN

İkinci Danışman: Yrd. Doç. Dr. Mohannad Kadhim SABIR

Elektrik ve Elektronik Mühendisliği Bölümü Anabilim Dalı

ÖZ

Erken tarama, Otizm Spektrum Bozukluğu (OSB) olan çocuklar için etkili müdahale ve rehabilitasyonun önemli bir parçasıdır. Gerçek zamanlı ve hassas izleme sağlayan Elektroensefalografi (EEG) sinyalleri, bu çalışmada ASD teşhisi için önerilen iki yöntemin geliştirilmesinde kullanılmıştır. 19 kanallı uyku EEG kayıtları kullanılarak 52 örnekten (22 ASD'li ve 30 kontrol) oluşan bir veri seti toplanmıştır. Yöntem 1: Bu yöntem, beynin sol ve sağ yarım küreleri arasındaki enerji farklarını kullanmıştır. Ön işleme adımları, azalma, bant geçiren filtreleme (< 0,5 Hz ve > 49 Hz istenmeyen frekansları reddetmek için), artefakt alt alanı yeniden yapılandırma ve genlik normalizasyonunu içermiştir. EEG sinyalleri beş frekans bandına ayrılmış ve her yarım küre için tepe kanal zarfı hesaplanmıştır. Maksimum, ortalama ve minimum enerji değerleri gibi özellikler, %12,5-%87,5 oranında değişen örtüşme oranları ile kayan pencere yöntemi kullanılarak çıkarılmıştır. Destek Vektör Makinesi (DVM) sınıflandırıcıları (Doğrusal, RBF ve Kuadratik çekirdekler) kullanılarak en iyi performans, maksimum enerji özellikleriyle DVM -D kullanılarak teta bandında elde edilmiştir: doğruluk %91,7, duyarlılık %91,4 ve F1 ölçüsü %91,6. Yöntem 2: Bu yaklaşımda, Irak ve Polonya'dan EEG verilerini otomatik şekilde analiz etmiştir. Ön işleme, gürültü giderme (< 0,5 Hz ve > 49 Hz istenmeyen frekansları bastırmak için) ve artefakt alt alanı yeniden yapılandırmayı içermiştir. EEG kanal güç spektral yoğunluğu özellikleri ve beyin topografya haritaları, derin özellik çıkarıcılar (örneğin AlexNet, GoogLeNet) kullanılarak işlenmiştir. Özellik seçimi için ANOVA uygulanmış, ardından DVM ve Doğrusal Ayırıcı Analiz (DAA) ile sınıflandırma yapılmıştır. Alfa bandı en iyi performansı göstermiştir. Doğruluk, Irak için %98 ve standart sapma (SS) %2,3'e ulaştı (GoogLeNet + ANOVA + DVM-D) ve Polonya için %96,5 doğruluk ile %3,6 SS (AlexNet-FC6 + ANOVA + DVM-D) olarak elde edilmiştir. Her iki yöntem de, EEG tabanlı sistemlerin düşük maliyetli ve doğru tanı araçları olarak potansiyelini vurgulamakta ve sağlık profesyonellerine OSB teşhisinde değerli bir karar destek mekanizması sunmaktadır.

Anahtar Kelimeler: Otizm Spektrum Bozukluğu (OSB), Elektroensefalografi (EEG), Otomatik Tespit, Destek Vektör Makinesi (DVM), Özellik Seçimi (ÖS).

EXTENDED SUMMERY

Autism Spectrum Disorder (ASD) is a neurodevelopmental condition characterized by challenges in social interaction, communication, and behavior. Early detection is critical to harness the brain's plasticity during childhood, enabling timely interventions that can significantly improve cognitive, emotional, and social outcomes. According to global statistics, the prevalence of ASD cases is rising annually, posing a growing concern. Developing an effective system for early detection is vital, as it can greatly enhance the skills and outcomes for individuals diagnosed at an early stage. EEG-based ASD detection has shown promise as a diagnostic tool due to its non-invasive, cost-effective, and real-time monitoring capabilities for brain activity.

This study analysed EEG signals in a dataset included 52 children: 22 with autism (average age: 4.8 years, Standard Deviation (SD): 1.5) and 30 typically developing (TD) children as controls (average age: 5.9 years, SD: 3.5). The control group was recruited from the EEG unit of the Pediatric department at the Children's Welfare Teaching Hospital. EEG signals for all participants were recorded using a Nihon Kohden EEG system (Tsurugashima, Japan) following the 10–20 international electrode system. The system utilized a 19-channel configuration, operated at a 500 Hz sampling frequency, resistance lower 10 k Ohm.

Two proposed methods have been used for ASD diagnosis. Despite its potential, challenges such as signal artifacts, data variability, and the limited size of available datasets pose significant barriers to achieving accurate classification.

To address these challenges, this thesis introduces two automated methods for ASD detection, utilizing EEG datasets from Iraq and Poland. Both methods implement robust preprocessing techniques, including (noise removal, EEG length equalization, artifact removal) is essential to improve EEG data quality. Pre-processing yields clean, equal-length EEG data free of noise and artifacts, which facilitate brain activity analysis and interpretation. First, the processing was accelerated by down-sampling the data to 256 Hz. Subsequently, the data were filtered using a zero-phase Hamming window of Finite Impulse Response Band-Pass Filter (FIR-BPF) to remove the frequency < 0.5 Hz and > 49 Hz to reject the baseline 50 Hz (DC, notch filter) and other unwanted frequencies. The filtered EEG data segments containing significant muscle and movement artifacts identified by Artifact Subspace Reconstruction (ASR) to eliminate artifacts, resulting in clean, high-quality data for analysis. These approaches provide valuable insights into temporal (energy-based) and both spatial (topographic) aspects of brain activity, contributing to the development of reliable and efficient diagnostic tools for ASD.

Method 1: Brain Hemisphere Energy Analysis

This method used a new approach to diagnosing ASD based on energy differences between the left and right hemispheres of the brain. The preprocessing stage included decimation, band-pass filtering to remove unwanted frequencies, ASR to eliminate artifacts, and amplitude normalization (AN) to preserve the relative relationships between the signal features, which were crucial for the subsequent analysis and classification. The normalized EEG signal was decomposed into different frequency bands using five zero-phase Chebyshev Type-II band-pass filters (BPFs). Each BPF was designed to extract one of the following EEG frequency bands: Delta (Δ, 0.5–4 Hz), Theta (θ, 4–8 Hz), Alpha (α, 8–13 Hz), Beta (β, 13–28 Hz), and Gamma (Γ, 31–49 Hz). The sixth-order filter, determined heuristically, provided the optimal balance between the signal attenuation and computational efficiency. For all filters, the stopband attenuation was set to 50 dB to ensure minimal signal distortion.

The EEG channel on the left and right brain hemispheres were divided into left electrodes (Fp1, F3, C3, P3, O1, F7, T3, T5, Fz, and Pz) and right electrodes (Fp2, F4, C4, P4, O2, F8, T4, T6, and Cz), the signals from each brain hemisphere were analysed separately by calculating the peak sensor's envelope and obtaining the mean envelope for each hemisphere, resulting in two mean signals (right and left). Features were extracted using a sliding window approach applied to the mean signals of each hemisphere, with varying overlap ratios (12.5% to 87.5%, in 12.5% steps) and the window length was 2000 samples (~8 Sec.). The maximum, mean, and minimum energy values were used individually as features. Three types of SVM kernels— linear (L), the radial basis function (RBF), and quadratic—were employed for classification.

Results of Method 1:

- The confusion matrix was used to evaluate the number of true positive, true negative, false positive, and false negative predictions. The precision of the θ band was compared with other frequency bands (δ, α, β, and γ) to assess their effectiveness in EEG-based ASD classification. The study also analysed the energy differences between the left and right brain hemispheres.
- For the θ band, the highest classification accuracy was achieved using a stride of 250 samples (87.5% overlap) and selecting the maximum energy window as features. Among all configurations, the θ band consistently outperformed others, particularly with the SVM-Linear classifier, yielding a mean accuracy of 91.73% and SD of 7% under these settings.
- The δ band also demonstrated strong performance, particularly with mean energy windows. For instance, using the SVM-Linear classifier, the δ band achieved a mean accuracy of 84.3% with an SD of 8.7%, and 85% with an SD of 9.2% with the SVM-Quadratic classifier under similar conditions. However, it did not surpass the θ band's superior performance.

- Higher overlap ratios and maximum energy windows generally enhanced classification accuracy, particularly for the θ band, by capturing more detailed EEG signals. Non-linear SVM kernels, such as RBF and Quadratic, further improved classification accuracy across frequency bands. The γ (Gamma) band, however, exhibited lower overall performance, with its best mean accuracy reaching 73.3% with an SD of 10.5%.

Finally, the θ band emerged as the most effective for early ASD detection, achieving the highest accuracy, sensitivity, and low standard deviation compared to other bands. This highlights its potential as a reliable feature for distinguishing between ASD and TD groups. The Theta band achieved the best results, with a mean accuracy of 91.7% with an SD of 7 %, mean sensitivity of 91.4% with an SD of 9.7 %, and mean of the specificity of 92.1% with an SD of 8.6% using a linear SVM with a 250-sample stride and 87.5 % overlap.

Method 2: EEG Topographic Mapping and Deep Learning Architecture

This method uses topographic brain maps (TBMs) as inputs to deep learning (DL) architectures for feature extraction and classification. AlexNet and GoogLeNet were used to extract meaningful features from EEG data, particularly focusing on the alpha band due to its high relevance in ASD detection.

To enhance efficiency and classification complexity, ANOVA-based feature selection was employed to reduce the dimensionality of the feature space. After feature extraction, used two types of classifiers (i.e., linear SVM (SVM-L) and Linear Discriminant Analysis (LDA)) were used to distinguish between ASD and non-ASD (TD) groups.

Results of Method 2:

- The results indicate that the alpha band consistently outperforms other EEG frequency bands in terms of performance metrics, including accuracy, sensitivity, specificity, precision, and F1 measure. This is particularly evident when combining CNN feature extractors (AlexNet-FC6, AlexNet-FC7, AlexNet-FC8, and GoogLeNet) with feature selection using ANOVA and classifiers like SVM-L and LDA. The integration of ANOVA significantly enhances accuracy across all bands, improves feature relevance, and reduces classification time.
- For the Iraq dataset, the configuration of GoogLeNet+ANOVA+SVM-L achieved the highest performance, with mean accuracy of 98% with an SD of 2.3% and mean of F1 measure of 97.9% with an SD of 2.9%. The second-best configuration, AlexNet-FC6+ANOVA+SVM-L, achieved a mean accuracy 97.8% with an SD of 2.8% and the mean of F1 measure of 97.3% with an SD of 3.6%.

- For the Poland dataset, AlexNet-FC6+ANOVA+SVM-L was the optimal combination, delivering a mean accuracy of 96.5% with an SD of 3.6% and a mean of F1 measure of 96.4% with an SD of 3.8%.
- The exclusion of ASR during preprocessing and ANOVA from the analysis resulted in a significant drop in accuracy to 59.5%, underscoring their importance. ANOVA effectively improved model performance by selecting relevant features, particularly in the alpha band, which emerged as the most informative for ASD detection. Previous research supports this finding, highlighting the role of alpha-band activity in distinguishing ASD from TD groups.
- SVM-L consistently outperformed LDA in classification tasks, providing better accuracy and reduced processing times. Among feature extractors, GoogLeNet required more computational resources due to its higher complexity, while AlexNet feature sets (FC6, FC7, and FC8) demonstrated comparable computational loads.

The study emphasizes that preprocessing methods and device differences significantly impact performance across datasets. The integration of ASR, ANOVA, and SVM-L with AlexNet-FC6 provided a robust and efficient approach, achieving high accuracy with reduced variability. These findings confirm the alpha band as a critical frequency range for ASD detection, offering potential for further advancements in automated diagnostic tools.

Finally, for the Iraq dataset, the GoogLeNet + ANOVA + SVM-L combination yielded 98% mean accuracy with a mean F1 measure of 97.9%. For the Poland dataset, AlexNet-FC6+ANOVA+SVM-L achieved 96.5% mean accuracy with a mean F1 measure of 96.4%. While both CNN architectures demonstrated high performance, GoogLeNet required more computational resources, making AlexNet-FC6 more efficient for real-time applications. The experiments also showed that removing ASR and ANOVA during preprocessing reduced classification accuracy to 59.5%, demonstrating the critical role of these steps in maintaining performance.

This thesis included both methods serves as a valuable resource for future designers and developers seeking to integrate and highlight this system's potential as an online decision-support tool to assist healthcare professionals in diagnosing autism.

Overall Conclusion

This study highlights the promising potential of EEG-based methods for the early detection of ASD, addressing a critical need in the field of neurodevelopmental research and healthcare. Two complementary approaches were developed and thoroughly evaluated, demonstrating the significance of signal preprocessing and advanced feature extraction techniques in achieving accurate diagnoses. The first method focused on analysing energy differences between brain hemispheres, revealing the theta band as a key discriminator between ASD and TD groups.

The second method utilized TBMs processed through deep learning architectures, particularly AlexNet and GoogLeNet. When combined with ANOVA-based feature selection, the alpha band emerged as the most informative frequency range for ASD detection, delivering high performance metrics. Preprocessing techniques, including ASR and BPF, ensured high-quality EEG data for analysis. The use of linear SVM classifiers further optimized accuracy while maintaining simplicity. Across both methods, the results demonstrated exceptional performance, achieving accuracies of up to 98% in the Iraq dataset and 96.5% in the Poland dataset, showcasing the methodologies' reliability across diverse populations and EEG systems.

It was mentioned that the first method provided the highest outcome in the theta band, and the second method was effective in the alpha band. As mentioned earlier, these two bands are located side by side to each other, that is, they are in the same plane. The 5-filters used in the first method had some overlap of the frequencies in the two bands and the effective frequency in both methods was 5 to 10 Hz, which might have caused these differences.

Future Work: Several directions for future research are proposed to enhance and expand upon the findings of this study. First, there is a need to collect larger and more diverse datasets to improve the generalizability of the models and address demographic variability. Second, developing real-time systems for clinical and educational settings could enable immediate ASD screening and intervention planning, bridging the gap between research and practice.

Integrating EEG data with other modalities, such as physiological signals, could provide a more comprehensive assessment of ASD. Additionally, optimizing deep learning models to create lightweight and efficient architectures would facilitate deployment in resource-limited settings. Exploring less commonly studied frequency bands may uncover further insights into ASD-related brain activity, while longitudinal studies could link EEG patterns to developmental trajectories and intervention outcomes.

Lastly, tailoring diagnostic tools to specific age groups, cultural contexts, and clinical requirements will maximize their effectiveness and accessibility. The robust preprocessing, advanced feature extraction, and scalable classification methods presented in this study lay a strong foundation for the development of automated, cost-effective, and non-invasive diagnostic tools for ASD.

GENİŞLETİLMİŞ ÖZET

Otizm Spektrum Bozukluğu (OSB), sosyal etkileşim, iletişim ve davranışta zorluklarla karakterize edilen bir nörogelişimsel durumdur. Erken tespit, çocukluk döneminde beynin plastisitesini kullanarak zamanında müdahalelerin bilişsel, duygusal ve sosyal sonuçları önemli ölçüde iyileştirmesini sağlar.

Bu çalışma, 52 çocuktan oluşan bir veri setinde EEG sinyallerini analiz etmiştir: 22'si otizmli (ortalama yaş: 4,8 yıl ve standart sapma (SS) = 1,5) ve 30'u tipik gelişim gösteren (TG) çocuklardan oluşan kontrol grubu (ortalama yaş: 5,9 yıl ve SS = 3,5). Kontrol grubu, Çocuk Refahı Eğitim Hastanesi Pediatri bölümünün EEG biriminden temin edilmiştir. Tüm katılımcıların EEG sinyalleri, Nihon Kohden EEG sistemi (Tsurugashima, Japonya) kullanılarak 10–20 uluslararası elektrot sistemi izlenerek kaydedilmiştir. Sistem, 19 kanallı bir konfigürasyonla çalışmış, 500 Hz örnekleme frekansında ve < 10 k Ohm direnç ile operasyona girmiştir.

Bu zorlukları ele almak için bu tez, Irak ve Polonya'dan elde edilen EEG veri setlerini kullanarak OSB tespiti için iki otomatikleştirilmiş yöntem sunmaktadır. Her iki yöntem de EEG veri kalitesini iyileştirmek için gerekli olan güçlü ön işleme tekniklerini, bunlar arasında gürültü giderme, EEG uzunluğu eşitleme ve artefakt giderme işlemlerini içermektedir. Ön işleme, gürültü ve artefaktlardan arındırılmış, eşit uzunlukta temiz EEG verileri elde edilmesini sağlar; bu da beyin aktivitesinin analizini ve yorumlanmasını kolaylaştırır. İlk olarak, veri 256 Hz'ye indirilerek işleme hızlandırılmıştır. Ardından, veriler, sıfır fazlı Hamming penceresi ve FIR bant geçiş filtresi (BGF) kullanılarak filtrelenmiş ve 0,5 Hz altındaki ve 49 Hz üstündeki frekanslar, temel 50 Hz (DC, notch filtresi) ve diğer istenmeyen frekanslar reddedilmiştir. Filtrelenmiş EEG verileri, Artefakt Alt Alan Rekonstrüksiyonu (AAAR) ile tanımlanan önemli kas ve hareket artefaktlarını içeren segmentlerden arındırılmıştır ve bu, analiz için temiz, yüksek kaliteli verilerle sonuçlanmıştır. Bu yaklaşımlar, beyin aktivitesinin zamansal (enerji tabanlı) ve her iki uzamsal (topografik) yönlerine dair değerli bilgiler sağlar ve OSB için güvenilir ve verimli tanı araçlarının geliştirilmesine katkıda bulunur.

Yöntem 1: Beyin Yarıküre Enerji Analizi

Bu yöntem, beynin sol ve sağ yarımküreleri arasındaki enerji farklarına dayalı olarak OSB teşhisinde yeni bir yaklaşım kullanmıştır. Ön işleme aşaması, istenmeyen frekansları kaldırmak için seyreltme, band geçiş filtresi uygulaması, artefaktları ortadan kaldırmak için AAAR ve sinyal özellikleri arasındaki göreceli ilişkileri korumak için genlik normalizasyonunu içermektedir. Normalize edilmiş EEG sinyali, beş sıfır fazlı Chebyshev Tip-II BGF kullanılarak farklı frekans bantlarına ayrılmıştır. Her bir BGF, aşağıdaki EEG frekans bantlarından birini çıkarmak üzere tasarlanmıştır: Delta (Δ, 0.5–4 Hz), Teta (θ, 4–8 Hz), Alfa (α, 8–13 Hz), Beta (β, 13–28 Hz) ve Gama (Γ, 31–49 Hz). Sezgisel olarak belirlenen altıncı dereceden filtre, sinyal zayıflatma ve hesaplama verimliliği arasında optimum dengeyi sağlamıştır. Tüm filtreler için durdurma bandı zayıflatması, sinyal bozulmasını en aza indirmek için 50 dB olarak ayarlanmıştır.

Sol ve sağ beyin yarımkürelerindeki EEG kanalları, sol elektrotlar (Fp1, F3, C3, P3, O1, F7, T3, T5, Fz ve Pz) ve sağ elektrotlar (Fp2, F4, C4, P4, O2, F8, T4, T6 ve Cz) olarak ikiye ayrıldı. Her bir beyin yarımkürenin sinyalleri, zirve sensörünün zarfı hesaplanarak ve her yarımküre için ortalama zarf elde edilerek ayrı ayrı analiz edildi, bu da iki ortalama sinyal (sağ ve sol) sonucunu verdi. Özellikler, her yarımküreye ait ortalama sinyallere uygulanan kaydırmalı pencere yaklaşımıyla çıkarıldı, değişen örtüşme oranlarıyla (yüzde 12,5'ten yüzde 87,5'e kadar, yüzde 12,5 adımlarla) ve pencere uzunluğu 2000 örnek (~8 saniye) olarak belirlendi. Maksimum, ortalama ve minimum enerji değerleri, özellik olarak ayrı ayrı kullanıldı. Sınıflandırma için üç farklı DVM çekirdeği türü—doğrusal (D), radikal bazlı fonksiyon (RBF) ve kare—kullanıldı.

Yöntem 1 Sonuçları:

- **Teta Bandının Üstünlüğü:** Teta (θ) bandının doğruluğu, hassasiyeti ve düşük standart sapması diğer frekans bantlarına kıyasla en yüksek değerleri sağlamıştır. θ bandı, OSB ile tipik gelişim gösteren (TG) gruplarını ayırt etmede en etkili özellik olarak öne çıkmıştır. Doğrusal DVM ile %91,73 ve SS = %7 doğruluk, %91,4 ve SS = %9,7 hassasiyet ve %92,1 ve SS = %8.6 özgüllük elde edilmiştir.
- **Diğer Frekans Bantlarının Performansı:** δ (Delta) bandı da güçlü bir performans göstermiştir. DVM -Doğrusal sınıflandırıcı ile, δ bandı %84,3 ve SS = %8,7 doğruluk ve DVM-İkinci Dereceden sınıflandırıcı ile %85 ve SS = %9,2 doğruluk sağlamıştır. Ancak, bu performans θ bandının üstün performansını geçememiştir.
- **Özellik Seçimi ve DVM Çekirdekleri:** Daha yüksek örtüşme oranları ve maksimum enerji pencereleri, özellikle θ bandında, EEG sinyallerini daha ayrıntılı yakalayarak sınıflandırma doğruluğunu artırmıştır. RBF ve ikinci dereceden gibi doğrusal olmayan DVM çekirdekleri, frekans bantları genelinde sınıflandırma doğruluğunu daha da artırmıştır. Ancak, γ (Gamma) bandı genel olarak daha düşük bir performans sergilemiştir, en yüksek doğruluk %73,3 ve SS = %10,5 ile sınırlı kalmıştır.

Bu sonuçlar, θ bandının OSB'nin erken teşhisinde güvenilir ve etkili bir özellik olarak kullanılabileceğini göstermektedir.

Yöntem 2: EEG Topografik Haritalama ve Derin Öğrenme Mimarisi

Bu yöntem, özellik çıkarımı ve sınıflandırma için topografik beyin haritalarını (TBH'ler) derin öğrenme mimarilerine giriş olarak kullanır. EEG verilerinden anlamlı özellikler çıkarmak için

AlexNet ve GoogLeNet kullanılmıştır; özellikle alfa bandı, OSB tespiti için yüksek önemi nedeniyle odak noktası olmuştur.

Verimliliği artırmak için ANOVA tabanlı özellik seçimi uygulanarak, özellik alanının boyutu azaltılmıştır. Özellik çıkarımından sonra, doğrusal (DVM-D) ve Doğrusal Ayırıcı Analiz (DAA) gibi sınıflandırıcılar kullanılarak OSB ve TG olmayan gruplar birbirinden ayrılmıştır.

Yöntem 2 Sonuçları:

Sonuçlar, alfa bandının doğruluk, hassasiyet, özgüllük, kesinlik ve F1 ölçütü gibi performans metrikleri açısından diğer EEG frekans bantlarını sürekli olarak geride bıraktığını göstermektedir. Bu, özellikle CNN özellik çıkarıcılarının (AlexNet-FC6, AlexNet-FC7, AlexNet-FC8 ve GoogLeNet) ANOVA tabanlı özellik seçimi ve DVM -D ile birleştirilmesiyle belirgin hale gelmiştir. ANOVA'nın entegrasyonu, tüm bantlarda doğruluğu önemli ölçüde artırmış, özelliklerin önemini geliştirmiş ve sınıflandırma süresini azaltmıştır.

DVM-D, sınıflandırma görevlerinde sürekli olarak DAA'dan daha iyi performans göstermiş, daha yüksek doğruluk ve azaltılmış işlem süreleri sağlamıştır. Özellik çıkarıcılar arasında, GoogLeNet daha yüksek karmaşıklığı nedeniyle daha fazla hesaplama kaynağı gerektirmiş, AlexNet özellik setleri (FC6, FC7 ve FC8) ise karşılaştırılabilir işlem yükleri sunmuştur.

Çalışma, ön işleme yöntemlerinin ve cihaz farklılıklarının veri setleri genelinde performansı önemli ölçüde etkilediğini vurgulamaktadır. AAAR, ANOVA ve DVM-D'nin AlexNet-FC6 ile entegrasyonu, yüksek doğruluk ve azalan değişkenlik ile güçlü ve verimli bir yaklaşım sağlamıştır. Bu bulgular, alfa bandının OSB tespiti için kritik bir frekans aralığı olduğunu doğrulamakta ve otomatik tanı araçlarında daha fazla ilerleme potansiyeli sunmaktadır.

- **Irak veri seti** için, GoogLeNet + ANOVA + DVM-D kombinasyonu %98 ve SS = %2,3 doğruluk ve %97,9 ve SS = %2,9 F1 ölçütü sağlamıştır.
- **Polonya veri seti** için, AlexNet-FC6+ANOVA+ DVM-D %96,5 ve SS = %3,6 doğruluk ve %96,4 ve SS = %3,8 F1 ölçütü elde etmiştir.

Her iki CNN mimarisi de yüksek performans göstermiş olsa da, GoogLeNet daha fazla hesaplama kaynağı gerektirirken, AlexNet-FC6 gerçek zamanlı uygulamalar için daha verimli bulunmuştur. Deneyler ayrıca, ön işleme sırasında AAAR ve ANOVA'nın çıkarılmasının sınıflandırma doğruluğunu %59,5'a düşürdüğünü, bu adımların performansı korumada kritik bir rol oynadığını göstermiştir.

Bu iki yaklaşımın kombinasyonu, klinik uygulamalarda kullanılabilecek, gerçek zamanlı ve invaziv olmayan OSB tanı araçlarının oluşturulması için bir temel oluşturmaktadır.

Genel Sonuç: Bu çalışma, nörogelişimsel araştırmalar ve sağlık hizmetleri alanında kritik bir ihtiyacı karşılayan, OSB'nin erken tespiti için EEG tabanlı yöntemlerin umut verici potansiyelini vurgulamaktadır. İki tamamlayıcı yaklaşım geliştirilmiş ve kapsamlı bir şekilde değerlendirilmiştir. Bu yöntemler, doğru tanıların elde edilmesinde sinyal ön işleme ve ileri düzey özellik çıkarma tekniklerinin önemini göstermektedir. İlk yöntem, beyin yarımküreleri arasındaki enerji farklarını analiz etmeye odaklanmış ve Teta bandını OSB ve TG gösteren gruplar arasında önemli bir ayırıcı olarak ortaya koymuştur. Özellikle, OSB vakalarında sağ yarımkürenin enerji seviyeleri daha yüksekken, TG bireylerde sol yarımküre baskın bulunmuştur.

İkinci yöntem, derin öğrenme mimarileri (özellikle AlexNet ve GoogLeNet) kullanılarak işlenen TBH içermektedir. ANOVA tabanlı özellik seçimi ile birleştirildiğinde, alfa bandı OSB tespiti için en bilgilendirici frekans aralığı olarak ortaya çıkmış ve yüksek performans metrikleri sunmuştur. AAAR ve band geçiş filtresi gibi ön işleme teknikleri, yüksek kaliteli EEG verilerinin analizini sağlamıştır. Doğrusal SVM sınıflandırıcılarının kullanımı, doğruluğu optimize ederken basitliği korumuştur. Her iki yöntem de, Irak veri setinde %98'e, Polonya veri setinde ise %96.5'e varan doğruluk oranları elde ederek, metodolojilerin çeşitli popülasyonlar ve EEG sistemleri arasında güvenilir olduğunu göstermiştir.

Birinci yöntemin Teta bandında en yüksek sonucu verdiği, ikinci yöntemin ise alfa bandında etkili olduğu belirtilmiştir. Daha önce de belirtildiği gibi, bu iki bant yan yana, yani aynı düzlemde yer almaktadır. Birinci yöntemde kullanılan 5 filtre, iki bant arasındaki frekanslarda bir miktar örtüşme göstermiştir ve her iki yöntemde de etkili frekans aralığı 5 ila 10 Hz arasında olmuştur; bu durum, bu farklılıkların nedeni olabilir.

Gelecek Çalışmalar: Bu çalışmanın bulgularını geliştirmek ve genişletmek için gelecekteki araştırmalar için çeşitli yönler önerilmektedir. İlk olarak, modellerin genelleştirilebilirliğini artırmak ve demografik farklılıkları ele almak için daha büyük ve daha çeşitli veri setlerinin toplanması gerekmektedir. İkinci olarak, gerçek zamanlı klinik ve eğitimsel ortamlar için sistemlerin geliştirilmesi, OSB taramasını ve müdahale planlamasını hemen mümkün kılabilir ve araştırma ile uygulama arasındaki boşluğu kapatabilir.

EEG verilerinin fizyolojik sinyaller gibi diğer modalitelerle entegrasyonu, OSB'nin daha kapsamlı bir değerlendirmesini sağlayabilir. Ayrıca, derin öğrenme modellerinin hafif ve verimli mimariler oluşturmak için optimize edilmesi, sınırlı kaynaklara sahip ortamlarda dağıtımı kolaylaştırabilir. Daha az çalışılmış frekans bantlarının keşfedilmesi, OSB ile ilgili beyin aktivitesine dair daha fazla içgörü sunabilirken, uzunlamasına çalışmalar EEG modellerini gelişimsel süreçler ve müdahale sonuçlarıyla ilişkilendirebilir.

Son olarak, tanı araçlarının belirli yaş gruplarına, kültürel bağlamlara ve klinik gerekliliklere göre uyarlanması, bu araçların etkinliğini ve erişilebilirliğini en üst düzeye çıkaracaktır. Bu çalışmada sunulan güçlü ön işleme, gelişmiş özellik çıkarma ve ölçeklenebilir sınıflandırma yöntemleri, OSB için otomatik, maliyet-etkin ve invaziv olmayan tanı araçlarının geliştirilmesi için sağlam bir temel oluşturmaktadır.

ACKNOWLEDGEMENTS

I would like to thank the University of Baghdad and Medical City, especially Dr. Ali Hussein Ali AL-HUSSEINY from the National Autism Center and Children's Welfare Teaching Hospital in Baghdad, Iraq, for confirming the diagnosis of pure ASD labeling. Special thanks to Dr. Noor H. AL-JANABI, who, as a Clinical Neurophysiologist currently working in the EEG unit, contributed significantly to the electroencephalography recordings.

I also extend my heartfelt gratitude to Prof. Dr. Sami ARICA for his invaluable assistance in data collection and preprocessing, which significantly contributed to this study.

A special acknowledgment goes to my co-supervisor, Assist. Prof. Dr. Mohannad Kadhim SABIR, for his guidance and support in obtaining data and sharing valuable information. I would also like to thank my supervisor, Assoc. Prof. Dr. Ahmet AYDIN, for accepting to oversee my thesis, supporting my academic journey, and providing ongoing assistance and encouragement throughout the study. Assoc. Prof. Dr. Ahmet AYDIN was also in close contact with me even during holidays, trips, and breaks, providing continuous assistance.

Lastly, I am deeply grateful to my family, especially my wife, Assist. Prof. Dr. Zainab H. Q., my lovely child, Hassen, my friends, and my loved ones for their unwavering moral support and encouragement, which helped me persevere and complete my PhD journey.

LIST OF TABLES

LIST OF FIGURES

SYMBOLS AND ABBREVIATIONS

AAAR	: Artefakt Alt Alan Rekonstrüksiyonu
ADOS	: Autism Diagnostic Observation Schedule
AI	: Artificial Intelligence
AN	: Amplitude Normalization
ANN	: Artificial Neural Network
ANOVA	: Analysis Of Variance
AOI	: Areas Of Interest
ASA	: Autism Spectrum Australia
ASD	: Autism Spectrum Disorder
ASR	: Artifact Subspace Reconstruction
Ave	: Average
BCI	: Brain-Computer Interface
BPF	: Band-Pass Filter
CAR	: Common Averaging References
CARS	: Childhood Autism Rating Scale
ciPLV	: Conditional Phase Locking Value
CNN	: Convolutional Neural Network
ConvLyr	: Convolutional Layer
CSTO	: Chronological Sewing Training Optimization.
CWT	: Continuous Wavelet Transform
DFT	: Discreet Fourier Transform
DL	: Deep Learning
DMN	: Default Mode Network
DÖ	: Derin Öğrenme
DRN	: Deep Residual Network
DSM	: Diagnostic and Statistical Manual
DT	: Decision Tree
DVM	: Destek Vektör Makinesi
DWT	: Discrete Wavelet Transform
EEG	: Electroencephalography
ERP	: Event-Related Potential
F1 measure	: Harmonic mean of precision and recall
FC	: Fully Connected
FC6	: Fully Connected Layer 6
FC7	: Fully Connected Layer 7

FC8 : Fully Connected Layer 8
Fe : Female
FE : Features Extrications
FFT : Fast Fourier Transform
FIR-BPF : Finite Impulse Response Band-Pass Filter
fMRI : Functional Magnetic Resonance Imaging
FN : False Negative
FP : False Positive
GARS : Gilliam Autism Rating Scale
GPU : Graphics Processing Unit
HT : Hilbert Transform
I_FAST : Implicit Function as Squashing Time technique
ICA : Independent Component Analysis
IIR : Infinite Impulse Response
IQ : Intelligence Quotient
KNN : K Nearest Neighbor
LDA : Linear Discriminant Analysis
LFCC : Linear Frequency Cepstral Coefficients
Max. : Maximum
Me : Male
Me : Male
Min. : Minimum
ML : Machine Learning
MRI : Magnetic Resonance Imaging
mRMR : Minimum-Redundancy-Maximum-Relevance
MS-ROM : Multi-Scale Ranked Organizing Map coupled
NAS : Neurodevelopmental Autism Spectrum
OSB : Otizm Spektrum Bozukluğu
PCA : Principal Component Analysis
PLV : Phase Locking Value
PSD : Power Spectral Density
QEEG : Quantitative Electroencephalography
RBF : Gaussian Radial Basis Function
ReLU : Rectified Linear Unit
RGB : Red, Green, and Blue
RIFG : Right Inferior Frontal Gyrus
RN : Random Forest

ROI	: Region of Interest
SD	: Standard Deviation
SI	: Sensory Integration
SMOTE	: Synthetic Minority Oversampling Technique
SNR	: Signal-to-Noise Ratio
SPWVD	: Smoothed Pseudo-Wigner-Ville Distribution
STBO	: Short-Term Behavioral Observation
STFT	: Short-Time Fourier Transform
SVD	: Singular Value Decomposition
SVM	: Support Vector Machine
SVM-L	: Support Vector Machine with Linear Kernel
TBH	: Topographic Brain Haritalama
TBM	: Topographic Brain Map
TD	: Typically Developing (Control Group)
TFD	: Time-Frequency Distribution
TG	: Tipik Gelişim
TN	: True Negative
TP	: True Positive
TWIST	: Task-Weighted Iterative Statistical Transformation
WHO	: World Health Organization
α	: (Alpha Band) 8-12 Hz
β	: (Beta Band) 12-30 Hz
γ	: (Gamma Band) 30-100 Hz
δ	: (Delta Band) 0.5-4 Hz
θ	: (Theta Band) 4-8 Hz

1. INTRODUCTION

Autism Spectrum Disorder (ASD) is a complex developmental disorder that is characterized by several genes, epigenetic modifications, environmental and immune triggers. It is mainly diagnosed in children and characterized by difficulties in social interaction and atypical patterns of behavior, interests, and activities. Symptoms are different in different people, and the functional patterns are atypical or maladaptive. While the root of ASD has not been identified, studies indicate that multiple genetic, biological, and environmental influences result in early brain developmental abnormalities (Ministry of Education, 2015).

Genetic Factors: There is strong evidence that genetics contribute to the development of ASD. Families with a history of autism are more likely to have children with the condition than families with no such history (Ohwovoriole, 2021).

Biological Factors: Neuroanatomical and neurochemical abnormalities are well documented in people with ASD. Functional MRI studies show that there is a deviation in certain areas of the brain in comparison with normal people. Furthermore, rapid brain development during the early years is another feature observed in many children with autism (Ohwovoriole, 2021).

Environmental Factors: Some factors in the environment may increase the chances of developing ASD. Some of the risk factors include infections during pregnancy, severe pollution during pregnancy, or preterm birth. However, these elements alone cannot lead to ASD and probably play a role in combination with genetic factors (Ohwovoriole, 2021).

Interaction of Multiple Factors: Researchers understand that ASD is caused by a combination of genetic, biological, and environmental factors. This makes it difficult to determine the root cause of the disorder as pointed out by the (Ministry of Education, 2015).

Knowledge of these contributing factors is important to diagnose the condition early and treat it. Consequently, early diagnosis and intervention improve the overall quality of life of these persons and provide the prospects for ASD treatment and inclusion in the community.

The ASD prevalence in the US increased from 1 in 68 in 2014 (Baio, 2014) to 1 in 36 as in 2018. Furthermore, ASD manifests 3.9 times more frequently in boys than girls (Autism Speaks, 2022; Maenner et al., 2018). The World Health Organization (WHO) reported that autism is diagnosed in 1 in 100 children worldwide. Autism Spectrum Australia (ASA) reported that autism prevalence has increased from 1 in 100 in 2014 to 1 in 70 people in 2018, which is a 40% increase (ASA, 2018). In 2023, about 42,700 people in South Korea were registered as having ASD, representing an increase of approximately 2,384 percent compared to the 1,514 registered cases in 2000. The number of registered cases has steadily increased each year, without any fluctuations (Statistics, 2024). Figure 1.1 displayed the number of people with autism in South Korea from 2000 to 2023 with annual growth rate. The data shows that the number of cases is increasing year by year from 2.4 thousand in 2000 to 42.7 thousand in 2023.

This increase represents a high-risk situation that should not be overlooked due to its steady progression over the years. The annual growth rate has been increasing year by year, the incremental increase is beginning from approximately 1.01 thousand cases per year in the early of 2000 and up to about 2.85 thousand cases per year in 2016. A pattern in such a manner reveals exponential increase over time, which means that whatever is being measured is on the increase in magnitude.

According to the observed trend, the number of cases could be estimated to be about 73.55 thousand in 2030. This projection was done by extrapolation, based on the current annual increment rate of 2.85 thousand cases. This estimate means that the 2016 value will be surpassed by more than a hundred percent and shows the need to act now and put measures in place to arrest this exponential growth. This is why the data provided also highlights the need to focus on the factors that are causing such an increase in the future.

However, the prevalence of autism exhibits significant variation among countries, with some nations reporting higher rates than others.

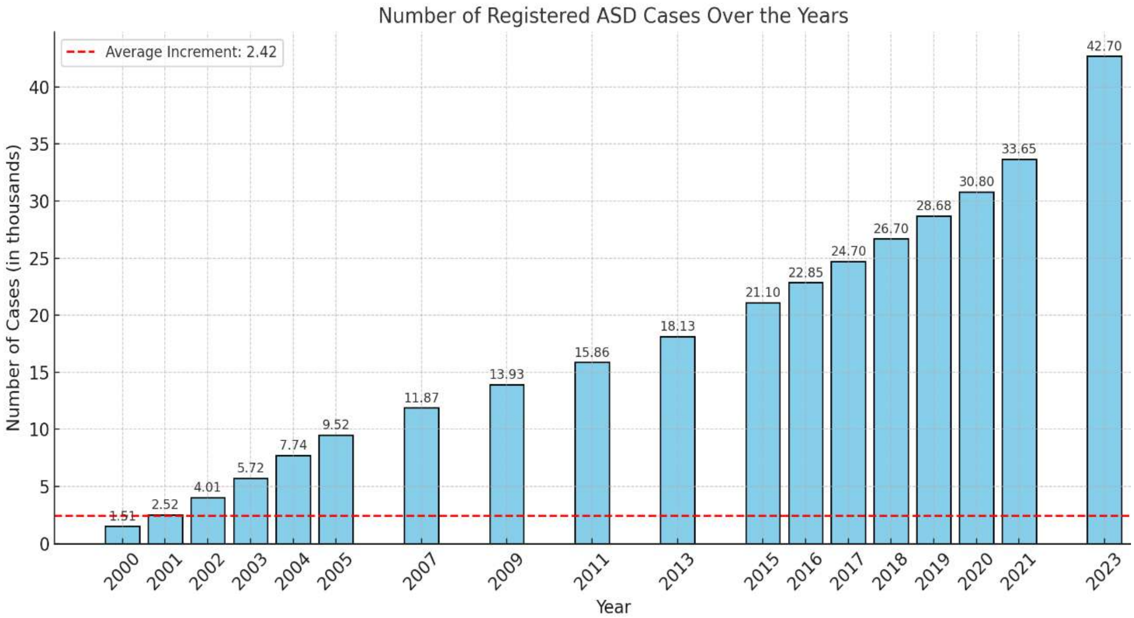

Figure 1.1. Number of people with ASD in South Korea from 2000 to 2023.

Research on high-risk infant siblings suggested that the specific behavioral traits associated with autism appear in the later stages of the first and second years of life (Ozonoff et al., 2010). The ASD severely impairs the ability to perform daily activities and participate in social interactions, which frequently hinders education, employment, and community involvement. Additionally, people with ASD are frequently victims of discrimination, abuse, and human rights violations globally reported by (WHO, 2024). While ASD has no cure, early intervention can positively affect brain development and enhance learning, social abilities, and communication.

The identification of autism requires an accurate, efficient, and highly effective diagnostic system. This thesis will bring arguments from different countries to show that the frequency of autism is on the rise presenting a real threat to the welfare of mankind and education. Therefore, the only way to enhance skills is to focus on early identification and treatment.

The rising prevalence of autism worldwide, as indicated by statistics across various nations, poses a significant challenge to both human well-being and educational standards. Therefore, prioritizing early detection and intervention is the optimal strategy to enhance skills.

While no cure exists, early intervention can positively impact brain development, enhancing learning, social abilities, and communication. An effective and efficient, and highly accurate diagnostic system is essential for autism identification.

1.1. Aim of Early ASD Detection

1.1.1. Improving Developmental Gains

ASD diagnosis allows children to receive specific treatments during the period of brain development when they are most receptive to learning, which is before the age of three. At this stage, the brain is plastic, and this is why early developmental, social, and communication interventions are effective. Those children who receive these services at an early age are likely to have appropriate physical, communication, and emotional development that will enable them to be independent (Faja et al., 2006). It has been established that the earlier the child is enrolled in an intervention program the higher the likelihood of the child attaining his or her full developmental potential in terms of social interaction and cognitive development.

1.1.2. Reducing Long-term Costs and Burdens

Early diagnosis of autism is not only helpful to the child but also helps to avoid the future economic and emotional costs for families and organizations. Research indicates that, if intervention is made before the child is 5 years old, the child may require fewer of these therapies and educational services in the future. This results in relief to families and has an economic impact on the healthcare and education sectors. This ensures that children with developmental delays are placed in normal learning classes thus minimizing the use of expensive individualized programs(Cancer Research UK, 2015).

1.1.3. Facilitating Social and Communication Development

The early identification of ASD is essential in improving communication and socialization gains. The strategies that target children's language development, and emotional, and social skills in their peer group are most beneficial when undertaken at an early stage. It has been found that early diagnosed children have the advantage of early intervention through therapies that foster basic interpersonal skills and enable them to engage in academic activities. They allow children to have more fulfilling lives and promote their social integration in subsequent phases of life (Cancer Research UK, 2015; Faja et al., 2006).

1.1.4. Personalized and Efficient Treatment Strategies

When the child is diagnosed early, the clinician and the family are in a position to come up with an individual plan that will fit the child. Such strategies can include a child's medical management by pediatricians, therapists, and educators, as well as developing supportive contexts for the child. This is because if the areas of need are identified early enough, the child can be provided with therapies that seek to exploit his/her potential as well as treat him/her for the areas of difficulty hence increasing his/her life chances (Faja et al., 2006) and (Zwaigenbaum et al., 2015).

The identification of young children with ASD is crucial for enhancing children's developmental achievements, increasing their social and cognitive gains, decreasing the necessity of extensive interventions, and alleviating the financial stress on families and facilities. Early intervention is the best strategy since the brain is most malleable during early childhood to help children on the autism spectrum get the best possible results.

Advanced signal processing and artificial intelligence have substantial potential for detecting ASD and facilitating early detection. This innovative approach can significantly benefit patients by enhancing diagnostic accuracy and efficiency. Furthermore, new technology, such as modern signal processing and artificial intelligence, increases the chances of detecting ASD and making a timely diagnosis. This original approach would also greatly contribute to diagnosis as it could increase the quality and speed of diagnostic methods.

1.2. Goal of Study

The main objective of this work is to design an accurate, fast, and explainable model for the screening of ASD in children based on EEG signals. ASD is a neurodevelopmental disorder and thus calls for early diagnosis so that children can be provided with the right therapies that can enhance their development and enhance their quality of life. However, clinical heterogeneity, high costs, and reliance on subjective assessment at present hinder the precision and availability of ASD diagnosis. This research seeks to address these challenges by developing new approaches that combine deep learning, machine learning (ML), and advanced signal processing of EEG signals to improve the accuracy, validity, and practicality of ASD diagnostic tools. This thesis proposed two methods for ASD identification as in the following:

1.2.1. Brain Hemisphere Energy-Based Methodology

The first methodology aims to explore energy distribution across the left and right brain hemispheres as an indicator of ASD. By calculating maximum, mean, and minimum energy values in overlapping time windows, this method investigates temporal EEG features relevant to ASD. A comparative analysis of three SVM kernels (linear, RBF, and quadratic) is conducted to determine the most effective classification technique. Additionally, the study examines how varying the time window overlap affects classification outcomes, focusing on the theta band, which has shown promising results in temporal energy analysis for ASD identification. The goal is to create an energy-based classification model that can function effectively on small datasets, providing a new dimension to ASD screening.

The analysis of the recorded EEG demonstrated changes in the patterns of hemispheric asymmetry in ASD subjects, with some reports suggesting that ASD subjects have greater power in the left hemisphere than in the right in a broad frequency range (Jun Wang et al., 2013). Addationally, neuroimaging investigations have suggested that in ASD there is increased right hemisphere activation which is or social, language delay and emotional processing (Floris et al., 2021). This focus on left-right hemispheric energy metrics is in harmony with these findings.

1.2.2. Topographic Brain Mapping (TBM) Methodology

The second methodology involves extracting features from TBMs generated from EEG data, with minimal pre-processing. Using CNNs, specifically AlexNet's fully connected layers (FC6, FC7, and FC8), in combination with classical ML classifiers (linear SVM-L and LDA), this method seeks to enhance the predictive accuracy of ASD detection. A key objective is to evaluate how feature selection with ANOVA and the use of transfer learning improve the model's performance in identifying a distinct subgroup of children with ASD, especially in the alpha band, which has been shown to exhibit significant class separation in previous studies. This aspect of the research not only aims to improve the early diagnosis of ASD but also demonstrates the model's interpretability by linking the predictions to specific EEG signal characteristics, facilitating validation for clinical use.

Employing these two approaches, the study will attempt to analyze both spatial and temporal aspects of EEG and provide a comprehensive view of ASD identification. This combined approach not only increases the accuracy of the prediction but also gives clinicians the possibility to interpret the results, which increases the reliability of the diagnosis. The overall aim of the study is to design an online decision support system that can be used by healthcare professionals in the early identification of ASD. This tool has the potential to close the gap between clinical research and practical application by reducing the need for human input, lowering diagnostic costs, and offering analysis based on the features of the EEG signal. Furthermore, the study intends to solve the problems of small sample sizes in EEG datasets through transfer learning and the use of feature selection methods that make the proposed methodologies feasible for clinical applications.

To sum up, the aim of the present work is to design an accurate, efficient, and explainable ASD detection system based on EEG data and employing preprocessing, feature extraction, DL models, and ML classifier methods. In this way, the study aims at the development of the field of

ASD, the enhancement of the possibilities of the diagnosis, and the enhancement of the quality of life of children with ASD.

2. PRELIMINARY WORK

Numerous studies (Haghighat, 2023; Seyed Fakhari et al., 2023; Sung et al., 2024) have detected autism from electroencephalograph (EEG) signals and functional magnetic resonance imaging (fMRI). These studies can be categorized broadly into ASD and typically developing (TD) based on their feature extraction methods, classification techniques, and brain network connectivity. Ongoing research consistently indicated that atypical structural and functional connectivity causes autism patients' behavioral and cognitive impairments. The most widely used method for ASD exploration focused on fMRI connectivity in the brain networks related to face processing, mentalizing, and mirroring. The results revealed significantly heightened connectivity within the ASD group between networks and hub regions to the brain rest. These differences may be linked to the diverse origins of ASD and rapid changes in brain activity, which is challenging to capture using fMRI.

A limitation of MRI is that patients are required to remain motionless in a confined tube (Blume et al., 2023; C. et al., 2017; Jung et al., 2019). This limitation renders MRI for children with autism only possible under sedation, which substantially alters brain activity. Overall, the disadvantages of MRI of pediatric patients are: 1) the only means of obtaining clear images from typically restless children is to sedate them, which may result in sedative side effects; 2) the enclosed MRI scanner can cause claustrophobia and anxiety, which may lead to the need for sedation or unsuccessful scanning; 3) the prolonged scan duration results in children encountering difficulty in remaining still, which results in more motion artifacts and poor image quality; 4) MRI machines emit loud, unpleasant noises that provoke anxiety in children even when earplugs are used; 5) the scarcity of MRI units in the most countries limits access due to long waiting lists for appointments and consequently delays diagnosis and treatment, which are more common in places without specialized pediatric facilities; 6) some MRI scans might require the use of contrast agents, which can cause adverse reactions, especially in children with kidney issues; and 7) MRI scans may be costly and impose an additional financial burden on families, specifically when additional scans or follow-up examinations are required.

The EEG is a widely available and economical alternative to fMRI, and its advantages in detecting ASD are that it is side-effect-free, suitable for babies, rapid, and cost-effective. Nevertheless, EEG signal analysis involves addressing numerous challenges to ensure accurate results. One significant challenge is the signal-to-noise ratio (SNR), which is critical for reliable analysis. (Bigdely-Shamlo et al., 2015; Jas et al., 2017). In controlled laboratory environments lead to variations in the SNR of raw EEG data caused by external factors such as blinking, odors, light, motion, temperature alterations and environmental elements. The inherent noise sources create difficulties for signal analysis because EEG processing algorithms need high-quality signals (Rashid et al., 2020). Signal pre-processing becomes more complex because noise from multiple sources including interference and artifacts makes accurate analysis difficult. Raw EEG data processing benefits from optimized electrode placement and high-quality electrodes while implementing advanced filtering and denoising algorithms and improved experimental setups to reduce the effects of low SNR and external noise sources.

Raw EEG data present processing challenges because their unique features lead to nonlinearity and non-stationarity and increased sensitivity to artifacts. The exploration of internal signal relationships becomes difficult because of these factors. The removal of EEG signal artifacts through pre-processing stands as an essential requirement before post-processing operations also known as artifact removal. (Steyrl et al., 2019).

ML and DL are widely successful in EEG classifications in seizures, which are the common symptoms of epilepsy and are characterized by abnormal and synchronized brain neuronal activities (Kbah et al., 2022). Early diagnosis and treatment, specifically for young children, is critical to maximize the probability of getting the maximum possible outcome in the child's best interest. A study of gender differences in emotional modifications enriched computational understanding of human emotions, thereby paving the way for more responsive emotion-oriented applications(N. K. Al-Qazzaz et al., 2021). The aforementioned study extracted linear and nonlinear features using EEG signals to detect emotional influences on gender behavior. Furthermore, the study intended to construct an automated gender identification model using optimization approaches to identify the most suitable channels for gender recognition from emotional-oriented EEG signals.

Another study described a novel method for classifying motor imagery EEG recordings in a brain–computer interface (BCI) task (Cao et al., 2024; de Melo et al., 2024; Firat Ince et al., 2006; Gaur et al., 2021; Liang et al., 2024), while five other studies (Fan et al., 2024; Fu et al., 2024; Kbah et al., 2022; Quan et al., 2023; Steyrl et al., 2019) examined emotional EEG classifications. Furthermore, gender differences were explored by analyzing emotional states (happiness, anxiety, surprise, anger, sadness, disgust) (N. Al-Qazzaz et al., 2021). The study collected EEG data from 10 healthy participants as they watched short emotional audio-visual video clips. Another study used the BCI as a communication interface between the human brain and an external device that transformed intent changes in EEG signals into control signals (Bah et al., 2023). The attempted movement altered EEG signals via the movement-related cortical potential originating from the attempts to move. The movement-related cortical potentials were classified using the delta band obtained through the Hadamard basis.

Dynamic applications have further demonstrated significant potential in EEG-based classifications. For example, movement-related EEG classifications have been explored to enhance BCI systems. In (Kim et al., 2019), researchers used EEG signals to decode movement intention during a reaching task, analyzing 30 movement types based on direction, distance, and target position. They demonstrated the potential for real-time control in movement-related BCIs, achieving the highest classification accuracy with premovement EEG for direction and distance. Similarly, (Robinson et al., 2013) investigated movement intention decoding using EEG for controlling BCIs. This study specifically focused on voluntary hand movement directions and low-frequency components ($\leq$ 6 Hz), achieving a high classification accuracy of 80% using a novel signal-processing approach for four movement directions.

The ML involves extracting time frequencies as EEG signal features. The features are used to classify autism through diverse ML-based algorithms. The ML-based classification relies on identifying significant features from EEG data. While many researchers used many autism detection methods, the issue of early detection remains unresolved. One study used connectivity with ML (Rogala et al., 2023) and the two metrics of integrated traditional statistical methods with ML techniques and connectivity. This concurrent strategy enhanced comprehension of model predictions generated from EEG signal attributes and simultaneously validated these predictions. Crucially, ML enabled the discovery of a distinct subclass of children accurately classified with autism based on the analyzed EEG features. The accuracies of the corrected imaginary part of the phase locking value (ciPLV), spectral, and phase-locking value (PLV) outcomes were 83% with an SD of 13%, 83%, and 86% with an SD of 16%, respectively.

One study addressed the shortcomings in current ASD screening models by integrating medical tests and demographic characteristics using conventional feature selection methods (Hazim Hammed et al., 2023). The study used seven ML classification techniques and a real dataset involving 45 features and 983 patients. The reported gradient boosting model outperformed other models and achieved 87% accuracy. Another study involved 97 children aged 3–6 years old (Kang et al., 2020). The children underwent EEG recording during rest and individual eye-tracking tests involving the stimuli of strangers' faces of their own and other races. The EEG analysis used power spectrum analysis, while the eye-tracking data focused on areas of interest (AOI) for face gaze analysis. The classification of autistic and TD children used the minimum-Redundancy-Maximum-Relevance (mRMR) feature selection method with support vector machine (SVM) classifiers. The results indicated that combining these data types yielded a maximum 85.4% classification accuracy.

One study introduced an effective autism diagnostic model utilizing EEG signals, which captured brain electrical activities (Singh et al., 2024). Noise was eliminated using Gaussian filtering, and statistical and spectral-based features were extracted and fed into a deep residual network (DRN) for improved efficiency. The ASD was detected using a chronological sewing training optimization-deep residual network (CSTO-DRN), where the DRN was pre-trained with the CSTO algorithm to optimize weights. The CSTO combines chronological and sewing training-based optimization (STBO) concepts. The CSTO-DRN model detected ASD with a high accuracy of 88.6%. Another report involved 58 ASD children and 50 TD children (Cheng et al., 2024). The children viewed videos depicting joint and non-joint intention. The children's gaze duration and frequency in various AOI were used to create classifier-based models, which were evaluated for accuracy, sensitivity, and specificity. Eight common classifiers were used and included SVM, Linear discriminant analysis

(LDA), decision tree (DT), random forest, and k nearest neighbor (KNN), and achieved a maximum 81.90% classification accuracy. Furthermore, using a feature reconstruction method with a DT classifier enhanced accuracy to 91.43%.

Another study combined two ASD screening datasets for toddlers. The study balanced data using the synthetic minority oversampling technique (SMOTE), followed by feature selection (Hajjej et al., 2024). The study introduced a two-phase system. The first phase used a range of ML models, including an ensemble of random forest and XGBoost classifiers, which achieved 94% accuracy in ASD identification. The second phase focused on identifying effective teaching methods for children with ASD by evaluating their physical, verbal, and behavioral performance. A different study examined and compared ASD prediction methods (Qureshi et al., 2023). The researchers focused on the application type, simulation method, comparison methodology, and input data to provide a unified framework for researchers in this field. The results demonstrated that random forest outperformed traditional algorithms, yielding the highest accuracy of 89.23%.

The authors of (Alhassan et al., 2023) proposed an energy-efficient sensor-based scheme for early autism detection using EEG data. An efficient signal transformation enabled the proposed scheme to achieve accurate classification through ML algorithms. The experimental results demonstrated impressive accuracy of 96%. Another study involved 15 ASD patients (13 boys, 2 girls; age: 7–14 years old; mean age: 10.4 years old) and 10 TD participants (4 boys, 6 girls; age: 7–12 years old; mean age: 9.2 years old) (Grossi et al., 2017). The children were diagnosed using Diagnostic and statistical manual of mental disorders: (DSM-V) criteria and confirmed using the Autism Diagnostic Observation Schedule (ADOS) scale. The researchers created invariant feature vectors by analyzing 60-second artefact-free EEG segments using Multi-Scale Ranked Organizing Map coupled (MS-ROM) with Implicit Function as Squashing Time technique (I_FAST) and Input Selection and Testing (TWIST). The ML achieved 84–92.8% accuracy in classifying autism cases using the leave-one-out protocol. The results were independent of the participants' ages, which indicated the recognition of underlying brain disconnection signatures.

In another study (Sheikhani, 2008), 15 children with ASD (13 boys, 2 girls, aged 6–11 years old) and 11 TD children (7 boys, 4 girls, same age range) underwent Quantitative Electroencephalogram (qEEG) evaluation across nine conditions. Spectrogram analysis revealed that the signals recorded during the relaxed eye-opened condition in the alpha band, viewing a stranger's picture in the beta band, and viewing an inverted stranger's picture in the same beta band exhibited the highest discrimination rates of 92.3%, 88.9%, and 88.9% respectively. Another group reported an efficient autism diagnostic system using EEG signals (M. N.A. Tawhid et al., 2020). Pre-processed EEG data were converted into time–frequency spectrogram images, and textural features were extracted and fed into an SVM classifier. The system achieved an average 95.25% accuracy, which demonstrated potential as a decision support tool for autism diagnosis.

Another group focused on ASD detection based on biological markers and highlighted the need for early diagnosis (Sharma, 2024). The EEG signal underwent band-pass filtering to isolate the gamma band. Subsequently, ASD and TD participants were differentiated by power spectral density and phase-locked values extracted from the gamma band. Statistical validation using analysis of variance (ANOVA) demonstrated a significant decrease in the aforementioned features in the ASD participants. Thus, EEG signal irregularities can be biomarkers for diagnosing ASD. Other researchers presented an efficient autism diagnostic model using EEG signals reflecting brain electrical activities to identify ASD (Singh et al., 2024). Noise was removed using Gaussian filtering, and statistical and spectral-based features were extracted. These features were inputted into a deep residual network (DRN) to enhance efficiency. ASD was detected using chronological sewing training optimization–DRN (CSTO-DRN). The CSTO combines the chronological concept with sewing training-based optimization (STBO). The approach pre-trained DRN using the CSTO algorithm to optimize weights, and CSTO-DRN achieved a notable 88.6% accuracy.

Various researchers used convolutional neural networks (CNNs) for classification tasks or feature extractors combined with ML for ASD detection. For example, EEG signals were analyzed using a multi-input one-dimensional (1D) CNN framework (Omar, 2024). Data augmentation and processing preceded input into the model, which included 1D convolutional layers, batch normalization, Rectified Linear Unit (ReLU) activation, and a fully connected layer. The researchers evaluated the effectiveness of the method using EEG data from King Abdulaziz University Hospital and various metrics. The first section of the study focused on specific EEG channels and reported an impressive 99.16% accuracy.

Authors in (Md Nurul Ahad Tawhid et al., 2021) proposed system involved pre-processing (re-referencing, filtering, normalization) raw EEG signals. Subsequently, the signals were converted into time–frequency (spectrogram) images using short-time-fourier transform (STFT). The images were assessed separately using DL and ML models. The ML approach extracted textural features and selected significant features using principal component analysis. The selected features were fed into six ML classifiers for classification. The DL approach involved testing three distinct CNNs. Testing on an autism EEG dataset determined that the proposed DL model had superior accuracy (99.1%) compared to the ML model (95.2%). Another study (Husna et al., 2021) focused on ASD biomarkers using neuroimaging fMRI. The study used the CNN models VGG-16 and ResNet-50 and achieved 63.4% and 87.0% accuracy, respectively, aiding doctors in quantifiable ASD detection beyond behavioral observations.

The study implemented an approach involving preprocessing, segmentation, and time-frequency distribution (TFD) using algorithms like STFT, continuous wavelet transformation (CWT), smoothed pseudo-Wigner-Ville distribution (SPWVD)]. These techniques generated spectrograms, scalograms, and SPWVD-TFD. These TFDs were integrated into pre-trained DenseNet-121 and ResNet-101 models, then fed into ASD-Net. DL models were employed to differentiate between ASD and Normal subjects based on TFD images, achieving a mean accuracy of 97.35% with the SPWVD-based TFD and ASD-Net model. The developed CNN model with five convolution layers demonstrated superior efficiency and computational speed compared to benchmark models (Lalawat et al., 2024).

One study (Mohi-Ud-Din et al., 2021) explores EEG and ML for detecting ASD. The study used trained CNNs (GoogLeNet and SqueezeNet) through transfer learning. The approach achieved 75% and 82% classification accuracies for ASD and the controls, respectively, which indicated the potential of EEG-based ASD classification. The authors of another study (Menaka et al., 2024) explored ML methods (K-NN, random forests, naïve Bayes, SVM) to predict ASD meltdowns. Additionally, the study evaluated the effectiveness of DL techniques (ResNet-50, VGG-16, AlexNet) using five cepstral coefficient features for detecting detection. The key contributions included incorporating cepstral coefficients in spectrogram construction and modifying the AlexNet architecture to enhance classification accuracy. The experimental results demonstrated that AlexNet with linear frequency cepstral coefficients (LFCC) achieved the highest accuracy at 85%, while a customised AlexNet with LFCC achieved 90% accuracy.

Another group used a hybrid lightweight deep feature extractor for high-performance classification in autism detection (Baygin et al., 2021). The group extracted EEG signal features using a unique signal-to-image conversion model using 1D local binary pattern (LBP) and generated spectrogram images by processing the features using Short Time Fourier Transform (STFT). Deep features were extracted using trained SqueezeNet, ShuffleNet, and MobileNetV2 models. The feature selection and ranking with a two-layered ReliefF algorithm yielded an SVM classifier with 96.44% accuracy. The authors of (Dong et al., 2021) addressed the limitations of existing EEG models in ASD evaluation by proposing a Q-learning method for fast CNN reconstruction adapted to individual participants. The method achieved higher accuracy (92.6%) than its counterparts, which demonstrated its efficacy in maintaining performance during participant shifts. The approach was a valuable contribution to EEG-based ASD assessment that considered individuality and non-stationarity in cognitive dynamics.

2.1. Knowledge Gaps

Although impressive achievements have been made for EEG-based ASD detection, some issues remain unclear or less investigated including the variability of the datasets, signal analysis, and clinical relevance. Another critical problem is the scarcity of datasets and their insufficient variety in terms of size. As has been seen in most of the studies including this thesis, the data sets used are small and are usually collected from a particular region or contain a particular type of population. The absence of diverse statistics poses the issue of how to transfer the results of a study to large groups, which creates a bias in the diagnostic models. Furthermore, the variation in the types of instrumentation used for recording EEG, how data was acquired, and how it was preprocessed further adds to the difficulty of comparing data across various investigations. Filling these gaps will need a coordinated effort to obtain much larger and more diverse data sets as well as to develop standard procedures for EEG data recording and processing.

The second major deficiency is in the analysis of spatial and temporal characteristics of EEG signals. Although this thesis provides approaches for interpreting EEG topographic maps and the energy distribution of brain hemispheres, the integration of spatial and temporal characteristics has not been well investigated. Present methods may analyze these features separately, which could lead to the loss of understanding of the temporal dynamics of the brain and its regions. This is a serious limitation in constructing other broader models necessary for modeling the complex neural activity associated with Neurodevelopmental Autism Spectrum (NAS) Disorder. Other research could involve spatial and temporal techniques for enhancing diagnostic capabilities based on EEG but also to understand and provide better results.

There is also an apparent gap in translation from basic research on EEG to clinical practice. While ML and DL models are being used in studies to develop diagnostic accuracy, there is still a question regarding real-world, real-time application of such models in clinical practice. Most seizure prediction models have employed computationally intensive approaches, like convolutional neural networks, until now, besides requiring artifact-free EEG data. Application of these kinds of models will be difficult to implement in realistic conditions. Besides this, most the models are not interpretable, and it's problematic in clinical practice. This gap will need the development of valid, interpretable, and user-friendly diagnostic tools that are easily integrated into existing practice.

Finally, the current method (2) use of conventional feature selection methods including ANOVA-based selection and linear classifiers raises the question of the need to employ more sophisticated and integrated approaches. Although these two techniques have been useful in some applications, they may not adequately possess the properties necessary to model non-linear and non-stationary patterns of EEG data. Nonlinear classifiers, inclusion, and combination of classifiers, and ensemble learning methods are a likely line of development that could yield extension beyond the effectiveness and flexibility of ASD detection. These are some of the gaps that need filling for the development of this field and to ensure EEG-based approaches can offer expected dividends by way of becoming accurate and inexpensive diagnostic tools for ASD.The study aims to optimize ASD prediction by comparing the effectiveness of two methods across frequency bands, with a particular focus on the alpha band for TBM analysis and the theta band for energy-based analysis. The ultimate goal is to create a reliable and interpretable clinical tool for early ASD detection that can handle small sample sizes, reduce diagnostic errors, and provide insights into EEG signal properties relevant to autism, thereby supporting healthcare professionals in real-time decision-making.

2.2. Thesis Outline

Thesis is organized into several sections to provide a clear structure and presentation of the study. The "**Materials** "outlines the EEG dataset utilized in the study and the collection tool employed. In the "**Preprocessing**", the processing of EEG signals to ensure freedom from noise and artifacts is detailed. The "**Proposed Methods**" elaborates on the autism screening methods utilized and the framework employed for analysis are presented in chapter 3. Following this, the "**Results Discussion**" chapter delves into the analysis and interpretation of the obtained results presented in chapter 4. Lastly, the paper concludes with a summary and final remarks in the "**Conclusion**" section. This structured approach facilitates a comprehensive understanding of the study's methodology, findings, and implications presented in chapter 5.

3. MATERIAL AND METHOD

3.1. History of EEG

The EEG was invented by a German scientist called Hans Berger. He made the first recordings of EEG and human subjects and those recordings were deemed as the beginning of clinical electroencephalography. To further deepen notions of interictal signals and clinical seizure patterns, Gibbs, Davis, and Lennox improved the clinical and scientific application of EEG in the 1960s (Pahuja et al., 2022). This progress occurred alongside the introduction of ML this advancement led to increased use of EEG in research and clinical practice, which in turn led to the development of the recurrent NN in 1982 (Bronzino, 1984).

Since then, frequency reduction (Nunez, 1973), mathematical frequency analysis (Houston, 1942), and classification techniques (Bronzino, 1984; Sanderson et al., 1980) have progressed EEG analysis. This evolution has been complemented by technical enhancements like videotape recording and remote real-time reading in the 1990s. In the 2000s, sophisticated algorithms like multi-class SVMs and probabilistic neural networks were introduced with the goal of minimizing artifacts and enhancing classification (Herman et al., 2008).

3.2. Materials (Datasets)

The system was examined based on two datasets. First, a case–control investigation was conducted at the Children's Welfare Teaching Hospital in Medical City, Baghdad, Iraq. The study period was from 5 March 2021 to 3 February 2024. Official approval for data collection was obtained from the University of Baghdad, AL-Khwarizmi College, Biomedical Engineering Department, and was approved by the local research ethics committee.

The EEGs were recorded during induced sleep. The participants in the chloral hydrate both groups received 50 mg/kg chloral hydrate syrup, with an additional 25 mg/kg dose if they did not fall asleep within half an hour (Limpornpugdee S, Thanawirattananit P, Yimtae K, Chayaopas N, Priprem A, Soontornpas C, Uppala R, Wongswadiwat Y, 2021). The resistance of all channels was lower than 10 k Ohm. The study used a 19-channel scheme with an EEG machine by Nihon Kohden Company (Tsurugashima, Japan) with a sampling frequency of 500 Hz. All the EEG data were real signals to obtain practical results as displlayed in Figure 3.1.

The dataset involved 52 children (ASD = 22 children, (average age = 4.8 years, SD: 1.5); TD = 30 children, (average age: 5.9 years, SD: 3). The data were validated using the Gilliam Autism Rating Scale (GARS) (Dumont et al., 2008), at Childhood Autism Rating Scale (CARS) (Schopler et al., 1980), medical history, and clinical assessment by child and adolescent psychiatrists according to DSM-5-TR (Tanguay, 2011) criteria for ASD diagnosis at the National Autism Centre. The control group was drawn from the pediatric department of an EEG unit, Child Welfare Teaching Hospital, Medical City, Baghdad, Iraq. The data were anonymized to ensure confidentiality and maintain ethical standards.

Second, autistic EEG datasets were obtained from the Institute of Mother and Child, Warsaw, Poland, and Warsaw University (Rogala et al., 2023), requested officially to assess the system and verify the accuracy of diagnosing ASD in the dataset. The retrospective analysis examined the clinical EEG recordings from the two patient groups, which each comprised 18 children (12 boys). The average age for both classes was approximately 3.9 years old. One group exhibited symptoms indicative of atypical development, while the other group comprised TD children. This development ensured that the participants' age, sex, and observed sleep stages during EEG recording were aligned. The provided Poland data was cleaned to ensure noise and artifact-free signals, with each patient's data consistently segmented into 2-second intervals containing 500 samples, as selected for the current study in the MATLAB® 2022b & EEGLABv 2023.1 data structure named "ALLEEG.data". However, it is crucial to mention that the data from our initial dataset is raw and directly sourced from the EEG machine.

The parents in both datasets did not report episodes that could be associated with epileptic seizures in any case, and the participants were recorded using the 10-20 international electrode positioning (Morley et al., 2016). Figure. 3.2 shows an example of 10-20 International Electrodes placements.

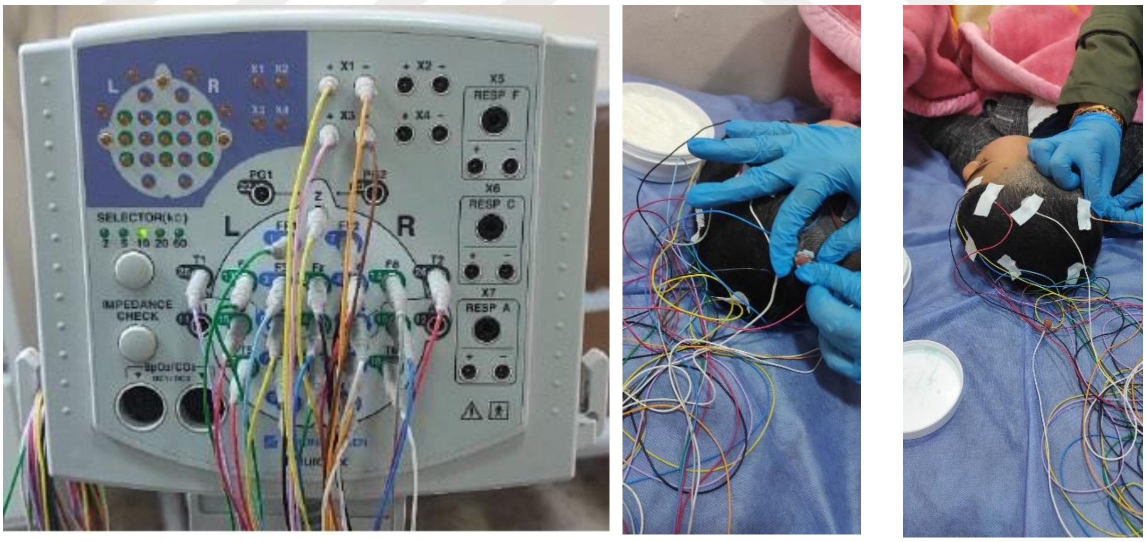

Figure 3.1. The used EEG machine by (Nihon Kohden), and example of EEG-channels connections.

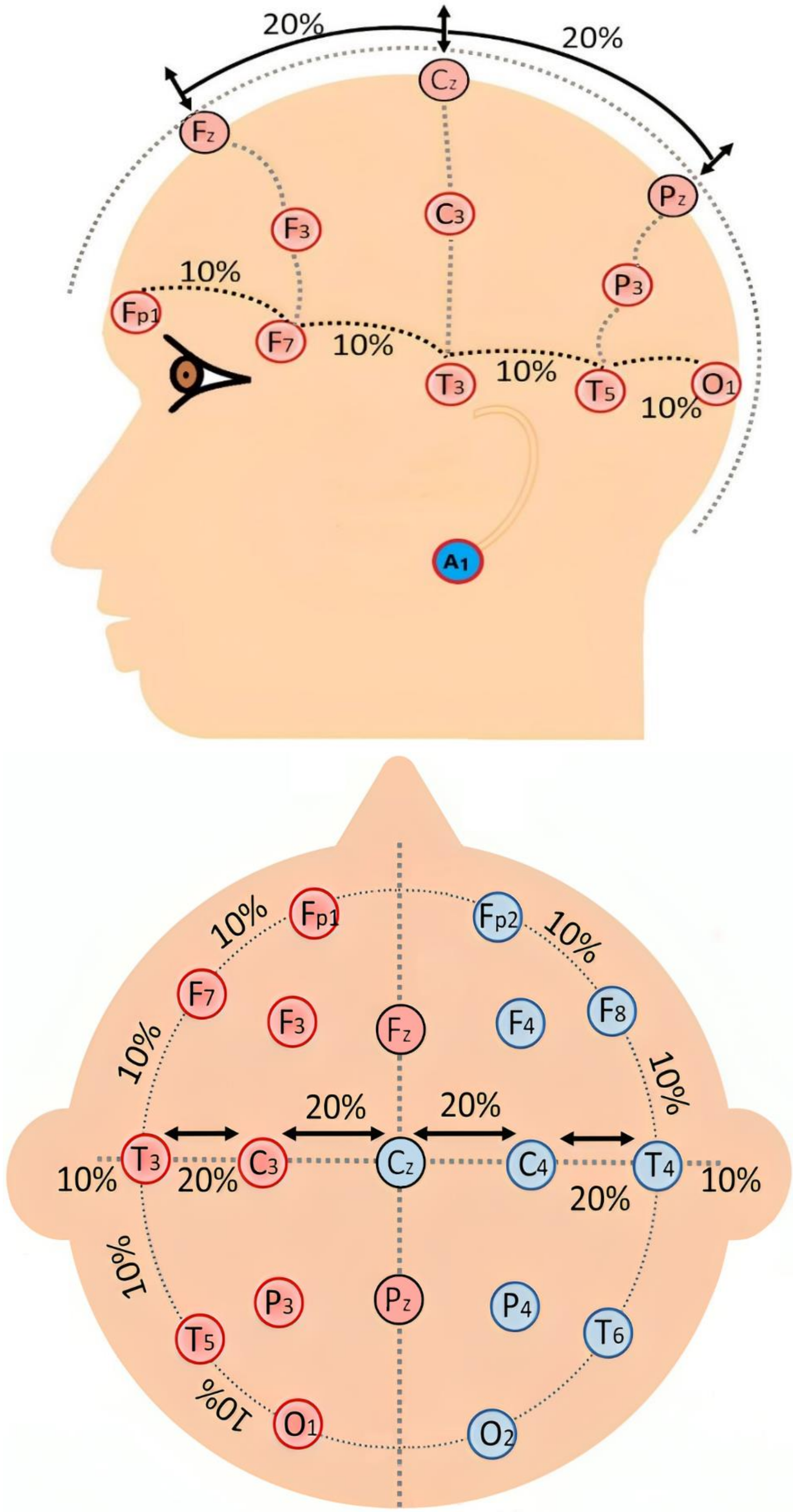

Figure 3.2. Diagram of the 10–20 international electrode placement system, showing standardized electrode locations on the scalp for EEG recording to ensure accurate and reproducible EEG data collection.

3.3. Method

In this thesis, two methods were proposed and utilized. Preprocessing was applied to both methods, which involved loading EEG data, selecting the used 19 channels, applying a frequencies below 0.5 Hz and above 49 Hz were removed using a zero-phase FIR-BPF. This step was designed to eliminate baseline 50 Hz noise and low-frequency components. The filter employed a Hamming window with a heuristic order, and the transition bandwidth was automatically estimated using EEGLABv2023.1 toolbox. The remaining EEG signal was reconstructed. All these steps will be explained in detail in the next sub-sections, and the preprocessing process was conducted using the EEGLABv2023.1 toolbox.

3.4. EEG Signals Processing

Analyzing EEG signals involves addressing numerous challenges to ensure accurate results. The EEG is a widely available and economical alternative to fMRI, and its advantages in detecting ASD are that it is side-effect-free, suitable for babies, rapid, and cost-effective. Nevertheless, EEG signal analysis involves addressing numerous challenges to ensure accurate results. One significant challenge is the signal-to-noise ratio (SNR), which is critical for reliable analysis. (Bigdely-Shamlo et al., 2015; Jas et al., 2017). In controlled laboratory settings, external influences (blinking, odurs, light, motion, temperature variations, environmental conditions) affect the SNR of raw EEG data. These inherent noise sources challenge signal analysis as EEG processing algorithms require high-quality signals (Rashid et al., 2020). Various sources of noise, such as interference and artifacts, complicate signal pre-processing further, which renders accurate analysis challenging. The effects of low SNR and external noise sources in raw EEG data processing can be mitigated by optimizing electrode placement, using high-quality electrodes, implementing advanced filtering and denoising algorithms, and improving experimental setups.

Raw EEG data exhibit unique characteristics, which complicate their processing due to nonlinearity, non-stationarity, and increased artifact susceptibility. These factors complicate the direct exploration of the internal relationships within the signals. Therefore, pre-processing is essential to remove EEG signal artifacts before post-processing, which is commonly known as artifact removal (Steyrl et al., 2019).

EEG signal processing is the methodology by which the quality of acquired EEG data is improved, and useless information is filtered out to further analyse the signals. The technique of EEG deals with signals that are connected with electric activity in the human brain, and such a signal requires preprocessing for cancelling the noises, artifacts, and other signals that interfere and that are undesirable for further analysis of these signals. So, various types of preprocessing techniques for the processing of EEG signals depend on the goals of a particular application and/or questions of a study. Here are some common types of preprocessing techniques used by various authors:

3.4.1. Common Averaging References (CAR)

A common reference electrode was used to average out noise sources across all channels, a technique that has been widely used in EEG to reduce common noise and thereby enhance the quality of EEG signals (Tsuchimoto et al., 2021). To do this, for each electrode, the deviation from the average activity will be determined by subtracting, from each channel's signal, the signal averaged over all electrode channels.

A CAR in EEG signals is important to achieve common noise reduction, preservation of relative neural activity, reference-independent analysis, improvement of spatial filtering, and compatibility with traditional analysis methods. The advantages mentioned above make the CAR a required technique to enhance the quality and interpretability of EEG data. Figure 2.3 (B) shows a sample output signal after applying the common averaging reference.

3.4.2. Detrending

A method that removes offsets or linear trends from time-domain input-output EEG data. It helps in detrending the data to eliminate systematic biases or drifts that may be operating in the data and ensures that the data is zero-centered or follows a stationary trend. While dealing with EEG signals, baseline shifts or slow linear trends are very common, which may distort the interpretation and analysis of the data. Detrending is done to eliminate these trends and focus on the dynamics of interest. (De Cheveigné et al., 2018). The technique involves estimating the trend component in the data and subtracting it to obtain detrended data.

Detrending is usually used as a preprocessing step to other analysis of EEG data such as AN, spectral analysis, event-related potential (ERP) analysis or time-frequency analysis. Detrending aids the next analysis and the identification of artifacts, the EEG features or patterns by erasing offsets or linear trends. Figure 3.3 (C). Shows an example of an output signal after detrending the difference is clear when compared with Figure 3.3 (A).

3.4.3. Amplitude Normalization (AN)

Absolute and relative amplitudes of the EEG signals may also differ from one recording or subject to another because of differences in electrode placement or impedance, or because of differences in the associated equipment. AN makes it possible for the signals that are recorded by the EEG devices from different sources, or from different individuals to be scaled to a certain range that makes it easy and direct to compare the signals between the different recordings as well as between the different subjects. It helps to maintain the uniformity of signal representation and enables comparison of different datasets on the basis of their meaningfulness. The EEG signals were also normalized to avoid problems of amplitude scaling when comparing samples. The goal of AN (Urbach et al., 2006), of EEG signals in signal processing is to scale the signal amplitudes to a standardized range, was selected between 1 to -1 This normalization process is carried out to achieve several objectives:

EEG signals can have varying amplitudes across different recordings or subjects due to factors such as electrode placement, impedance differences, or recording equipment variations. AN ensures that EEG signals from different sources or individuals are scaled to a common range, facilitating comparison and analysis across different recordings and subjects. It promotes consistency in signal representation and allows for meaningful comparisons between different datasets.

AN of EEG signals to a standardized range, were chosen between 1 to -1, aims to ensure consistency, comparability, efficient utilization of the dynamic range, enhancement of the signal-to-noise ratio, and facilitation of subsequent data processing and analysis. Figure 3.3 (D). Shows an example of an output signal after AN the difference is clear when compared with Figure 3.3 (C). Will be explained with more briefly with mathematical equations in the next.

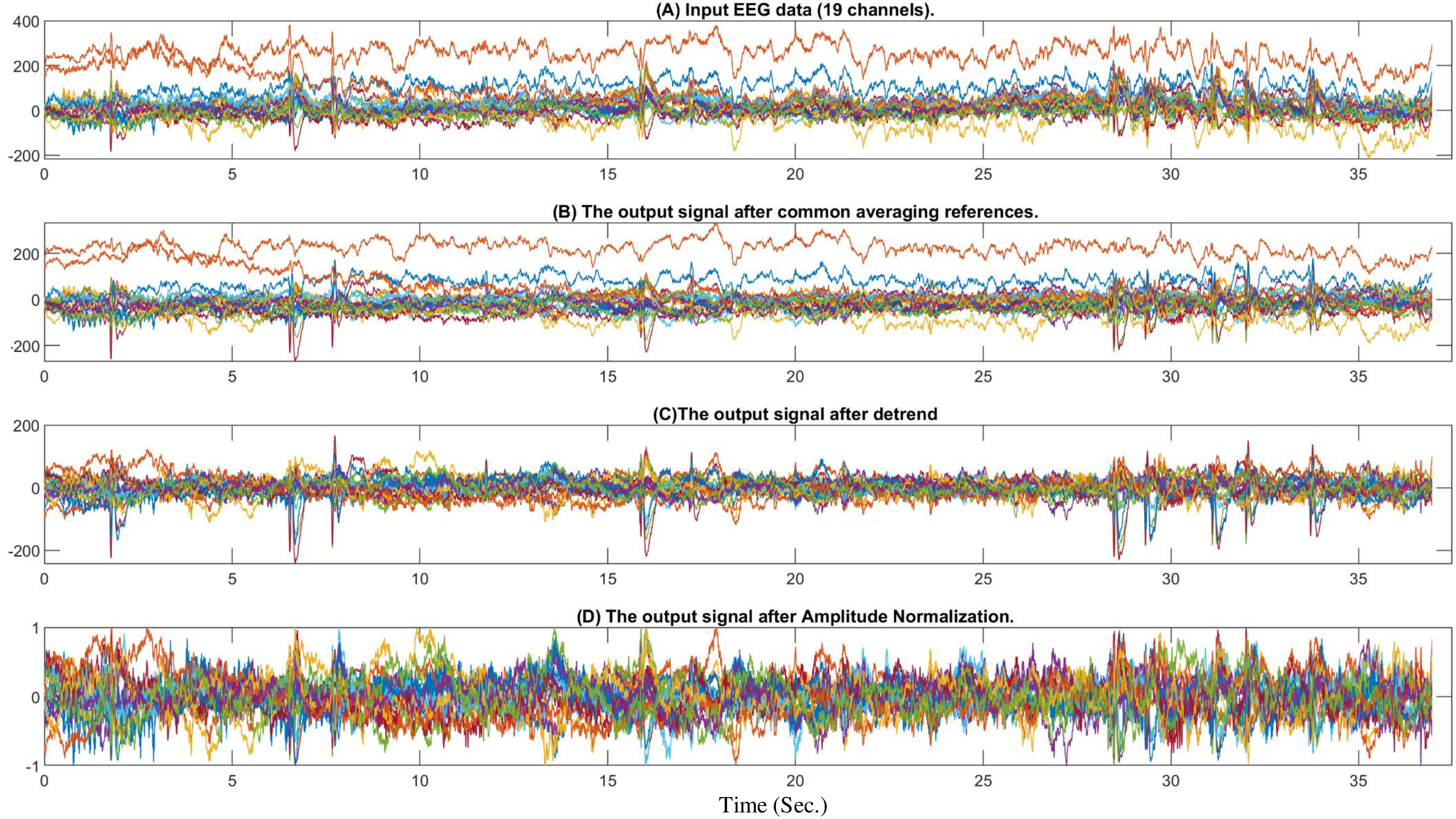

Figure 3.3. The output of the pre-processing in each step.

3.4.4. Downsampling

Downsampling the EEG channels is a method that aims to lower the various EEG signals' sampling rate for the purposes of lowering the level of processing involved and the complexity of the process as well. The concept of down sampling is that the important information of the brain activity is still contained in the lower sampling rate. EEG signals are usually recorded at a high frequency; in this study, the signals are recorded at 500 samples per second (Hz) to capture the fast dynamics of brain activity. However, some purposes or limitations in computation may mean that downsampling is to be used. Downsampling is the process of decreasing the number of samples per second, which means that less data has to be analyzed. In our study, the EEG signals were downsampled by ~two times from 500 Hz to 256 Hz for the Iraq dataset and 250 Hz for the Poland dataset. Such downsampling of EEG channels should consider the Nyquist-Shannon sampling theorem, according to which the sampling should be done at least twice the maximum frequency component in the signal to avoid aliasing.

Thus, care must be taken to avoid information loss or distortion during down-sampling. Down-sampling EEG channels can be a viable approach to reduce processing complexity, but it should be done carefully, considering the specific application requirements and potential information loss. Figure 3.4. Demonstrated of the EEG signals – 19 channels before and after downsampling algorithm.

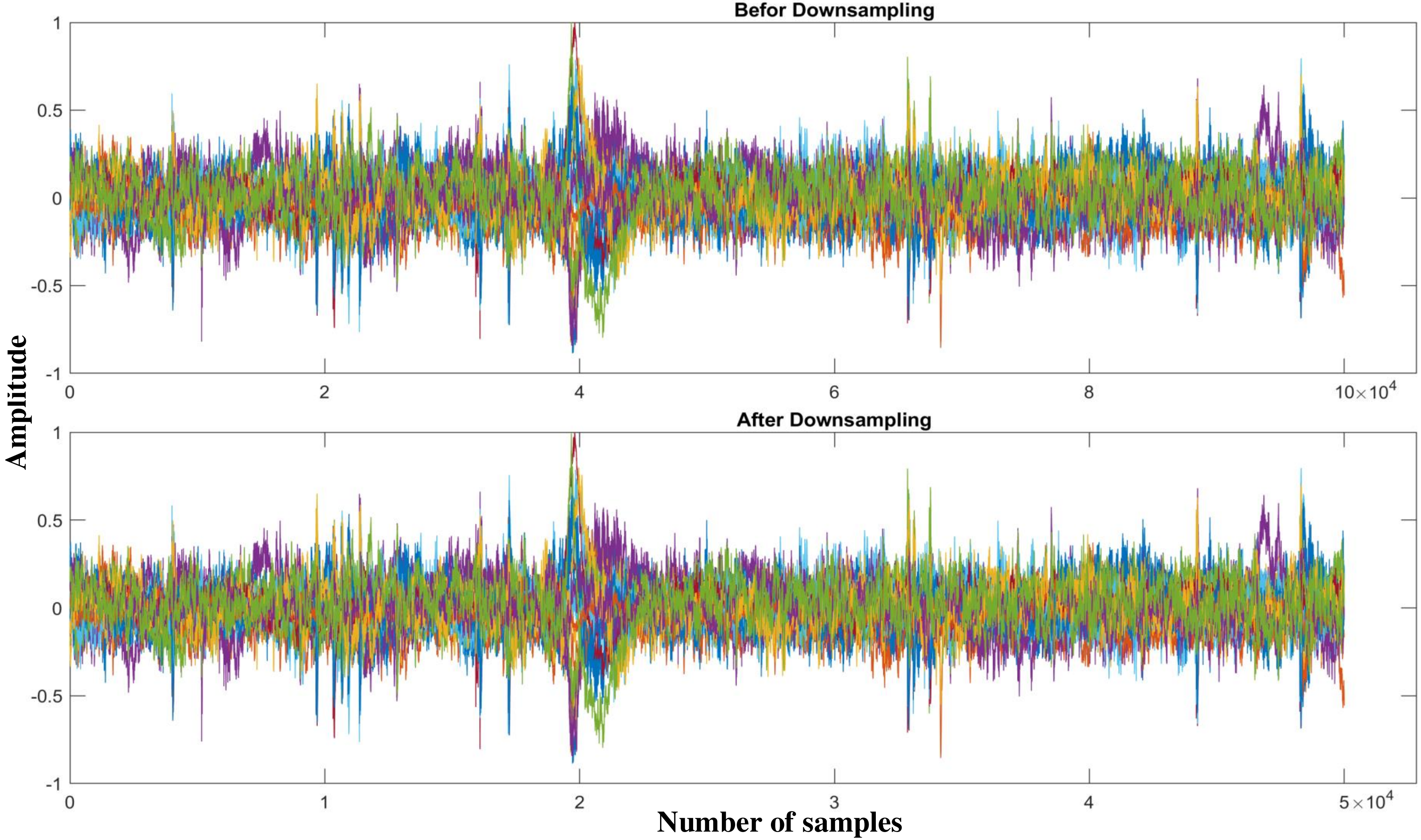

Figure 3.4. EEG signals – 19 channels before and after downsampling algorithim.

3.4.5. EEG bands decomposition

The raw EEG data was preprocessed by filtering to obtain the desired frequency bands of interest such as delta, theta, alpha, beta, gamma. Every band has its own set of frequencies. Can be selected by filtering. In this study, we employed different types of filtering methods (e.g., wavelet transform 6 levels, IIR filters). More pre-processing methods like appropriate bandpass or notch filters were used for further removal of noise in the signal. Banding of the EEG is a standard process in the analysis of EEG data to extract certain frequency bands of interest and reject other frequencies or interference. Among the filters used it worked with wavelet filters and IIR filters such as Chebyshev, Butterworth, and Elliptical filters. The type of filter to be used depends on the nature of the analysis and the nature of the EEG data. For example, Butterworth filters provide a flat frequency response, Chebyshev filters provide steep roll-offs with little ripples in the passing band and elliptic filters have very good control of bandwidth (Podder et al., 2014).

Wavelet filters

Wavelet filters are inherently useful for analysing signals at multiple resolutions or scale, which make them particularly useful for analysing features in the frequency domain at the local and global levels. Wavelet based filtering encompasses use of wavelet transform to break down the EEG signal according to the frequencies of the wavelets and then filtering is done on the required sub bands to reconstruct the signal. Due to a good time-frequency resolution, wavelet filters are recommended for detecting transient or time-variant characteristics in EEG signals (Khalid et al., 2020). In this study, the wavelet function chosen was “sym32” and the number of levels was six. However, the wavelet outputs were not useful in providing a perfect separation of the sub-bands since there was an overlap of the bands as shown in Figure 3.5. In addition, a 50 Hz baseline artifact was also observed in the same figure suggesting another source of interference that made the signal even less distinguishable. This artifact demonstrates the difficulties in obtaining accurate signal decomposition and the necessity for better methods to enhance signal processing.

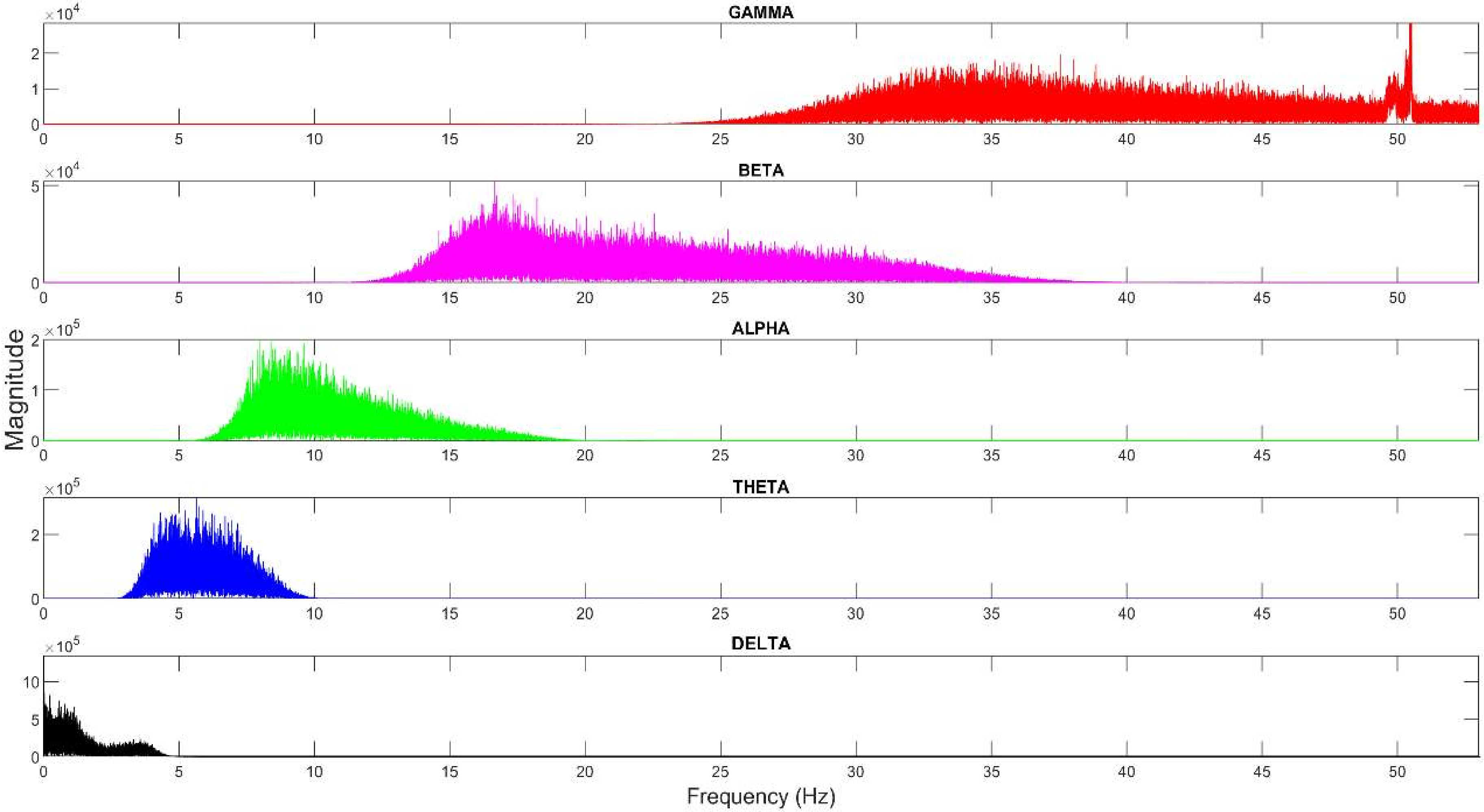

Figure 3.5. The output of the Wavelet packet 6 levels.

Finite Impulse Response (FIR)

Applying filters to EEG data is important for eliminating the interference frequency components. Many of the filters used are high-pass filters and low-pass filters that remove all the signals below or above the required frequency. In this regard, the first BPF used is of the FIR type with a linear phase as depicted in Figure 3.6. The filter has a low pass cut off of 0.5 Hz and a high pass cut off of 49 Hz thus eliminating the 50 Hz power line noise. The pre-filtering was done using EEGLABv2023.1 for all the input signals where the filter order was set to be automatically calculated. This automated selection provides the best filter characteristics for the input EEG data in order to achieve the best filtering results.

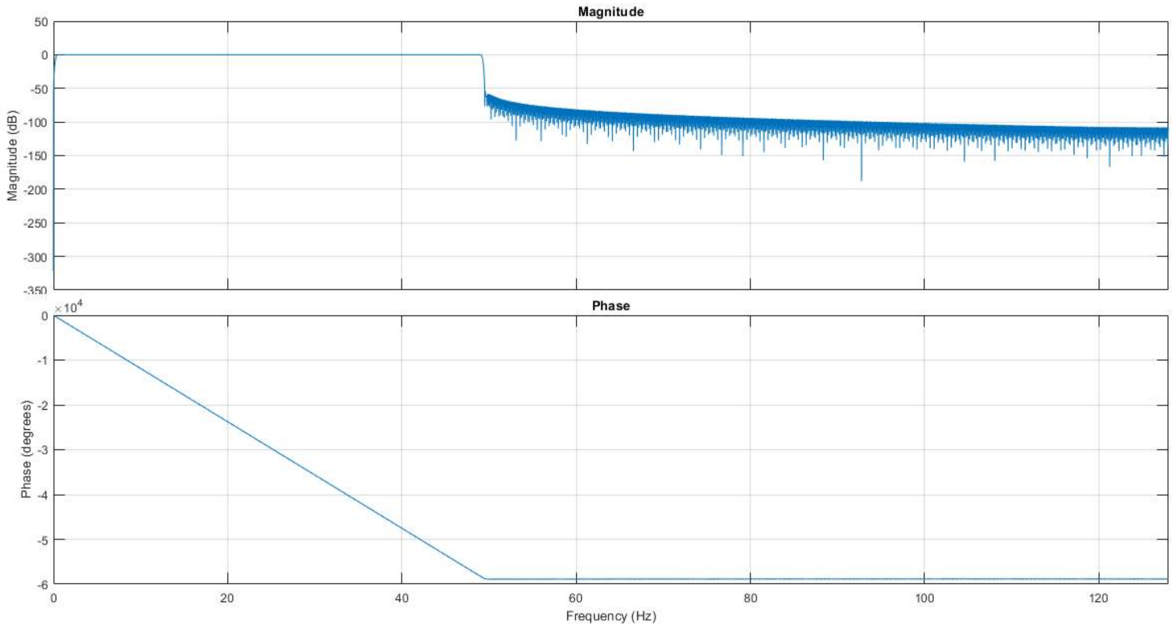

Figure 3.6. The response of FIR filter [0.5 - 49] Hz.

Infinite Impulse Response (IIR)

The Chebyshev filter, an IIR filter, was selected as an alternative to the wavelet due to its ability to balance stopband attenuation and passband ripple. Designed based on the Chebyshev approximation, it offers a steeper roll-off and better stopband attenuation compared to other filters like the Butterworth filter. In this study, the Chebyshev Type II filter was chosen for its sharper cutoff and significant attenuation of specific frequency components.

The selected Chebyshev Type II filter is a 6th-order Band Pass Filter (BPF) with a stopband attenuation of 50 dB below the peak passband value. This filter type was preferred because it provides a maximally flat passband and a slower roll-off (passband-to-stopband transition) compared to the Chebyshev Type I filter. The MATLAB function ‘filtfilt’ was employed for signal filtering, as it offers zero-phase filtering by applying the filter in both forward and reverse directions. This approach cancels out phase delays from the forward and backward and reverse directions. This approach cancels out phase delays from the forward and backward filtering, resulting in no effective filter delay. An example of the BPF response for the Alpha band is illustrated in Figure 3.7.

While any filter operating in real-time is considered a causal filter—where the output at time t_0 depends only on events occurring at $t \leq t_0$—non-causal filters, such as MATLAB's "filtfilt" function, leverage the knowledge of events at $t > t_0$. The filtfilt function applies the filter forward, reverses the output, and applies the filter again, eliminating phase delay. This process is not applicable in real-time scenarios due to its reliance on future data. However, as this study deals with recorded data, the lack of real-time applicability does not pose a limitation. In contrast, the Wavelet packet method provided a 6-level decomposition, as shown in Figure 3.5. However, overlapping between sub-bands limited its effectiveness, making the Chebyshev filter a more suitable alternative.

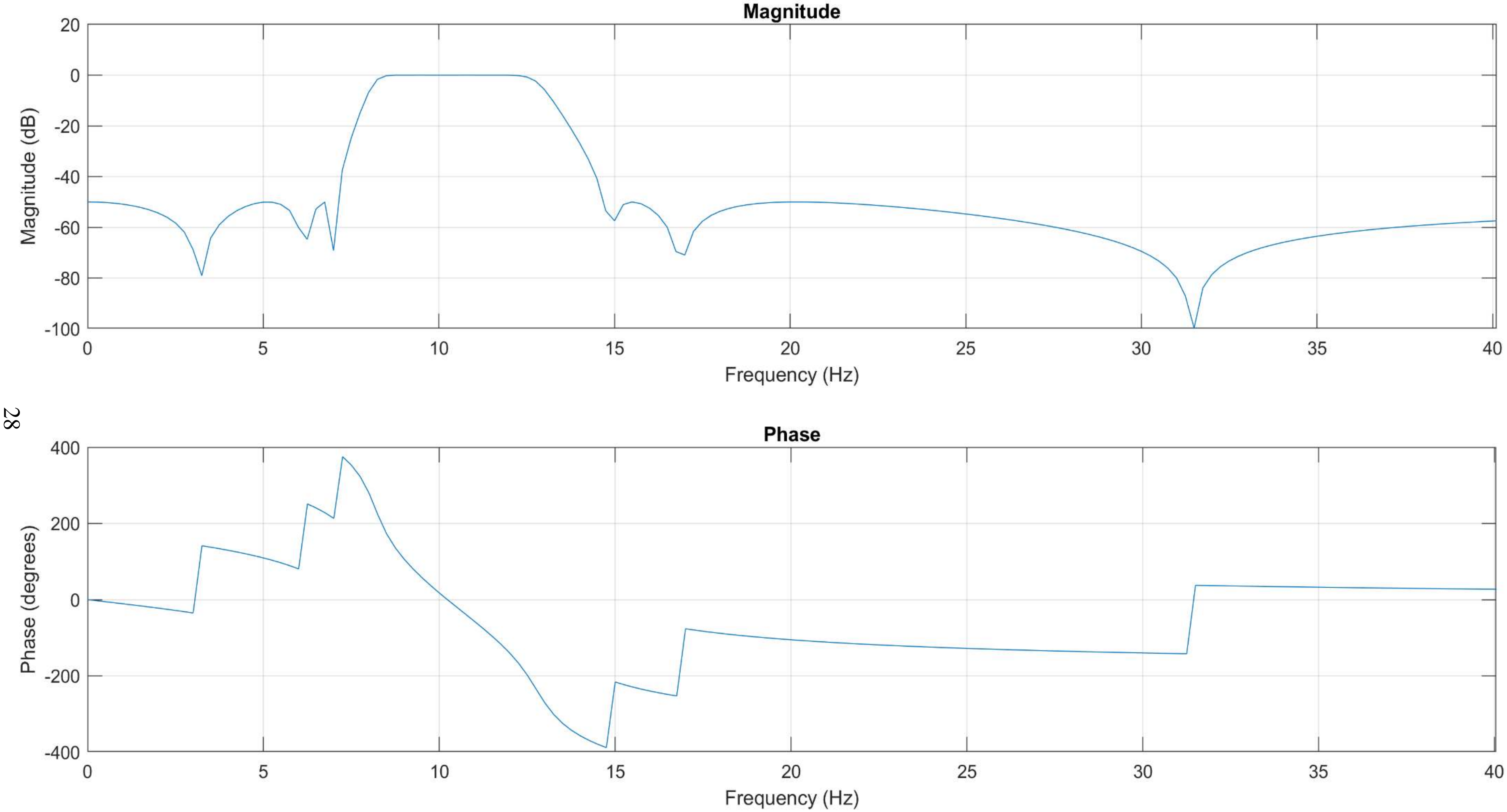

Figure 3.7. The response of Chebyshev type II filter designed for Alpha band example.

The Chebyshev Type II filter outperformed wavelet filters and all other filter types including elliptical and Butterworth filters. A filter's performance depends on three key elements which include EEG signal characteristics together with targeted frequency bands and data quality affected by noise and artifacts. The Chebyshev Type II filter proved ideal for this application because it provided superior noise reduction and unwanted frequency suppression while maintaining precise sub-band decomposition.

The Chebyshev Type II filter achieved optimal performance by offering rapid rolling and robust blocking of unwanted signals among competing filtering solutions. The selection of filters depends on precise understanding of EEG signals and analysis requirements to achieve desirable performance. The selection of optimal filters requires a systematic evaluation process which includes examination of frequency response alongside stopband attenuation and passband ripple and phase distortion and computational complexity and their impact on targeted frequency bands and features.

The first method used five zero-phase Chebyshev Type-II band-pass filters (BPFs) to separate the signal into distinct frequency bands. Each BPF was designed to extract one of the following EEG frequency bands: Delta (δ, 0.5–4 Hz), Theta (θ, 4–8 Hz), Alpha (α, 8–13 Hz), Beta (β, 13–28 Hz), and Gamma (γ, 31–49 Hz).

The results supported the hypothesis that the Chebyshev Type II filter successfully minimized the 50 Hz baseline noise, especially in the γ band as illustrated in Figures 3.5 and 3.8.

The output for the γ band was then filtered using a band-pass filter with the maximum frequency of 49 Hz. As illustrated in Figure 3.8, the performance of the filters is higher than that of the Wavelet approach with six levels. This superiority stems from less spectral overlap of the decomposed EEG sub-bands and the elimination of the 50 Hz baseline noise in the γ band response.

Furthermore, we achieved accurate segmentation of the EEG signals and identified the characteristics of each sub-band in time and frequency domain. This segmentation allowed for the assessment of dynamic and spectral properties for each sub-band, providing a better insight into the activity of the brain at the frequencies of interest. Some of these sub-bands are depicted in the frequency domain in Figure 3.8 and in the time domain in Figure 3.9, where the peculiarities of each band, as used in Method 1, are emphasized.

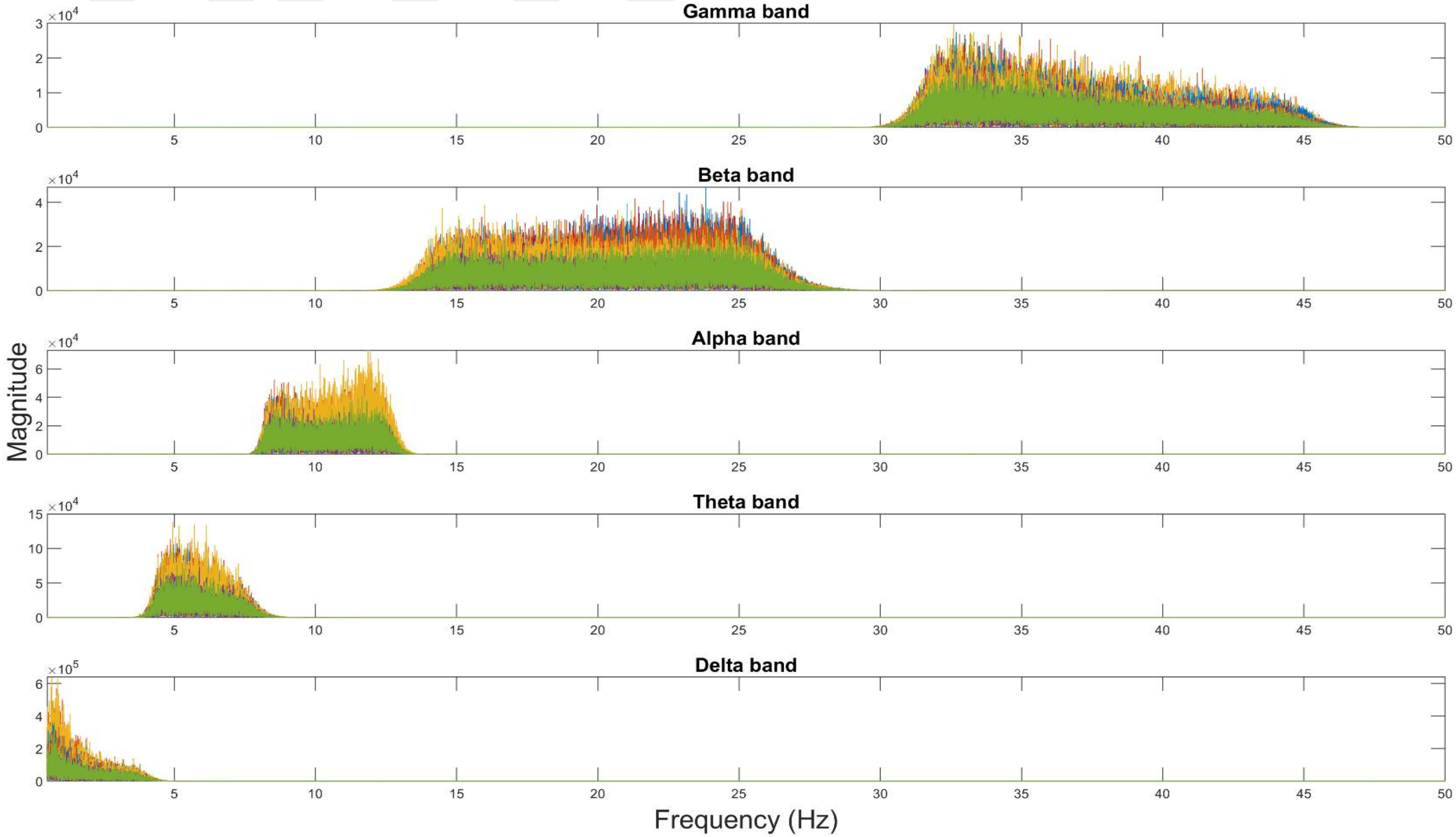

Figure 3.8 . FFT representation of each decomposed EEG band (Delta, Theta, Alpha, Beta, and Gamma) in the frequency domain after zero-phase filtering. Each color in each sub-band represents an EEG channel. The sixth-order Chebyshev Type-II band-pass filters, with a stopband attenuation of 50 dB, effectively separate the EEG signal into distinct frequency ranges, ensuring minimal signal distortion and clear isolation of each band

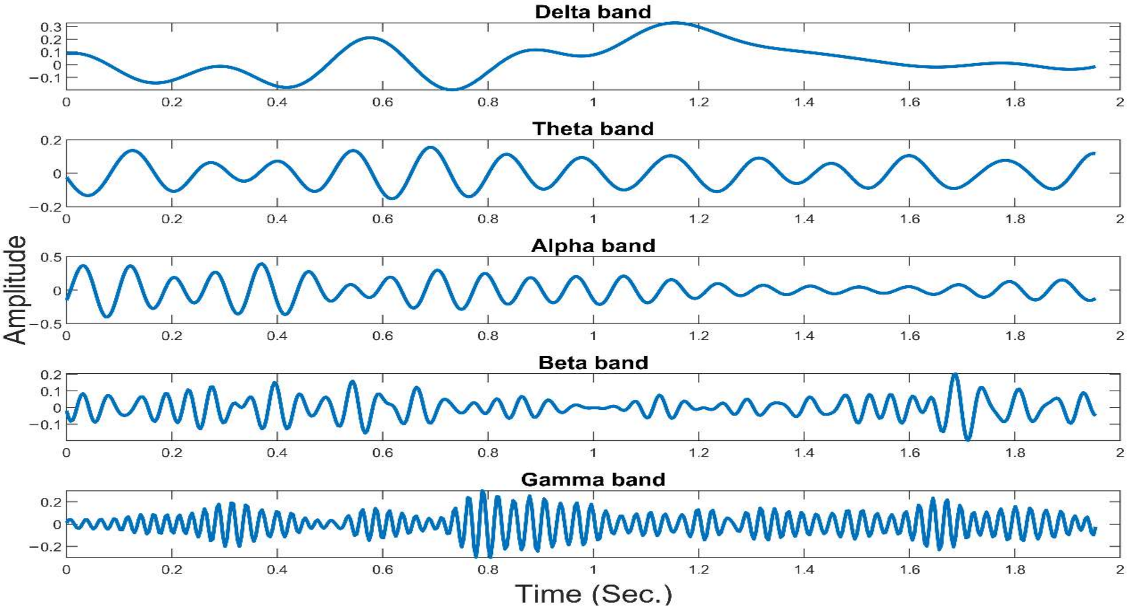

Figure 3.9. The presentation of each decomposed EEG band (Delta, Theta, Alpha, Beta, and Gamma) in the time domain after zero-phase filtering. The sixth-order Chebyshev Type-II band-pass filters, with a stopband attenuation of 50 dB, effectively separate the EEG signal into distinct frequency ranges, ensuring minimal signal distortion and clear isolation of each band.

3.4.6. Cleaning EEG data (Artifacts rejection)

Cleaning EEG data EEG data cleaning is a process of preparing and refining EEG data to enhance its quality and reliability for analysis. It typically involves several steps to eliminate unwanted artifacts, noise, or interference that may be present in the raw EEG recordings. Here's a brief description of some common techniques that we used in my study involved in EEG data cleaning:

Artifact Removal: Identifying and removing artifacts, which are unwanted signals in the EEG data, is crucial. Artifacts can arise from various sources, such as eye blinks, muscle activity, or external interference (Jas et al., 2017).

Artifact Subspace Reconstruction (ASR)

Artifact Subspace Reconstruction (ASR) is an algorithmic approach to remove high-frequency and high-amplitude noise from the EEG signals, including muscle activity and external interference, while preserving the neural signals of the brain. It works by detecting the artifact-contaminated segments and then estimating the underlying artifact-free segments based on a statistical model fitted from clean calibration data, preserving non-artifactual brain signals (Blum et al., 2019). It is performed using EEGLAB v2023.1 with MATLAB® 2022b. Figure 3.10 shows the ASR algorithm and the removal of bad regions and channels that have been discussed in this chapter.

Core Principles, ASR operates in a subspace, isolating portions of the signal that deviate significantly from expected clean signal behavior. It compares short time windows of incoming EEG data to clean calibration data and identifies segments that exceed a predefined threshold.

- **Threshold Calculation:**

The primary equation used in ASR for thresholding is:

$$\Gamma_i = \mu_i + k \cdot \sigma_i \tag{3.1}$$

Where, Γ_i is the artifact detection threshold for the i^{th} segment, μ_i is the mean value of the clean calibration data, σ_i is the standard deviation of the calibration data, and k is a multiplicative factor (usually between 20 and 30) that determines the threshold's sensitivity. This threshold determines whether a data segment contains artifacts. If the deviation in a windowed segment exceeds Γ_i, the segment is flagged for artifact correction.

Lower k values result in more aggressive removal, potentially eliminating some brain signals and Higher k values focus on extreme artifacts, ensuring minimal signal loss (Plechawska-Wójcik et al., 2019; Plechawska-Wójcik et al., 2023).

- **Covariance Matrix Calculation:**

ASR leverages the covariance matrix of the clean EEG data to model the expected signal distribution:

$$C = \frac{1}{N} \sum_{i=1}^{N} (X_i - \mathbb{X})^T \tag{3.2}$$

Where, X_i is the i^{th} EEG sample (vector form), $\mathbb{X}$ is the mean vector of the clean EEG samples, N is the total number of samples, and C is the covariance matrix representing variance and covariance of the clean data.

The covariance matrix projects the incoming EEG data into the artifact subspace, enabling the detection and correction of deviations.

- **Artifact Subspace Detection and Reconstruction:**

After projection into the artifact subspace, ASR identifies components exceeding the threshold Γ_i. If a segment contains artifacts, it is reconstructed using a low-rank approximation to suppress the artifact-dominated subspace.

Let X be the original data matrix, and U and V be matrices derived from the singular value decomposition (SVD) of X:

$$X = U\Sigma V^T \tag{3.3}$$

The clean data Ĥ is reconstructed by retaining only components below Γ_i:

$$\hat{H} = U\Sigma_{filtered}V^T \tag{3.4}$$

Where $\Sigma_{filtered}$ contains singular values below the threshold. This process eliminates high-amplitude artifacts while preserving essential brain signals.

- **Sliding Window Approach in ASR:**

ASR processes EEG signals in sliding windows. For each window, it calculates the mean and variance of the calibration data, compares it to incoming data, and reconstructs the signal if needed. For completeness, consider adding a mathematical representation of how the sliding window operates, such as: $X_{windowed} = [x_t, x_{t+1}, \ldots, x_{t+w}]$, where w is the window size, and t indicates the start of the window. This helps formalize the windowing process. The w and overlap percentage are adjustable, typically chosen to balance sensitivity and computational efficiency.

Applications and Effectiveness

ASR is particularly effective in removing high-amplitude, short-duration artifacts, such as eye blinks and muscle movements, without compromising core brain signals (Figure 3.10). It is often combined with Independent Component Analysis (ICA) for more comprehensive artifact correction in complex datasets. The choice of k, the threshold multiplier, impacts the aggressiveness of artifact removal:

Applications of ASR include Online EEG monitoring: Corrects artifacts in real-time, Neurofeedback and BCI systems: Ensures clean signals for accurate applications, and Clinical EEG analysis: Reduces noise from involuntary movements in clinical recordings.

Bad Channel Detection and Elimination

In addition to artifact removal, ASR can identify and eliminate bad channels or regions in EEG recordings. This feature is essential in preprocessing, as faulty channels or noise-contaminated areas degrade signal quality and impair analysis.

Bad channels are identified by comparing each channel's statistical properties (e.g., variance and mean) with the calibration data. Channels with consistently high deviations beyond the threshold are flagged as bad (Figure 3.11). These channels can either be excluded from further analysis or reconstructed using data from neighbouring channels to minimize information loss. This process ensures that compromised channels do not distort the results (Plechawska-Wójcik et al., 2023).

Limitations in bad channel detection method despite its strengths, ASR did not perform well in our proposed Method 2, primarily because all channels were need to used for plotting the TBM with PSD distribution across sensor positions. This limitation highlights the need for alternative approaches when analyzing data with this methodology.

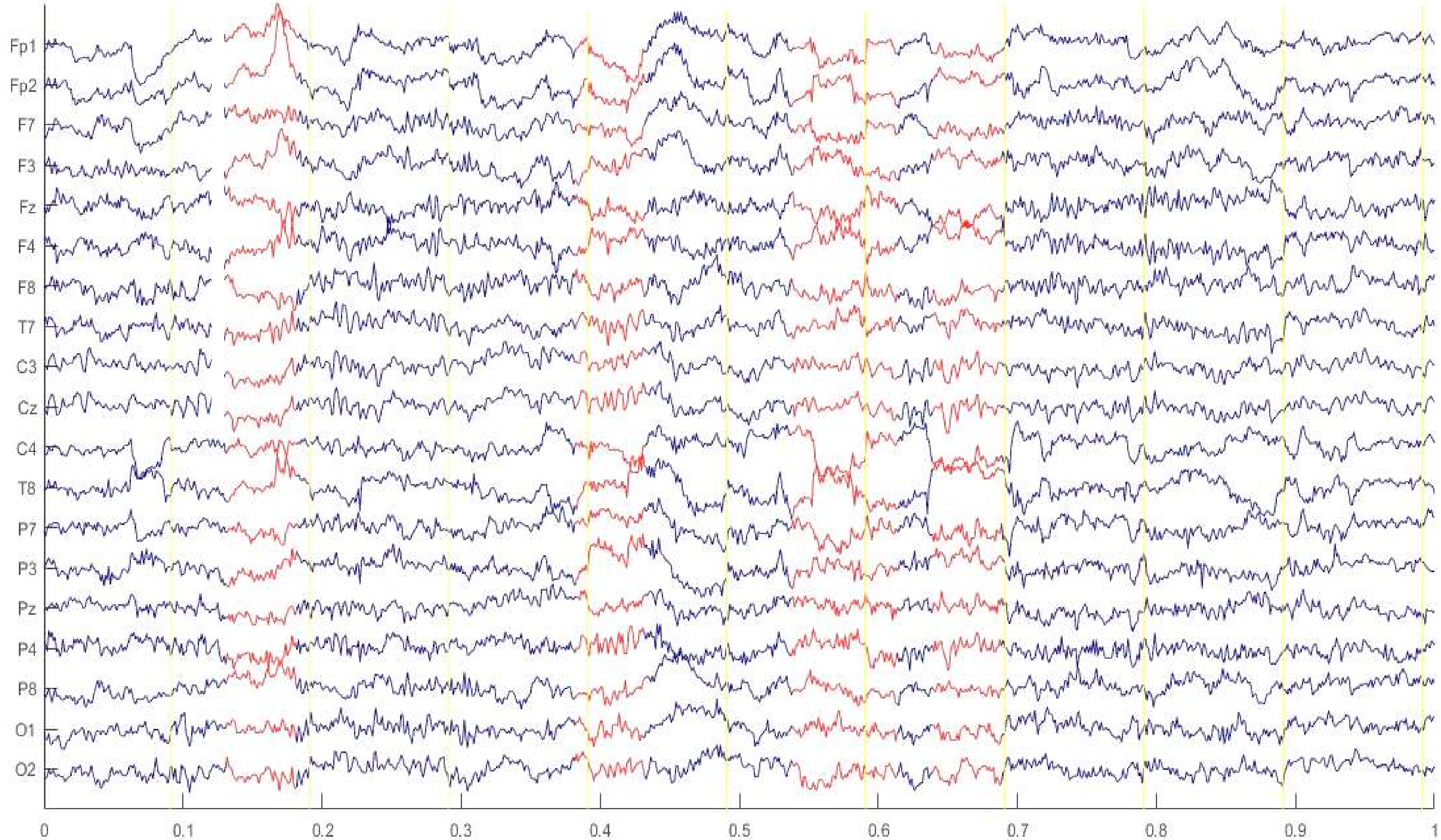

Figure 3. 10. The ASR results: red segments show excluded artifacts, while blue segments represent the reconstructed, artifact-free signasl for clean EEG analysis.

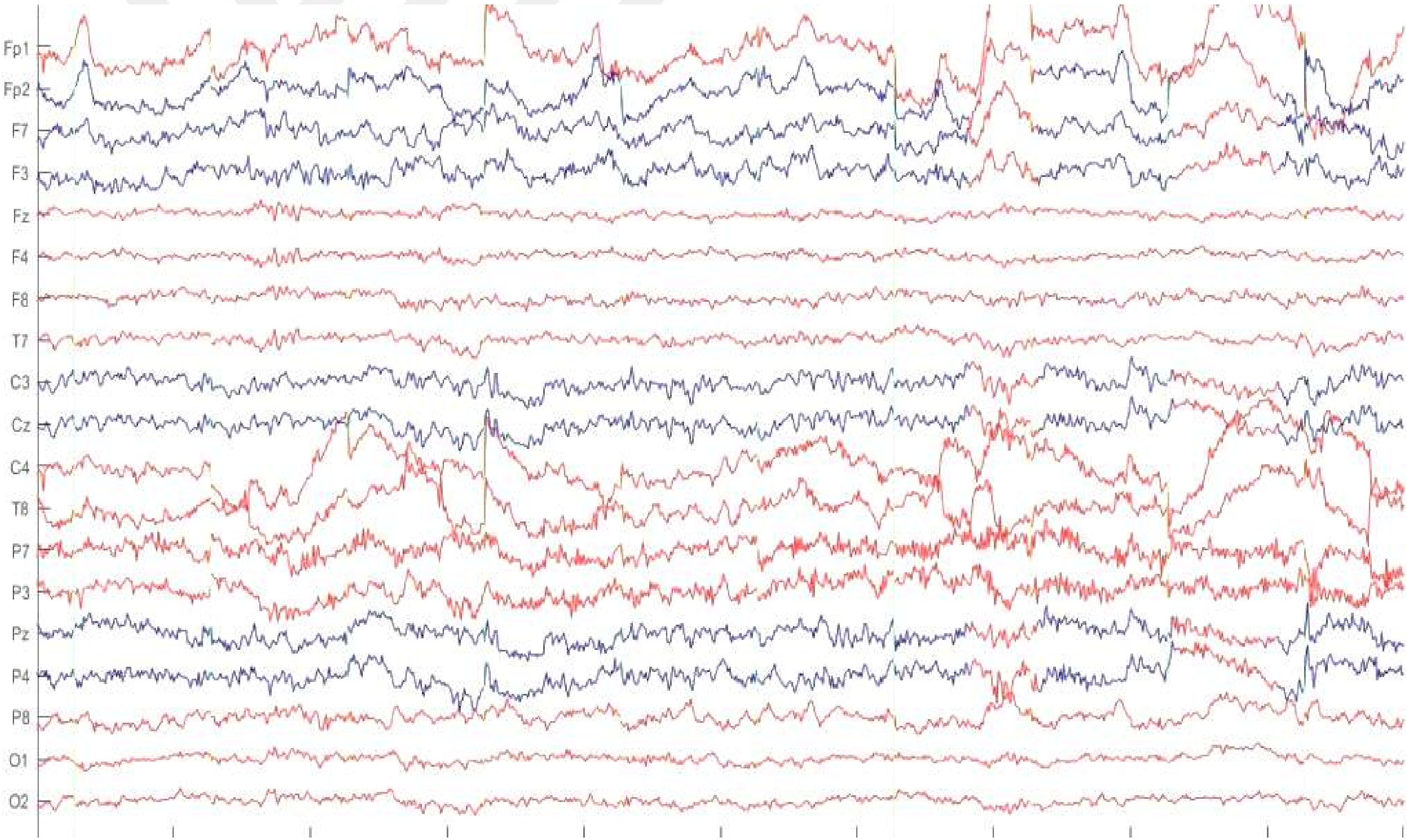

Figure 3.11. The output of one example of rejection bad channel by ASR. The channels marked in red were rejected (bad channels), and the channels marked in blue, which contain some red segments, had these red areas excluded from the signal as they represent artifacts.

Independent Component Analysis (ICA)

ICA is a computational technique used to separate multivariate signals into additive, statistically independent components (Castellanos et al., 2006) . When applied to EEG data, ICA separates the EEG signal into statistically independent components, allowing for the identification and removal of specific components related to artifacts such as eye blinks, muscle activity, cardiac signals, and environmental noise, thus providing a cleaner EEG signal. The ICA-runica technique was employed in this study, successfully correcting EEG signals, as illustrated in Figure 3.12. However, ICA did not contribute significantly to my overall methods, as ASR proved to be more effective for artifact correction in this approach.

The principle worke of ICA treats observed EEG signals as linear mixtures of independent source signals and decomposes them into statistically independent components (Bell et al., 1995). This decomposition helps in separating out non-neural artifacts from brain signals, which is crucial in producing a cleaner dataset for further analysis.

For EEG, ICA methods such as runica and ASR—implementation available in EEGLABv 2023.1 (Arnaud Delorme et al., 2004)—are commonly used. The algorithm works by iteratively estimating the unmixing matrix to maximize the statistical independence of the separated components. Artifacts like eye movements and muscle contractions are typically spatially distinct, and ICA excels at isolating such artifacts, enabling the removal of unwanted signals while retaining valuable brain data.

Advantages of ICA in EEG Analysis

- **Artifact Correction**: ICA has been widely used for its ability to effectively identify and remove artifacts, thereby enhancing signal quality for brain analysis. Eye blinks and muscle movements are effectively isolated (Iragui, 2014).
- **Functional Network Analysis**: ICA also helps reveal brain functional networks by identifying independent sources that may correspond to distinct neural populations or activities (Makeig et al., 1995).
- **Data Representation**: By transforming the EEG into independent components, ICA can reveal unique sources of activity, providing insights into different brain functions.

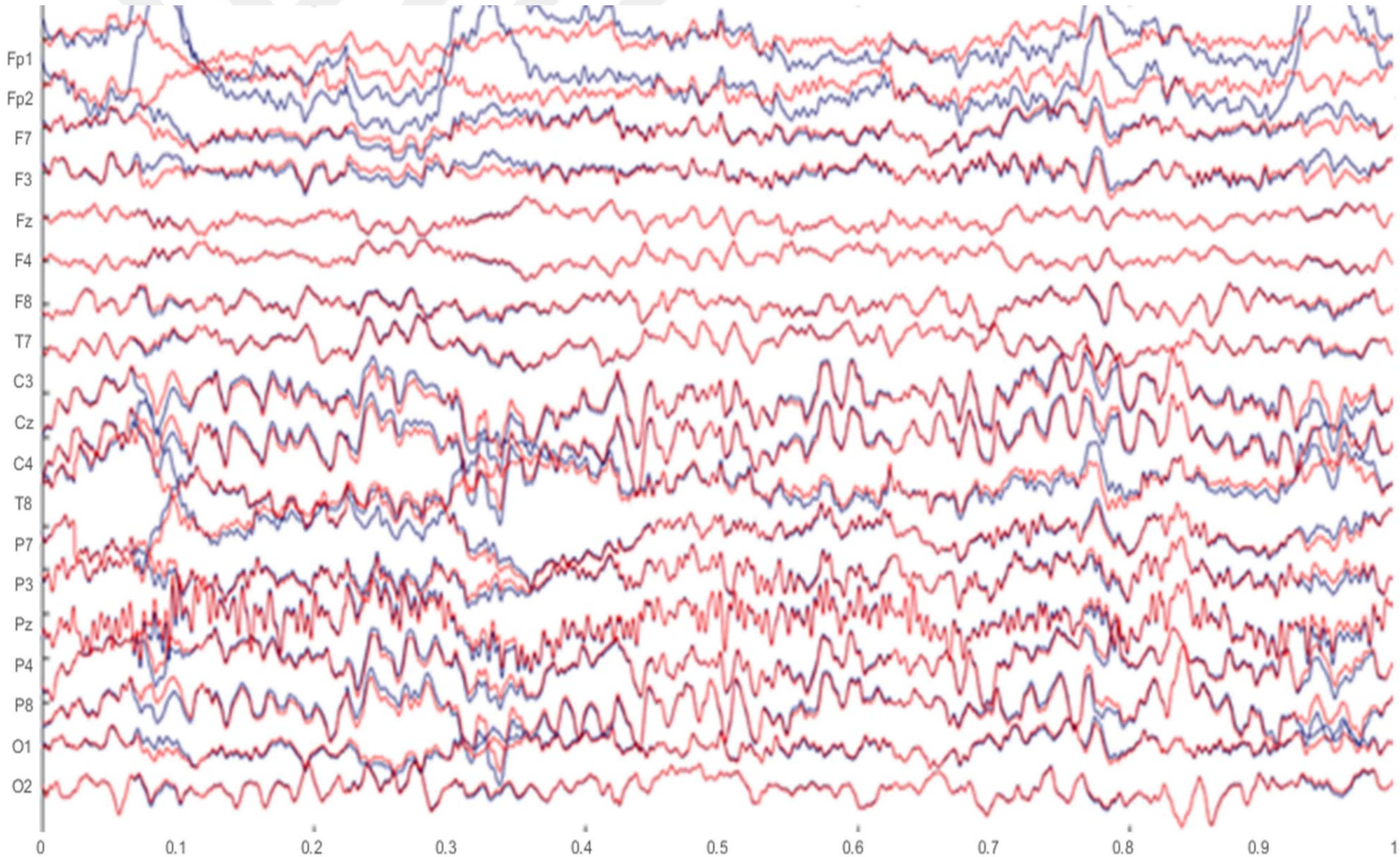

Figure 3.12. An example of EEG prosseced by ICA; Red color represented after correction, and Blue color before corrections.

In contrast, ASR emerged as a superior method in this study. ASR, developed by (Mullen et al., 2015), offers several advantages over ICA.

First, ASR provides automatic detection and correction of artifacts. It automatically reconstructs artifact-contaminated subspaces by identifying deviations from a reference signal, significantly reducing the need for subjective manual identification of artifacts. This approach allows ASR to effectively clean data segments without removing valid neural information, preserving the integrity of the EEG signals for further analysis (Chang et al., 2020).

Second, ASR demonstrates efficient and consistent performance. Compared to ICA, ASR is faster and more efficient, making it an ideal choice for practical applications. It can detect and reconstruct high-amplitude artifacts in real time, which is especially valuable for scenarios requiring immediate data processing.

These benefits highlight ASR as a robust and reliable method for preprocessing EEG signals, ensuring high-quality data for subsequent analysis while minimizing the potential loss of critical neural information.

Improved Signal Quality, by automatically rejecting artifact components and reconstructions the remining EEG signals, ASR improved the accuracy of subsequent feature extraction and classification in this study.

ICA is a valuable tool for EEG signal preprocessing, widely recognized for its ability to decompose EEG into independent components. However, in this study, it did not significantly contribute to improving the performance of the proposed method. Instead, ASR showed superior performance by automating artifact removal and reconstruction the remining signals and maintaining consistent quality without requiring extensive manual intervention.

Finally, the preprocessing stage prposed for both methods is displayed in Figure 3.13.

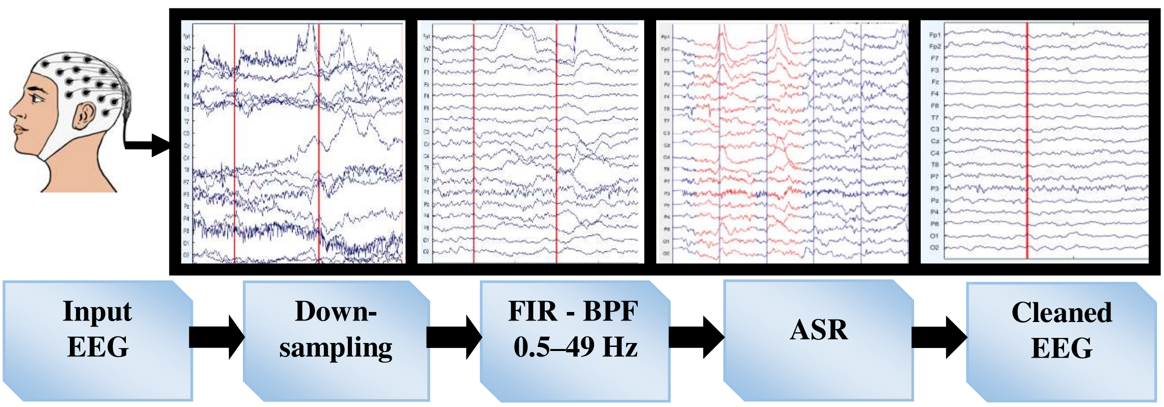

Figure 3.13. The bloke diagram of raw EEG data cleaning

3.5. Feature Extractıons (FE)

After the preprocessing stage, which involves removing unwanted frequencies and artifact removal, the next crucial step is feature extraction from EEG signals. Feature extraction is an essential part of EEG signal processing that aims to identify relevant characteristics from raw EEG data for further analysis, such as classification. Given the high dimensionality and complexity of EEG signals, extracting features helps to highlight significant information while reducing redundancy and noise (Subasi A, 2007).

There are various methods for extracting features, including Time Domain features and Frequency Domain features, which utilize specific mathematical approaches to capture meaningful information from the signals. These methods aim to enhance the accuracy of subsequent classification tasks by emphasizing significant features in the data while filtering out irrelevant information. Each type of FE used in each method will be explained in detail in the following sections.

3.6. Method (1)

The preprocessing stage included decimation see Figure 3.13., band-pass filtering to remove unwanted frequencies, artifact subspace reconstruction to eliminate artifacts, and AN to preserve the relative relationships between the signal features, which were crucial for the subsequent analysis and classification. Five band-pass filters were applied to decomposing the EEG signals. For each decomposed band, the signals from each brain hemisphere were analysed separately by calculating the peak sensor's envelope and obtaining the mean envelope for each hemisphere, resulting in two mean signals (right and left) as displayed in Figure 3.2. Features were extracted using a sliding window approach applied to the mean signals of each hemisphere, with varying overlap ratios (12.5% to 87.5%, in 12.5% steps). The maximum, mean, and minimum energy values were used individually as features. Three types of SVM kernels— linear (L), the radial basis function (RBF), and quadratic—were employed for classification as explained briefly in the next:

The 1st algorithm under consideration consists of three main components: (1) cleaning the raw EEG data, (2) extracting features, and (3) performing classification.

3.6.1. Preprocessing Raw Data

The preprocessing stage involved the following steps:

3.6.2. Down-Sampling

The raw EEG data were downsampled from 500 Hz to 256 Hz to accelerate the processing and reduce the computational complexity.

3.6.3. Unwanted Frequency Removal

Frequencies < 0.5 Hz and > 49 Hz were removed using a zero-phase finite impulse response band-pass filter (FIR-BPF). This step was designed to eliminate baseline 50 Hz noise and low-frequency components. The filter employed a Hamming window design with a heuristic order, and the transition bandwidth was automatically estimated using EEGLABv2023.1 (A Delorme et al., 2004).

3.6.4. Artifact Rejection and Reconstruction

Filtered signal artifacts were addressed using the artifact subspace reconstruction (ASR) method. This process involved three steps: (1) extracting reference data from the raw EEG signals, (2) determining thresholds to identify artifact components, and (3) rejecting the artifact components while reconstructing the remaining signals (Chang et al., 2020). The ASR method enables the rejection of artifacts while reconstructing the signals based on physiological activity, thereby enhancing the quality and reliability of the subsequent analyses. The rejected portions of the signal are marked in red in Figure 3.10, which highlights the artifact segments excluded from the cleaned signals (blue segments).

3.6.5. Amplitude Normalization (AN)

AN of EEG signals to a standardized range, were chosen between 1 to -1, aims to ensure consistency, comparability, efficient utilization of the dynamic range, enhancement of the signal-to-noise ratio, and facilitation of subsequent data processing and analysis. Figure 3.3 (D). Shows an example of an output signal after AN the difference is clear when compared with Figure 3.3 (C).

The ASR implementation in EEGLAB was configured with the following parameters, selected experimentally: BurstCriterion of 20, WindowCriterion of 0.25, Euclidean distance for artifact reconstruction, and with FlatlineCriterion, ChannelCriterion, LineNoiseCriterion, and Highpass set to off. These parameters were chosen to balance between preserving valid EEG data and mitigating artifacts. The artifact reconstruction process used the Euclidean distance metric with a conservative threshold to retain physiological activity. This plays a critical role in enhancing the reliability, interpretability, and efficiency of EEG signal analysis, particularly in neuroscience, clinical applications, and BCI systems (Chang et al., 2020; Halaki et al., 2012).

In this study, the clean EEG data, denoted as ($x_{clean}[n]$), were processed to find the minimum (min) and maximum (max) values of $x_{clean}[n]$. AN was then applied to scaling the signals to the desired range [A to B], which in this case was selected as [-1 to 1]. The normalized signal $x_{nor}[n]$ was calculated using Equation (3.5):

$$x_{nor}[n] = \left((B - A) \times \left(\frac{x_{clean}[n] - \min(x_{clean})}{\max(x_{clean}) - \min(x_{clean})}\right)\right) + A \tag{3.5}$$

This ensures that the normalized signal ($x_{nor}[n]$) ranges between [-1 to 1], effectively centering the signal around zero and removing the DC component. Therefore, this normalization process maintains the relative relationships between signal features, which are crucial for further analysis and classification.

3.6.6. Divided Brain Hemispheres

EEG Bands Decomposition: The normalized EEG signal $x_{nor}[n]$ was decomposed into different frequency bands using five zero-phase, Chebyshev Type-II band-pass filters (BPFs). Each BPF was designed to extract one of the following EEG frequency bands: Delta (δ, 0.5–4 Hz), Theta (θ, 4–8 Hz), Alpha (α, 8–13 Hz), Beta (β, 13–28 Hz), and Gamma (γ, 31–49 Hz).

The sixth-order filter, determined heuristically, provided an optimal balance between signal attenuation and computational efficiency. For all filters, the stopband attenuation was set to 50 dB to ensure minimal signal distortion. The normalized EEG signal ($x_{nor}[n]$) was in to sub EEG bands $x_{BPF}^{\delta}[n]$, $x_{BPF}^{\theta}[n]$, $x_{BPF}^{\alpha}[n]$, $x_{BPF}^{\beta}[n]$, and $x_{BPF}^{\gamma}[n]$. Figures 3.10 and 3.11 illustrate the separation of the five EEG bands in the frequency domain and time domain, respectively, with each decomposed band shown according to its corresponding frequencies.

Figure 3.9 illustrates a two-second window of each decomposed EEG band, clearly showing that the δ band represents the lowest frequency range, while the γ band corresponds to the highest frequency range. Additionally, Figure 3.8 presents the Fast Fourier Transform (FFT) of each decomposed band, demonstrating that the filters effectively separate the bands within their respective frequency ranges.

Divided brain hemispheres: The EEG sensors on the left and right brain hemispheres were divided into left (red) electrodes (Fp1, F3, C3, P3, O1, F7, T3, T5, Fz, Pz) and right (blue) electrodes (Fp2, F4, C4, P4, O2, F8, T4, T6, Cz), as shown in Figure 3.2, following the 10–20 electrode placement system. For a given signal $x_{BPF}^{\text{band}}[n]$, the signals were further separated into hemisphere-specific signal $x_{band,hemisphere}[n]$.

3.6.7. Feature Extraction (FE)

This study used peak envelope analysis (Yang, 2017), mean of envelopes for each brain hemisphere, and sliding window for energy calculation as a feature extraction method. The following steps were performed for feature extraction:

Peak Envelope for Each channel

Peak envelope analysis aims to detect and emphasize the signal peaks or maximum amplitudes. For a given signal $x_{band,hemisphere}[n]$, the peak envelope $e_{band,hemisphere}[n]$ can be computed using the Hilbert Transform (HT). The peak envelope is expressed mathematically by Equation (3.6):

$$e_{band,hemisphere}[n] = \sqrt{x_{band,hemisphere}[n]^2 + \hat{h}_{band,hemisphere}[n]^2} \tag{3.6}$$

Where the HT $\hat{h}_{band,hemisphere}[n]$ of a real valued signal $x_{band,hemisphere}[n]$. The HT is defined as the convolution operation ($\otimes$) of the signal $x_{band,hemisphere}[n]$ with the filter impulse response $h[n]$. This is mathematically represented by Equation (3.7):

$$\begin{aligned} \hat{h}_{band,hemisphere}[n] &= x_{band,hemisphere}[n] \otimes h\,[n] \\ &= \sum_{k=-\infty}^{\infty} h\,[n-k] \times x_{band,hemisphere}\,[k] \end{aligned} \tag{3.7}$$

Where $h[n-k]$ is the HT filter impulse response, a 10-tap HT filter was used, which specifies the number of samples around each local maximum considered for interpolation.

Mean Envelope for Each Hemisphere

The mean envelope $\hat{e}_{band,hemisphere}[n]$ for each decomposed band and brain hemisphere was calculated by averaging the envelopes across all EEG channels in that hemisphere. This can be expressed mathematically by Equation (3.8):

$$\hat{e}_{band,hemisphere}[n] = \frac{1}{m}\sum_{i=1}^{m} e_{(i),band,hemisphere}\,[n] \tag{3.8}$$

Where m is the total number of channels in each hemisphere, $e_{(i),band,hemisphere}[n]$ is the envelope signal from the i^{th} sensor at time n, and $\hat{e}_{band,hemisphere}[n]$ is the average signal at time domain as displayed in Figure 3.14 provides an example of an ASD case, where the mean envelope in the θ band for the right hemisphere was calculated from ten individual sensor envelopes.

The mean of the envelopes for each decomposed band and brain hemisphere was subsequently computed, resulting in a single envelope signal per hemisphere. Figure 3.15 illustrates the difference between the mean envelopes of the left and right hemispheres, highlighting the variation in signal characteristics across the two sides of the brain.

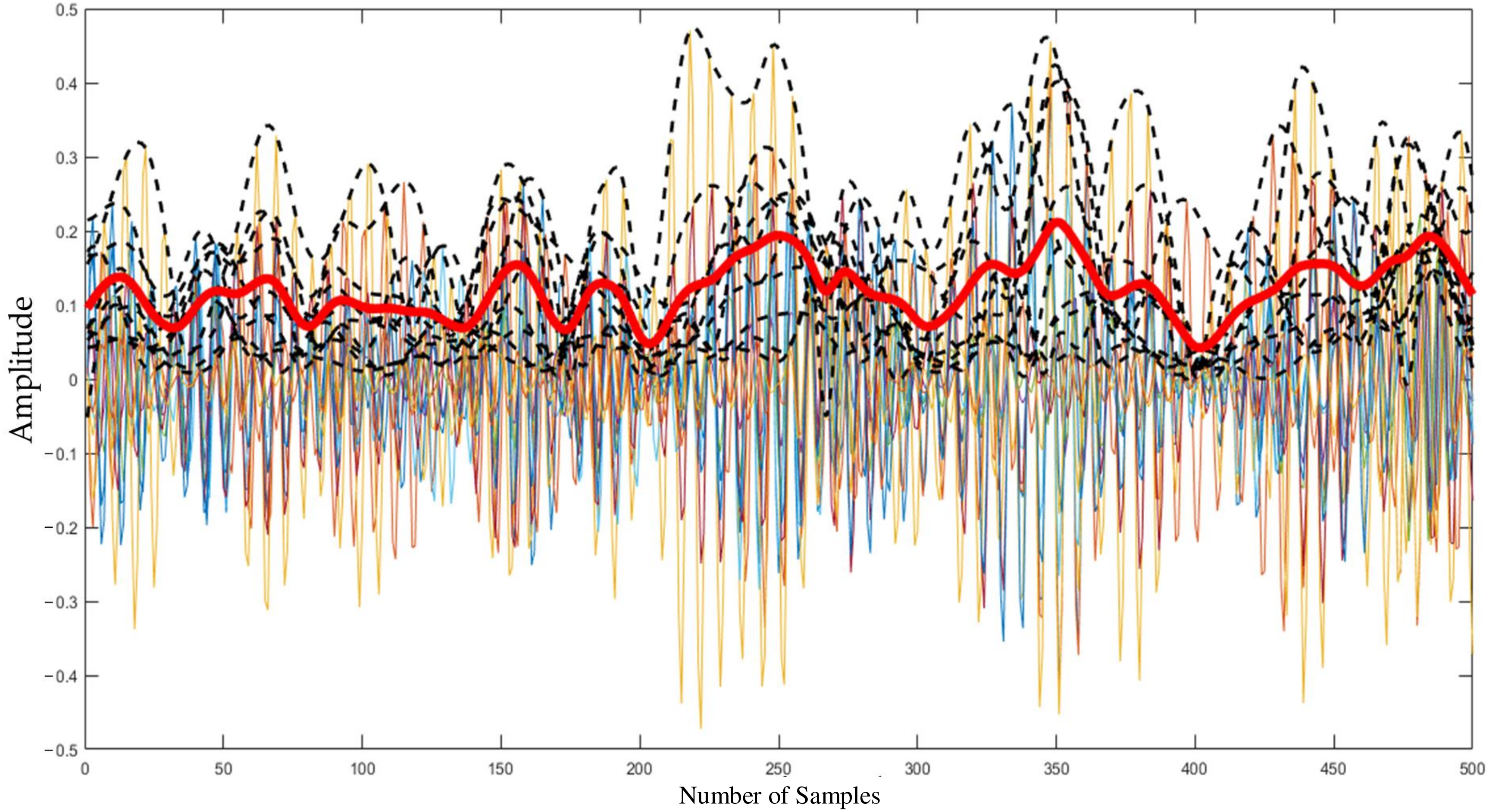

Figure 3.14. Example of a peak envelope: The Black dotted lines represent the envelopes of each of the 10 individual sensors, while the red line indicates the mean of 10 envelopes from the left hemisphere.

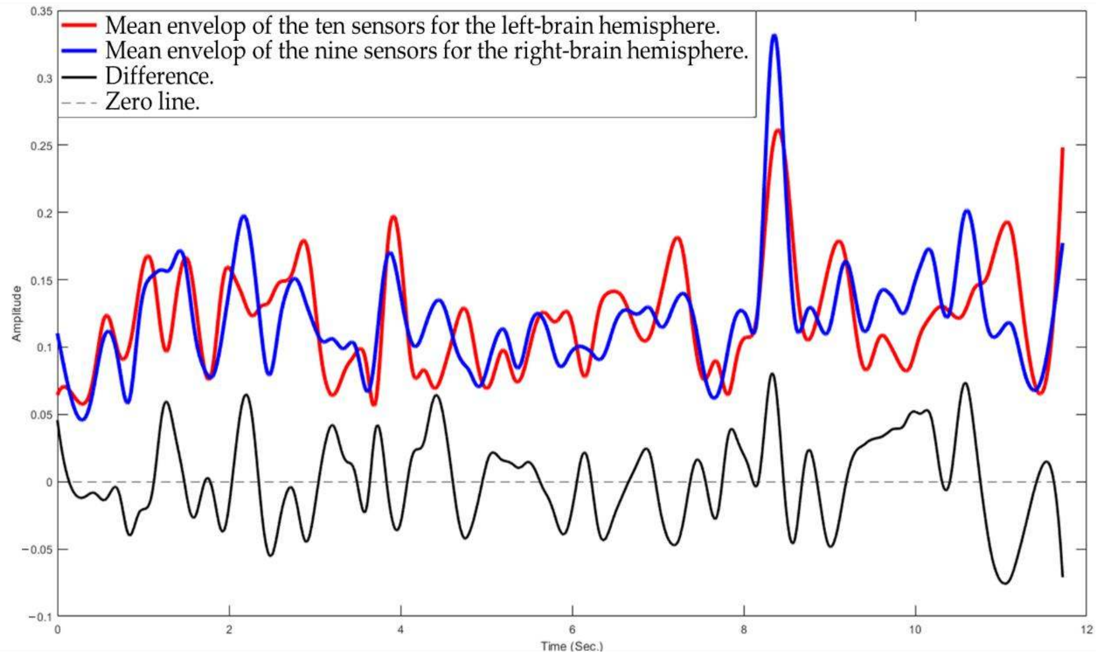

Figure 3.15. Difference between the mean envelops of the left and right brain hemispheres.

Energy Computation

The computed energies were derived using a sliding window approach applied to the mean envelope in each brain hemisphere for each sub-band separately. The envelope signals $\hat{e}_{band,hemisphere}[n]$ were divided into overlapping windows. Let w represent the window index, N the window length (set to 2000 samples, approximately equivalent to 7.8 seconds, selected experimentally). Research suggests that 8 seconds provides valuable information for certain types of EEG analyses (Urbach et al., 2006).

Different overlap ratios were tested, ranging from stride of 1750 samples to stride of 250 samples by step 250 samples, to determine the ratio that yields the best performance. The windowed signal envelope $\hat{e}_w^{band,hemisphere}[n]$ is defined by Equation (3.9):

$$\hat{e}_w^{band,hemisphere}[n] = \hat{e}_{band,hemisphere}\,[n + w.(N - \tau)] \tag{3.9}$$

Where τ represents the number of overlapping samples. The energy $En_w^{band,hemisphere}$ of the envelope within each window is computed as the sum of the squared envelope values over the window, as shown in Equation (3.10):

$$En_w^{band,hemisphere} = \sum_{n=0}^{N-1} |\hat{e}_w^{band,hemisphere}[n]|^2 \tag{3.10}$$

Overlapping windows help maintain the continuity of the EEG signal and ensure that important features between successive windows are not missed see Figure 3.16. This overlap improves feature capture and enhances the model's performance. A slight overlap enables the model to detect patterns that might otherwise be missed with non-overlapping strides as see in Figure 3.19. Research has demonstrated that overlapping sliding windows positively impact classification accuracies (Banos et al., 2014; Dehghani et al., 2019; Janidarmian et al., 2017). Without overlap, each window is independent, potentially missing transitional features (Lara et al., 2013), see Figure 3.19 illustrates a non-overlapping sliding window example with a length of 2 seconds and a stride of 2 seconds.

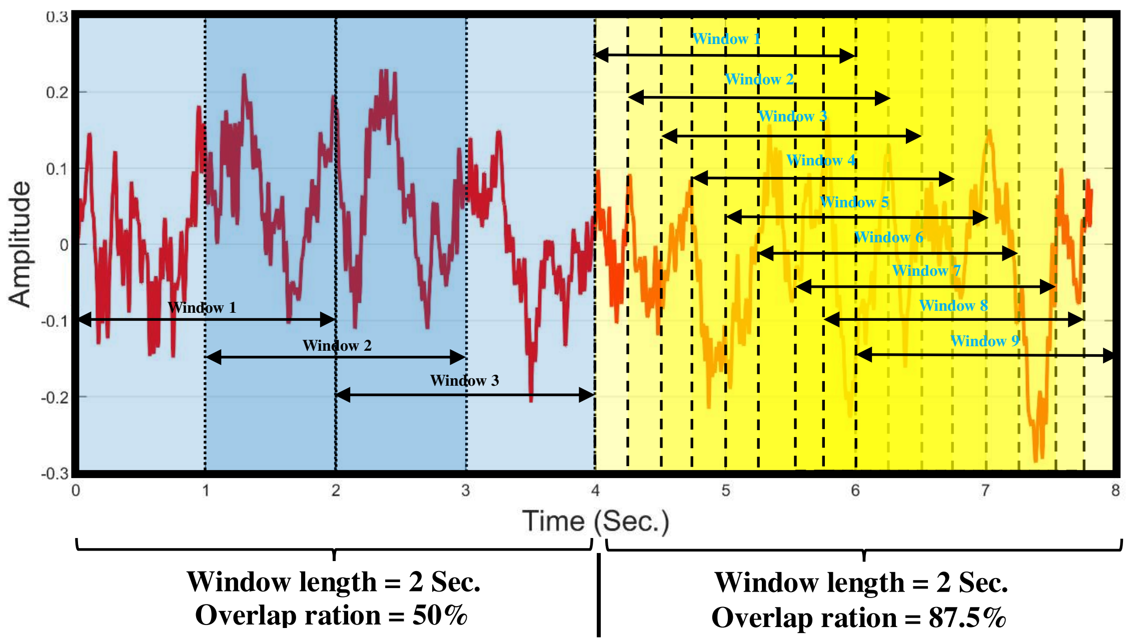

Figure 3.16. Two examples of Sliding window techniques; Blue windows show 50% overlap and yellow windows 87.5% overlap ratio.

Energy Features

For each hemisphere and EEG band, the maximum, mean, and minimum energies across all windows are selected as features. These values are calculated as follows:

$$
\begin{aligned}
&En_{w,max}^{band,hemisphere} = max\left(En_{w}^{band,hemisphere}\right) \text{, For max.}\\
&En_{w,mean}^{band,hemisphere} = \frac{1}{L}\sum_{n=1}^{L} En_{w_n}^{band,hemisphere} \text{, For mean}\\
&En_{w,min}^{band,hemisphere} = min\left(En_{w}^{band,hemisphere}\right) \text{, } For\ min.
\end{aligned}
\tag{3.11}
$$

Where L is the total number of energy windows, and $En_{w_n}^{band,hemisphere}$ refers to the energy value from the n^{th} window. For each decomposed frequency band, two features are extracted—one for each hemisphere. For example, the maximum window features for a given frequency band are expressed as:

$$[En_{w,max}^{band,left}, En_{w,max}^{band,right}]$$

This approach yields two features per EEG band, effectively capturing the most informative segments of the EEG signals. A classifier with these two-dimensional features can leverage this information to improve the classification accuracy between ASD and TD groups.

3.6.8. Classification

For the classification of extracted features from EEG signals into ASD or TD categories, this study utilized Support Vector Machine (SVM) supervised ML for both linear and non-linear problems. SVMs are widely used in classification tasks as they define a linear decision boundary in a high-dimensional space where input vectors are transformed non-linearly. Based on the nature of the optimal hyperplane (Huang et al., 2018; Platt et al., 1999; Scholkopf et al., 1997), SVMs can be categorized into three types: linearly separable, linearly non-separable, and non-separable. For non-linear mappings, a kernel function is used to implicitly map the inputs into a higher-dimensional space.

Linear kernel (L)

The SVM linear classifier seeks to find the optimal hyperplane that separates data into distinct classes see Figure 3.17. The parameters used in MATLAB were: Kernel Function = 'linear' and Standardize = true. The decision boundary is determined by Equation (3.12):

$$0 = w \cdot x + b \tag{3.12}$$

Where w is the weight vector perpendicular to the hyperplane, x is the input feature vector, and b is the bias term. The classifier minimizes the following objective function, as shown in Equation (3.13):

$$0.5\ |w|^2 + \lambda\left(\sum_{i=1}^{n} max(0,1 - y_i(w\ \cdot x_i\ ) + b)\right) \tag{3.13}$$

Here, λ controls the trade-off between maximizing the margin and minimizing classification errors, and y represents the label of the data.

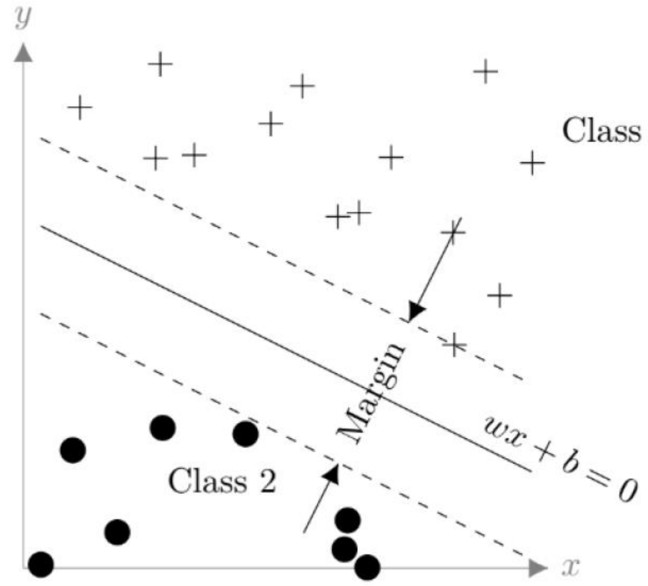

Figure 3.17. Illustrates the operation of a linear SVM with 2-D features (Saffar, 2020).

Gaussian Radial Basis Function (RBF) kernel

Kernel is commonly used for non-linear mappings. The kernel function, $k(x_i, y_j)$, is expressed as follows in Equation (3.14):

$$k(x_i, y_j) = \phi(x_i) \cdot \phi(y_j) \tag{3.14}$$

Where k is the kernel function, and the weight vector to the hyperplane is defined by Equation (3.15):

$$w = \sum_i y_i \ \alpha_i \ \phi(x_i) \tag{3.15}$$

The SVM classifier minimizes the following objective function, shown in Equation (3.16):

$$\lambda |w|^2 + \left(\frac{1}{m} \sum_{i=1}^{m} max(0{,}1 - (w^T \cdot x_i) - b) \right) \tag{3.16}$$

Where $\lambda > 0$ represents the trade-off between the size of the margin and its flexibility in classification. The MATLAB parameters were: Kernel Function = 'rbf', and Standardize = true.

2.1.1.1. Quadratic or Polynomial kernel (Quadratic)

A quadratic or polynomial kernel of degree (d = 2) is used in SVM to map the original features into a higher-dimensional space. This enables SVM to classify data that is not linearly separable in the original space (Cristianini et al., 2000). The kernel function is defined in Equation (3.17):

$$k(x_i, y_j) = (x_i \cdot y_j)^2 + 2c(x_i \cdot y_j)^2 + c^2 \tag{3.17}$$

Where, c is a constant used to adjust the influence of higher-order terms in the polynomial. Typically, $c \geq 0$ and $\wedge^{2}$ indicates that this is a quadratic kernel (degree 2).

The MATLAB-2022b hyperparameters were: Kernel Function = 'polynomial', Polynomial Order = 2, Kernel Scale = 'auto', Box Constraint = 1, and Standardize = true.

This expansion ensures that the kernel incorporates not only the dot product of the original features but also squared terms and cross-products, enabling the SVM to capture more complex patterns in the data.

For all SVM models, the features were standardized to have zero mean and unit variance. Within EEG signal classification, the SVM utilized the maximum, mean, and minimum energy computations from each band and brain hemisphere as features. These features were fed into the SVM, which calculated the optimal decision boundary to distinguish ASD from TD cases. Figure 3.18 illustrates the workflow of the proposed method, including feature extraction, standardization, and classification using SVM with different kernels.

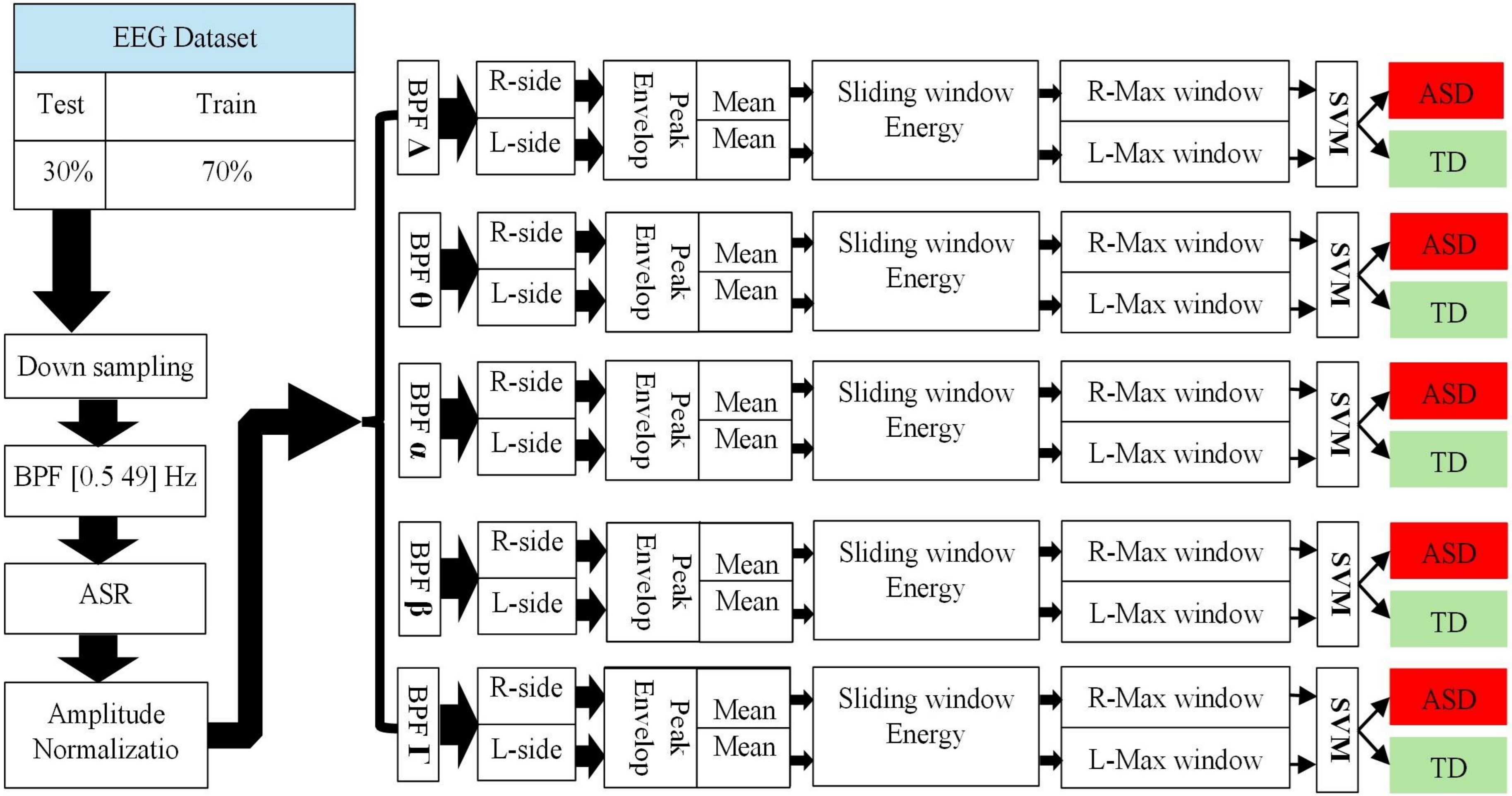

Figure 3.18. Workflow of EEG-based ASD classification (Method 1): preprocessing, band decomposition, feature extraction, and SVM-based classification of hemisphere features into ASD or TD.

Following the success obtained with Method 1, we were able to show a difference between the brains of ASD and TD children. This finding pointed to the possibility of further exploration of the patterns of brain activity.

In order to extend these findings, we planned to develop a system that displays the energy density for each frequency band across all the brain regions. These mappings will be analyzed using even deeper learning techniques given they should prove more accurate and intellectually richer.

The proposed system will present it in next section (Method 2) will include all brain regions because it may be that the distinguishing area is localized to a particular area, for instance the anterior part of the right hemisphere. This consideration concurs with the findings made in Method 1 where attempting to target individual areas in the brain provided significant effectivity and outstanding effectiveness were realized.

3.7. Method (2)

This method introduces an automated method for ASD detection using EEG data from Iraq and Poland. Pre-processing involved noise removal with a finite impulse response band-pass filter and artifact subspace reconstruction same in method 1. Features were extracted from EEG channel power spectral density, and topography brain maps were input to deep feature extractors (e.g., AlexNet, GoogLeNet) combined with ANOVA for feature selection. Classification was conducted using SVM and LDA explıaned breafely in the next sections.

The algorithm under consideration comprises two primary phases: 1) initially, the cleaning of EEG raw data, followed by 2) converting the cleaned EEG signals into images for feeding into the CNN-ML interconnection, as outlined in the subsequent subsections of the workflow.

3.7.1. Pre-processing

Raw EEG data Pre-processing (noise removal, EEG length equalization, artifact removal) is essential to improve EEG data quality. Pre-processing yields clean, equal-length EEG data free of noise and artifacts, which facilitate brain activity analysis and interpretation. First, the processing was accelerated by down-sampling the data to 256 Hz. Subsequently, the data were filtered using a zero-phase Hamming window of FIR-BPF to remove the frequency < 0.5 Hz and > 49 Hz to reject the baseline 50 Hz (DC, notch filter) and other unwanted frequencies. The filtered EEG data segments containing significant muscle and movement artifacts identified by ASR, which is explaind brefely in previous sections, see Figure 3.10 presented how ASR rejected parts colored in red were automatically excluded and the remining blue color were reconstracted. Finally, segment lengths of 8.5 minutes per participant were selected. The Block diagram of cleaning EEG signals is presented in Figure. 3. 13.

3.7.2. Topography Brain Maps (TBM) Images

Spectral analysis was conducted using EEGLABv2023.1 with the pop_spectopo function(Arnaud Delorme et al., 2004). Each trace was examined for the channel or component index to ensure data continuity. Subsequently, the spectra were computed using the parameters of no overlap, a window length of 256 (1 Sec.), and FFT window length (N =256 points). FFT is an efficient algorithm to compute the Discrete Fourier Transform (DFT). The DFT equation (3.18) is given as:

$$F(i) = \sum_{n=0}^{N-1} f(n) \cdot e^{-j\frac{2\pi}{N}in} \tag{3.18}$$

Where, $F(i)$ is the DFT of the sequence $f(n)$, $f(n)$ is the input signal, i = 0, 1, 2, ..., (N−1) represents the frequency index, and $e^{-j\frac{2\pi}{N}in}$ is the complex exponential, with j representing the imaginary unit. Figure 3.19 illustrates an example of a non-overlapping sliding window with a length of 2 seconds.

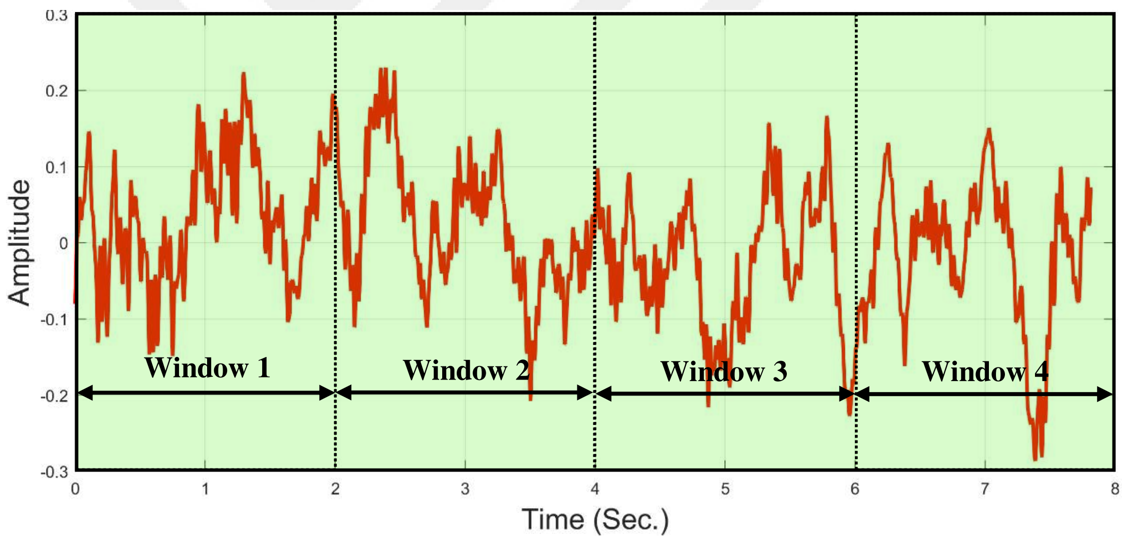

Window length = 2 Sec., Strid = 2 Sec., and Overlap ration = 0%

Figure 3.19. An examples of Sliding window techniques with non-overlap windows.

During this process, the clean EEG signal frequency components were analyzed within the selected time range to understand their spectral characteristics. Using the EEGLAB pop_spectopo function (Arnaud Delorme et al., 2004) involved selecting a single frequency value within each EEG band i.e., the bands are: delta (γ), 0.5–4 Hz; theta (θ), 4–8 Hz; alpha (α), 8–13 Hz; beta (β), 13–30 Hz; gamma (γ), 30–49 Hz, to plot the required TBMs. The TBMs were plotted by determining the optimal frequency within each EEG band as shown in Figure 3.20, by computing the power spectral density (PSD) mean across 19 channels, can be calculated by the fellowing Equation (3.19):

$$PSD_{db} = 10\ Log_{10}\left(\frac{(\mu Volt)^2}{Frequency}\right) \tag{3.19}$$

Subsequently, the optimal frequency was identified as the frequency range per decomposed band with the highest PSD on the mean value curve across these channels. Figure 3.20 illustrates the process for selecting the most effective frequency within each EEG band and provides an example of a TBM image with five decomposed EEG bands, such as Delta, Theta, Alpha, Beta, and Gamma. Figure 3.21 displayed EEG bands examples of TBMs.

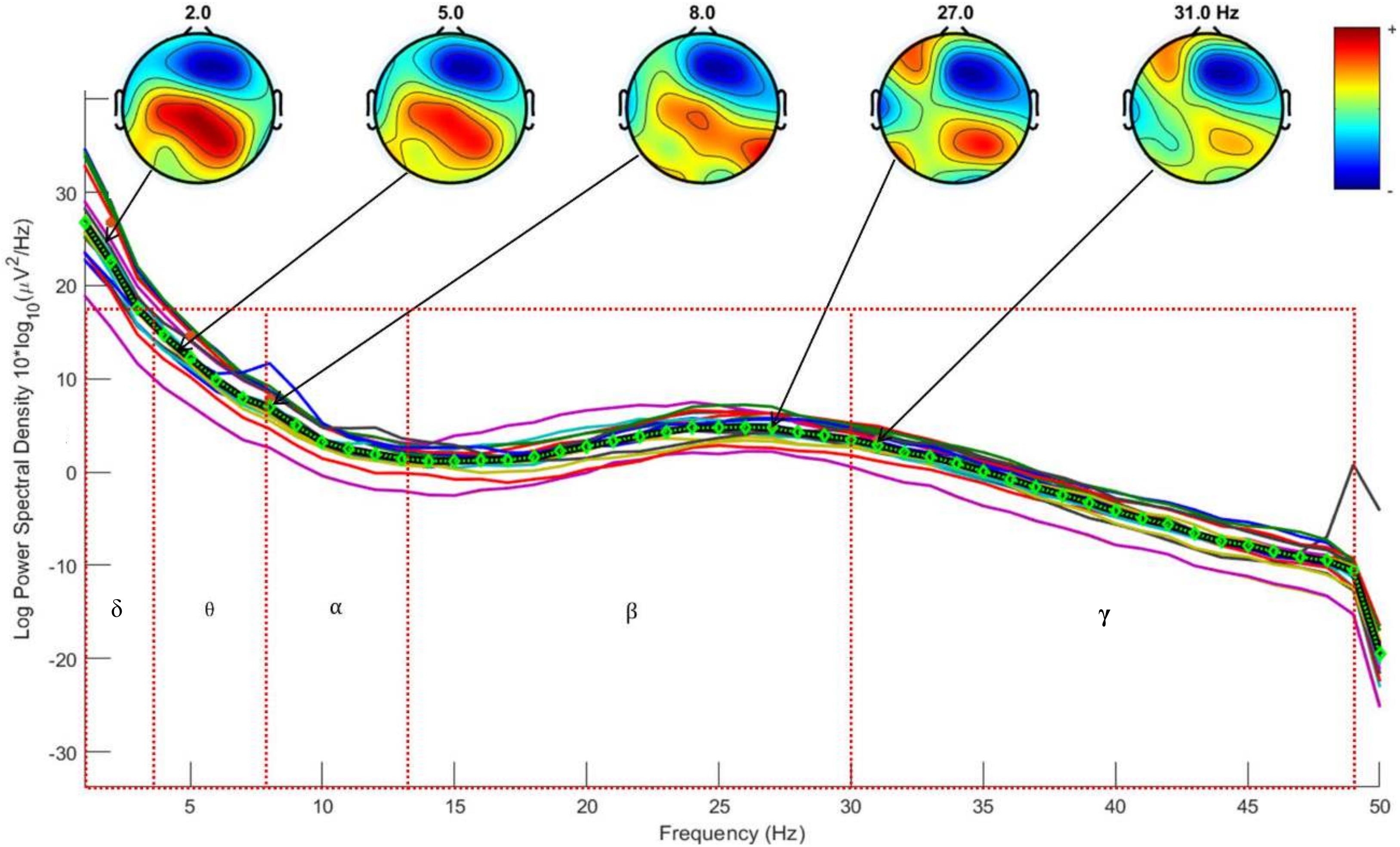

Figure 3. 20. Illustrates the approach of selecting the superior frequency to generate TBMs from the PSD distribution across all electrodes. The black and dotted green lines represent the mean values across the 19 electrodes. Subsequently, TBMs were plotted for each EEG band, with the superior frequency selected for each plot.

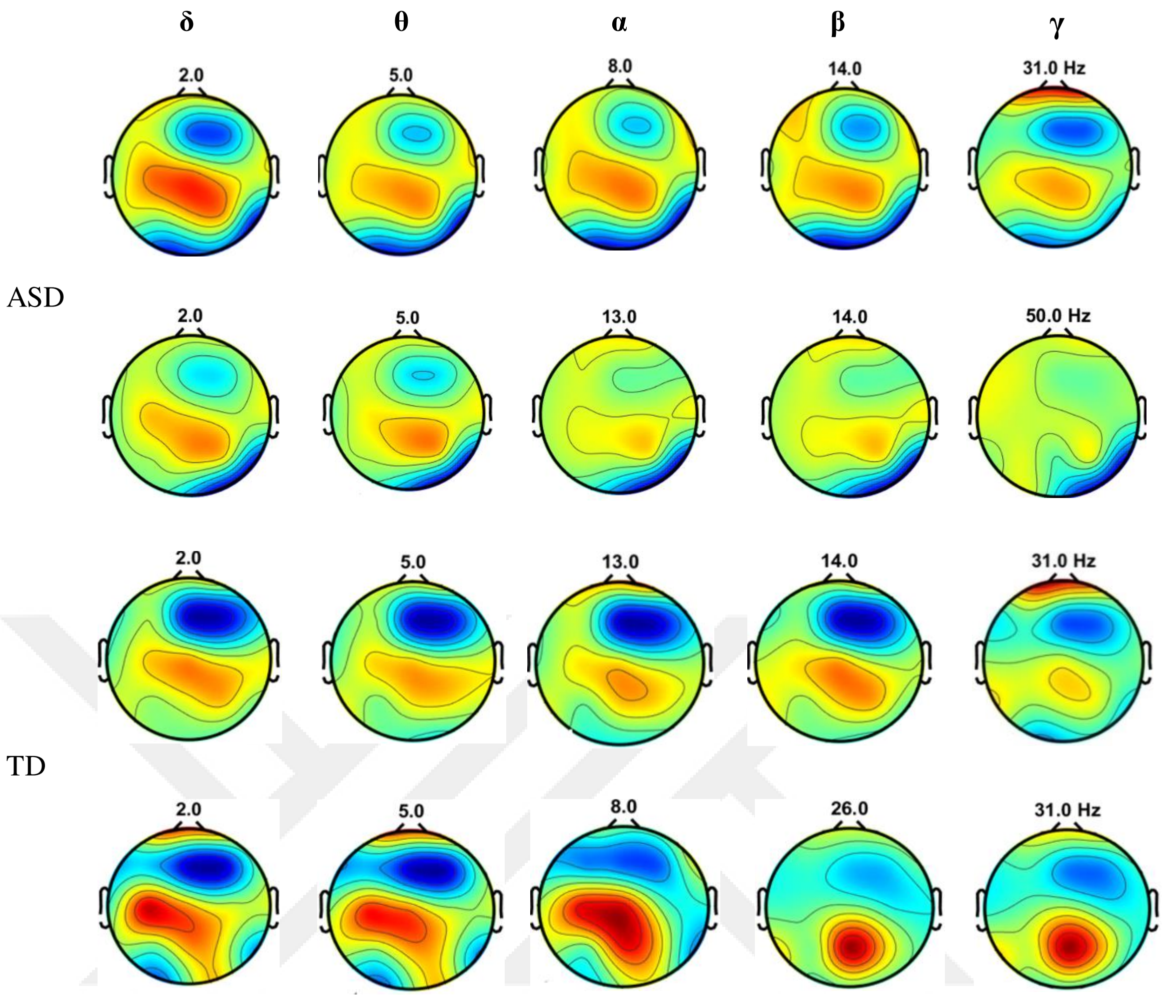

Figure 3.21. The example of distribution of PSD across scalp regions to both cases ASD and TD-Iraq datasets.

3.7.3. Deep Learning (DL)

ML has long been a field dedicated to building models that extract patterns from data. Traditionally, it required extensive knowledge of statistical methods, computation, and access to data, which were not always readily available. Over the past two decades, however, the field has undergone a significant transformation. With advancements in statistical modeling and programming, powerful ML models capable of achieving high accuracy can now be developed more efficiently.

DL, a subfield of ML, automates the extraction of meaningful patterns from data using neural networks and optimization techniques. Today, libraries like neural networks and DL enable the rapid development of sophisticated models. These libraries leverage the abundance of available data, Graphics Processing Unit (GPU)-based parallel processing for neural network computations, and various efficient initialization and computation strategies that enhance learning.

DL has driven remarkable advancements in areas such as face recognition, image classification, speech recognition, text-to-speech generation, self-driving cars, recommendation systems, games, and machine translation.

In (Krizhevsky et al., 2012) introduced AlexNet, one of the pioneering CNN architectures designed to classify numerical data in images. Over the past two decades, DL has emerged as a transformative and widely adopted technology. Deep networks, a subset of neural networks, distinguish themselves through certain key characteristics: they feature more neurons and deeper layers, their layers are interconnected in more intricate ways, resulting in a dramatic increase in the number of parameters from thousands to millions, and they enable automatic feature extraction. The architecture of deep networks has significantly evolved over this period, and ongoing research continues to push the boundaries of their capabilities. CNNs are well-known for their capability in pattern recognition and image classification tasks. Here are the main layers in CNNs and their functions:

Convolutional Layer (ConvLyr)

A ConvLyr performs convolution operations on input data using a set of learnable filters, known as kernels. One at a time they slide over the input, taking dot products of feature weights to the input values covered by the filter as shown in an example of Convlyr with one channel input in Figure 3.22 (Prijono, 2018). This process allows the layer to divide features such as edges, texture, and patterns of input images where early layers provide simple features and the deeper layers provide complex patterns. The complete red, green, and blue (RGB) image with convolutional layers is presented in Figure 3.23.

For each feature map X of dimensions $H \times W$ with three input channels, and a filter F of size $K(n_H) \times K(n_W)$, the output at position (i , j) in the feature map can include a bias b added to the result of the convolution. This process is expressed by Equation (3.20):

$$Y_{i,j} = \sum_{m=1}^{K} \sum_{n=1}^{K} \sum_{c=1}^{3} X_{i+m-1,j+n-1,c} \cdot F_{m,n,c} + b \qquad (3.20)$$

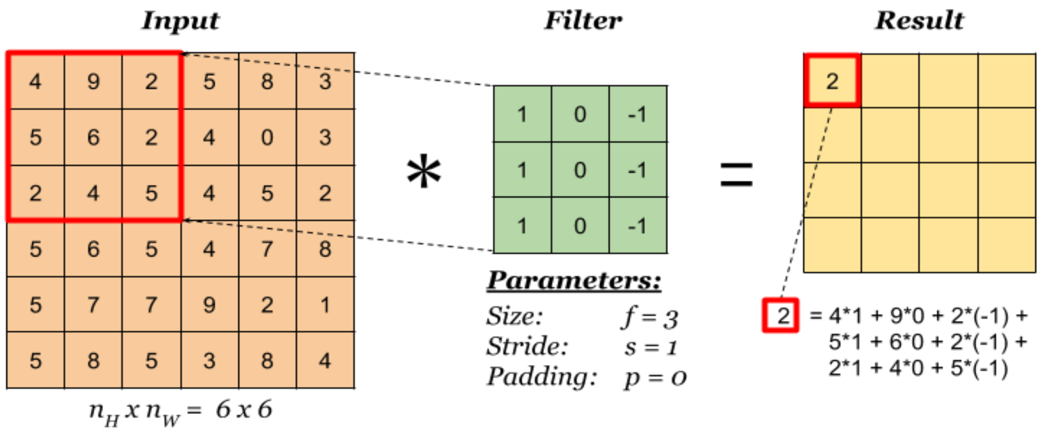

Figure 3.22. An example of one-channel convLyr work. Filter size 3×3, Stride =1, and no padding (Prijono, 2018).

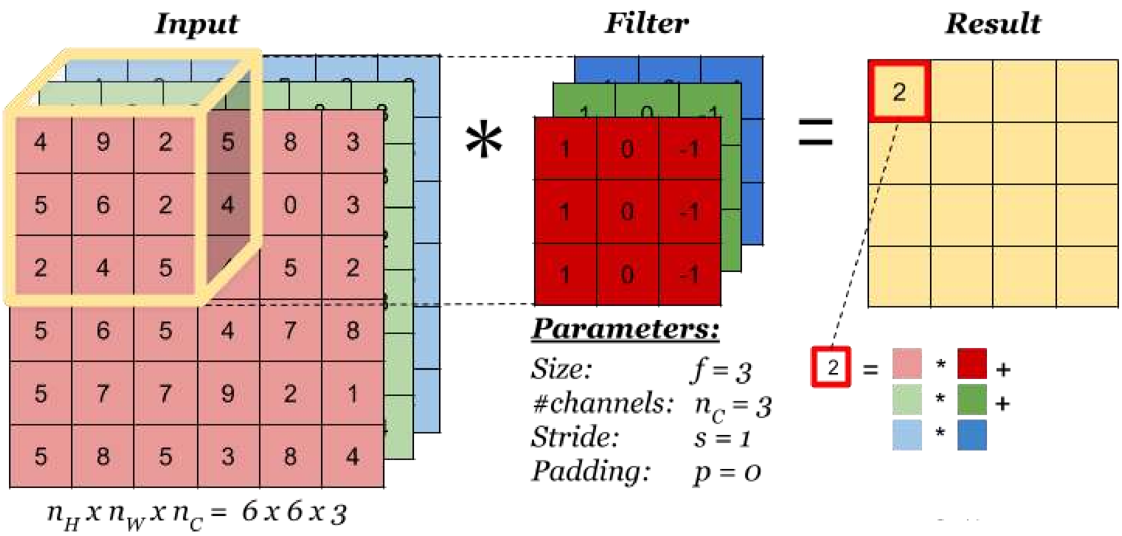

Figure 3.23. Convlayr with RGB channels. The total number of multiplications to calculate the result is (3 × 3 × 3) × (4 × 4) = 432 (Prijono, 2018).

Stride (s)

Amied to determines the number of cells the filter shifts across the input to compute each subsequent value in the output. Figure 3.24 and Figure 3.25 displyed the strid =2 in X and Y axiess.

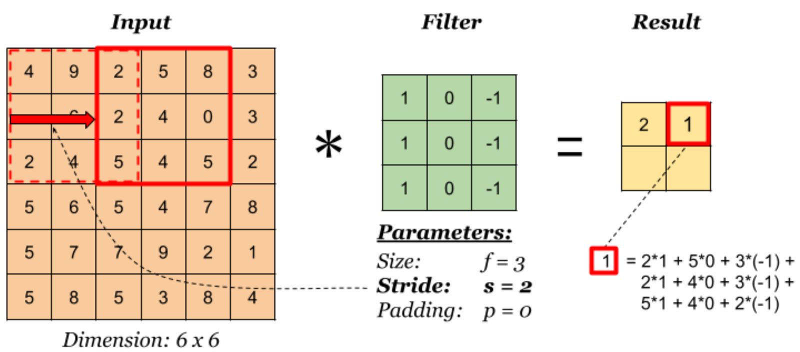

Figure 3.24. An example of one-channel convLyr work. Filter size 3×3, Stride =2, and no padding (Prijono, 2018)

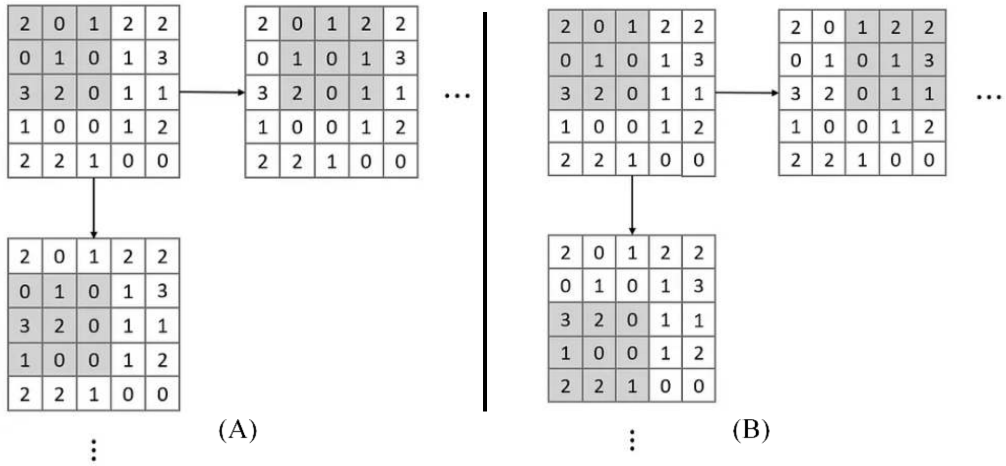

Figure 3.25. Examples of one-channel convLyr work. Filter size 3×3, Stride = [1 1] in (A) and in (B) [2 2].

Padding offers several benefits

It requires convolution without decreasing height and width of volumes that is important in the construction of deeper networks for otherwise these dimensions would be progressively diminished by layers. Furthermore, padding retains more data around the image border so that edge pixel affects values in the next layer. Figure 3.26. displayed the 1-channel N × M dimension with pading =1.

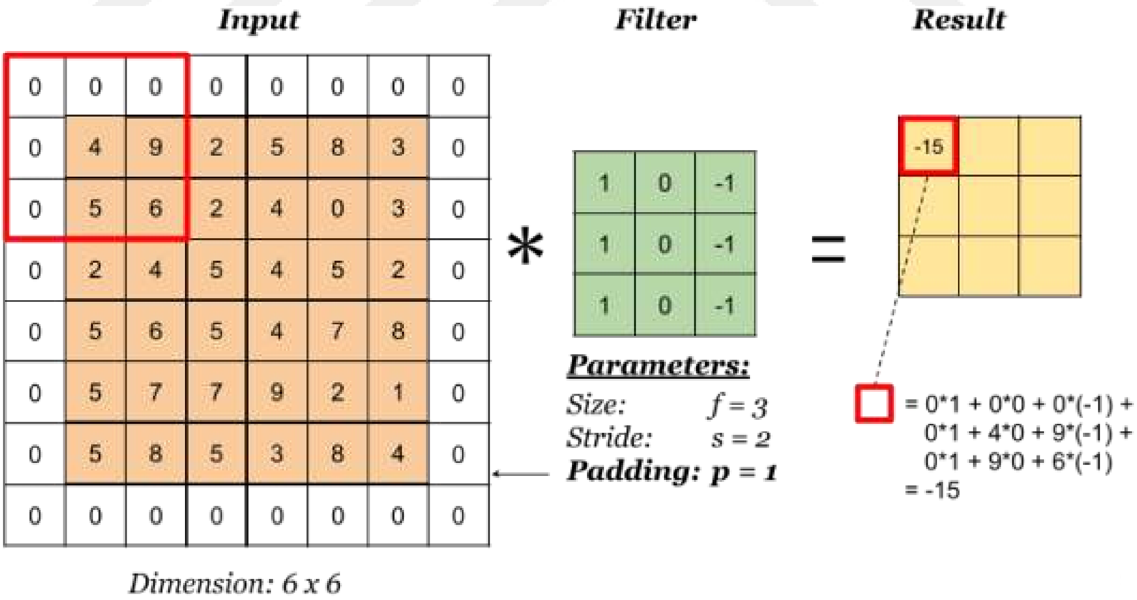

Figure 3.26. Displayed the worke of adding zero padding and p=1, (Prijono, 2018).

Activation Layer (ReLU)

Just after the convolution operation the data passes through the ReLU activation function to add non-linearity to the model. This enables the model to capture more complicated structures to work with nonlinearity in data. ReLU(i)=max (0, i), achieves this by map ing negatives to zero and leaving posit i ves as is. Figure 3.27 Displayed the ReLU work input and output features map.

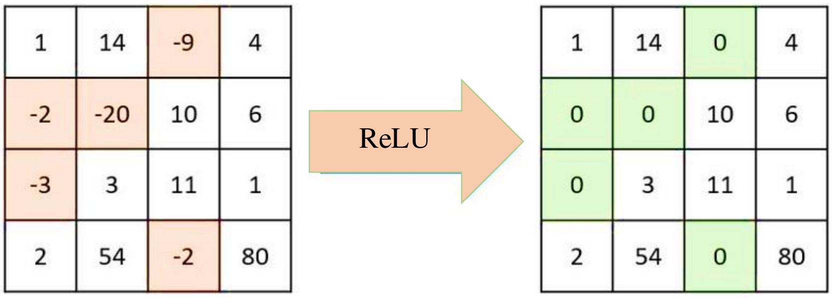

Figure 3.27. Displayed the worke of ReLU activation fuction

Pooling Layer

This layer sub-sample the width and height of the feature maps while maintaining the most important information. Standard types of pooling involve max which takes the maximum values in a region and average which computes the mean of the region. Purpose: This scheme saves computational complexity, reduces memory load and the least probable overfitting due to simplification of the feature maps (Shivhare et al., 2021). Figure 3.28. Shows examples of maximum and average (Ave) pooling for 1-channel (A) and 3-channels (B) features map.

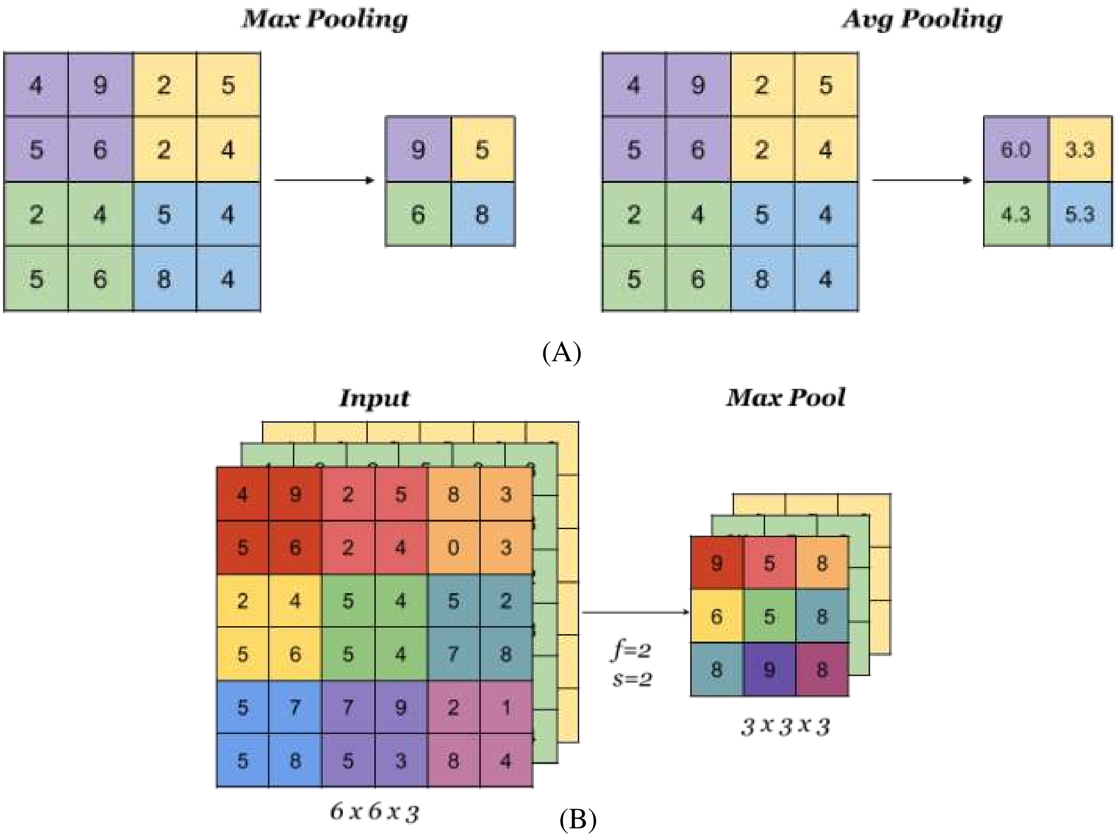

Figure 3.28. An example of one channel feature map for two type of pooling Max. and Ave. pooling presented in (A). In (B) presented an example of max. pooling with 3-channels feature maps which are defined R,G, and B, (Prijono, 2018).

Fully Connected (FC) Layer

This layer makes the output of previous layers to be flat and creates a relationship between each neuron in a given layer and every neuron in the other layer. Its goal is to gather the learned features together and use them for the final prediction either in classification providing a set of probabilities or in regression providing a set of continuous values (Jingjing Wang et al., 2021). In current study we used this layer to get feature vectors to feed ML classifier to build Deep- ML interconnections. Figure 3.29 presented a principal work of the FC layer.

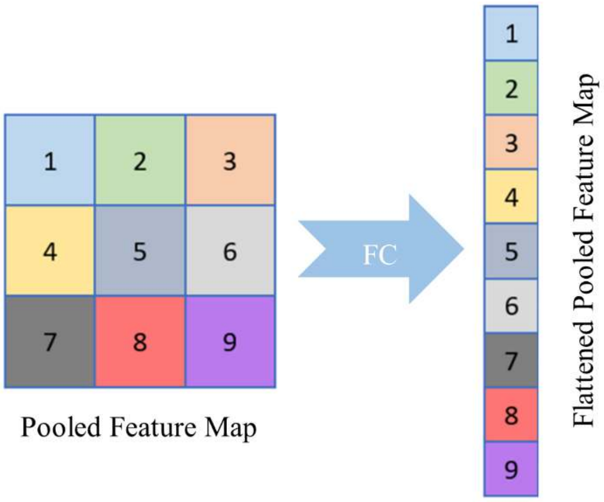

Figure 3.29. The primary function of the fully connected (FC) layer is to transform feature maps into vectors.

Dropout Layer (Optional)

This layer randomly excludes a part of neurons during training. This makes the equations a lot better in preventing over fitting since it decreases the dependent on those neurons and increases the chances of learning other improving features.

Softmax Layer

However the final stage is just a fully connected layer from which the softmax function is used to transform raw scores to probabilities. It is applied to the multiclass classification problems, which provide the probability distribution of the samples on the several classes. In curent study we used 2 poupluer model of CNN which are will discribe breifelly in the next.

CNNs automatically extract meaningful features from raw input images, which enables them to discern intricate patterns and accurately classify images (Akin et al., 2000). Many studies used CNN models due to their effectiveness in resolving image-related issues (Al-Saffar et al., 2023; Menaka et al., 2024; M. N.A. Tawhid et al., 2020; Md Nurul Ahad Tawhid et al., 2021).The proposed method used AlexNet (Krizhevsky et al., 2012) and GoogleNet (Tang et al., 2017) as deep feature extractors form TBM images which are will be described breifelly in the fellowing:

- **AlexNet**

The architecture of the AlexNet (Krizhevsky et al., 2012) is made of five Convlyrs, max-pooling layers, and dropout layers and only three fully connected (FC) layers for deep feature extraction, which are; (FC6–FC8) with feature lengths of 4096, 4096, and 1000, respectively. Figure 3.30 and Figure 3.31 display the AlexNet architecture.

The output of the fully connected layer (FC8) is passed through a 1000-node SoftMax layer that produces the probability distribution of each class (Krizhevsky et al., 2012). The tester images have to be resized to 227 × 227 × 3 and pass through the first convolution layer with 96 filters of the size 11 × 11 × 3 and strides of 4. The second Convlyr takes the normalized and pooled output of the first layer, and uses sixty-four kernels of size 5 × 5 × 48. The next three Convlyrs are connected connaturally, and there are no normalization or pooling layers between the layers. The third Convlyr has 384 kernels of size 3 × 3 × 256 which are connected with the second layer. The fourth and fifth Convlyrs have 284 and 256 kernels respectively with the kernel size of 3 × 3 × 192. The layers of the FC layers are both composed of 4096 neurons. With 60.9 M total leanables. As the model employs two GPUs, the layers are only interwoven at certain phases of the computation (Krizhevsky et al., 2012).

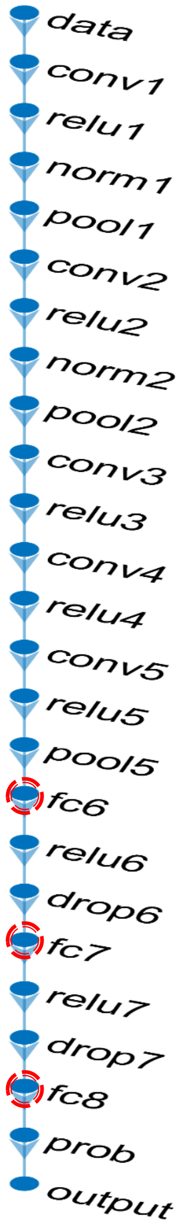

Figure 3.30. The workflow of AlexNet Artitecture.

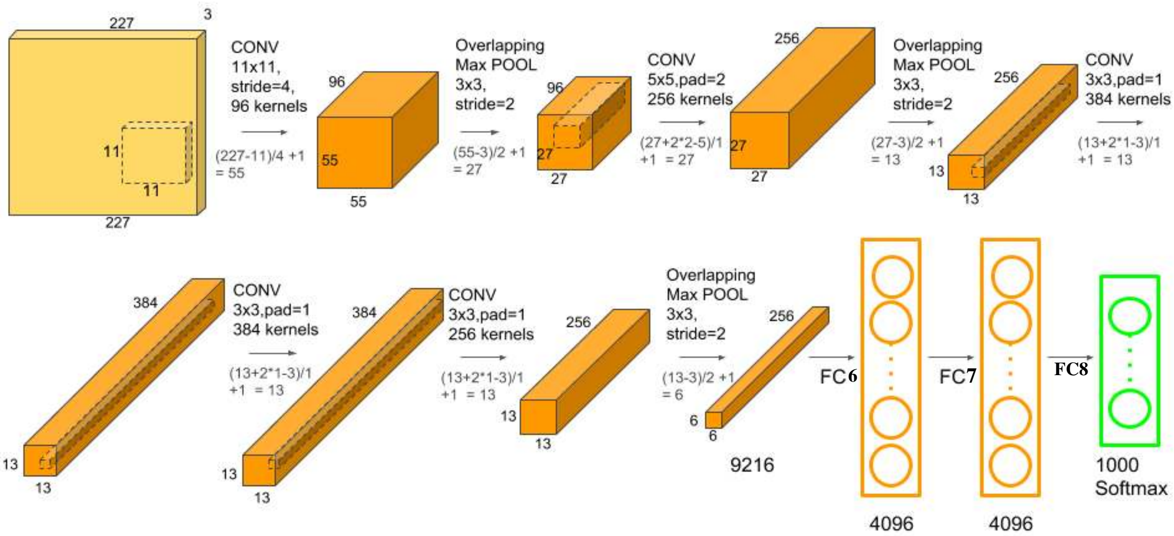

Figure 3.31. The block diagram of AlexNet architecture (Krizhevsky et al., 2012)

- **GoogleNet**

Presented by (Tang et al., 2017), is deep CNN built for its competition on ImageNet competition and this contains more than 10000 images with 1000 classes. This PET is well known for its high-performance capability in the field of image prediction tasks and is used effectively as a feature extractor in a number of fields, including medical and neurodevelopmental. The GoogLeNet architecture is of twenty-two layers comprised of 144 individual layers that are optimized to apply layers of feature extraction on the inputted images as shown in Figure 3.32. The network is expected to take RGB images of size 224 × 224 × 3 (width × height × color channels) of the input image. All of them act as specific filters that work with some specific attributes of input data. The first layers aim at detecting very simple features, such as color, edges, and textures that are probably relevant for a vast majority of categories. Such early filtering operations smooth down the raw input data while maintaining some important features for the next stages of consideration. At the reception, it is then processed by the deeper layers to extract features in a progressive manner with the data searching for increasingly or more abstract features that are exclusive to the image category. This type of architecture helps to exclude categories, thus providing very high accuracy for GoogLeNet. New to GoogLeNet, there are Inception modules that improve the performance of FE by applying various convolutions in a single layer. These modules work at different resolutions, allowing the network to extract both local and global information at the same time. Such multi-scale processing capabilities not only enhance the performance of category recognition but also lessen the computational complexity compared with previous generations of CNNs.

Because of its flexibility and speed, GoogLeNet should not be limited only to image recognition. Due to its capability of extracting significant features from raw data including EEG-derived topographic brain maps, it has been used in higher-level areas like neurodevelopmental disorder diagnosis, especially for ASD. From the hierarchical feature extraction of GoogLeNet, new approaches to the analysis of EEG signal features can be studied from the spatial and temporal dimensions and help in establishing robust diagnostic EEG signal analysis systems automatically.

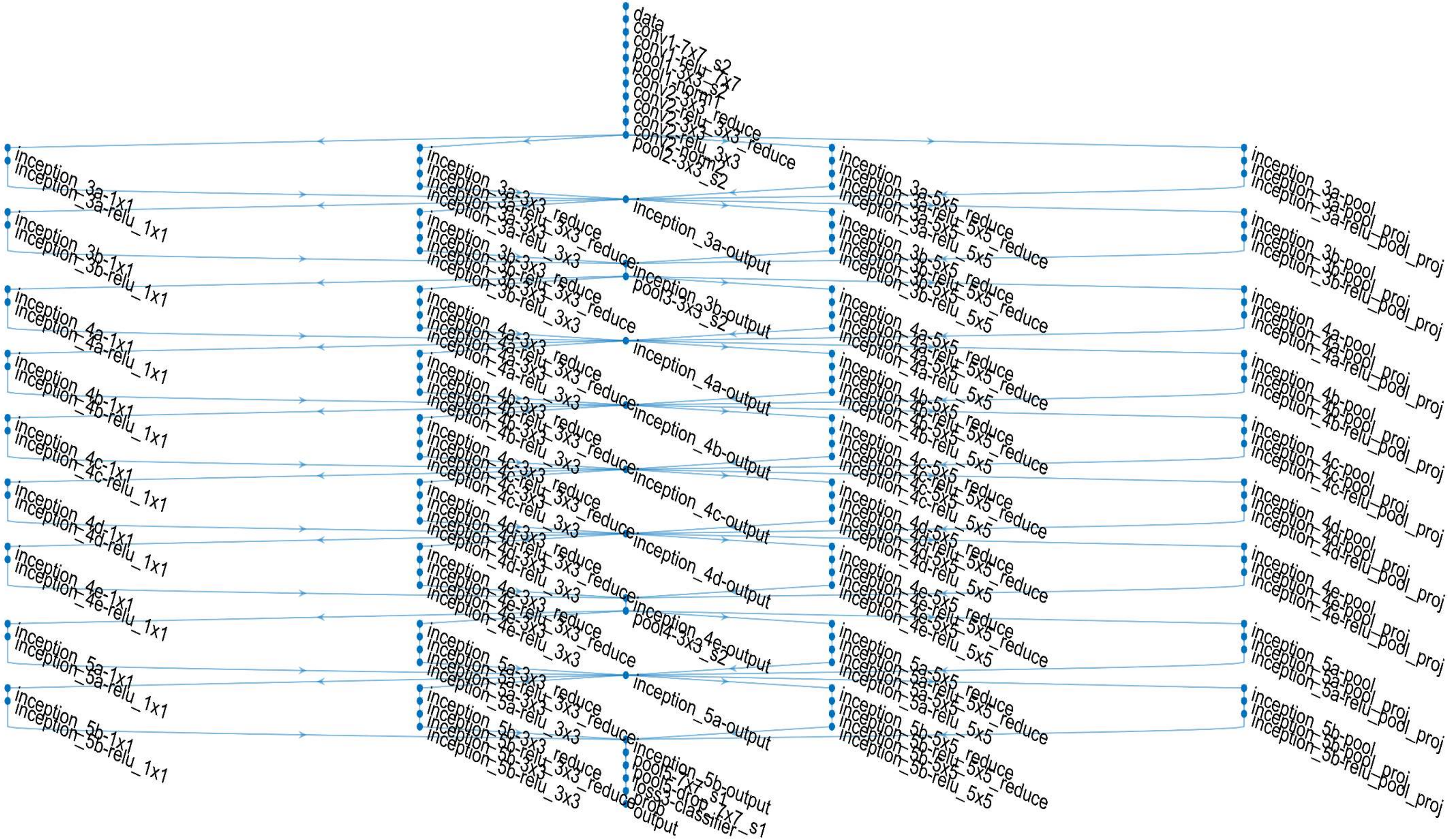

Figure 3.32. The Architecture of GoogLeNet.

3.7.4. Feature Selection

The number of features was reduced to fifty features, they were experimentally using ANOVA (Ding et al., 2014) feature selection approach. Dimensionality reduction is crucial before applying a classifier as it enhances model efficiency and interpretability (Li et al., 2005). Choosing the most relevant features eliminates irrelevant or redundant information, which reduces classification time and data dimensionality, improves performance, enables a more concise data representation, and facilitates better decision-making during classification (Li et al., 2005). Finally, ASD was detected using an SVM-L (Rambabu et al., 2014) and LDA (Balakrishnama et al., 1998) classifiers were compared to select the system that provided both faster performance and higher accuracy with lower standard deviation, ensuring greater stability in the results. Figure 3.33 illustrates the flow work of the proposed method 2.

3.7.5. Classification

In the second method, we utilized two types of classifiers, as outlined below:

Support Vector Machine (SVM)

A supervised ML classifier that finds the best hyperplane from a set of feature vectors which are related to the class labels in a dataset (Rambabu et al., 2014). Consider a set of feature vectors $x_i \in \mathbb{R}^n$, corresponding to TBM images I_i where $i \in$ [1,2 …, k], and the set of class labels y = [y_1, y_2,…, y_k]. The goal is to find the optimal linear hyperplane the classifier has been explained with details in subsection 3.6.8.

Linear Discriminant Analysis (LDA)

LDA type of supervised learning that works through the projection of data onto a higher-dimensional space using hyperplanes for the classification of data. In the case of only one EEG dataset, LDA separates classes using maximizing the distance between class means while concurrently minimizing variance within each class. LDA tries to achieve the best possible separation by finding an optimal linear combination of the features (Balakrishnama et al., 1998). However, LDA works well for linearly separable data, as it suffers with highly non-linear data, and will probably not be able to capture very elaborate patterns. Another critical problem that LDA may experience is overfitting, which can happen whenever there is a small sample size or the dimensionalities are high, reducing the ability for generalization Virous authors recommended to use of LDA to classify EEG signals (Fu et al., 2019; Hasan et al., 2015; Melinda et al., 2023).

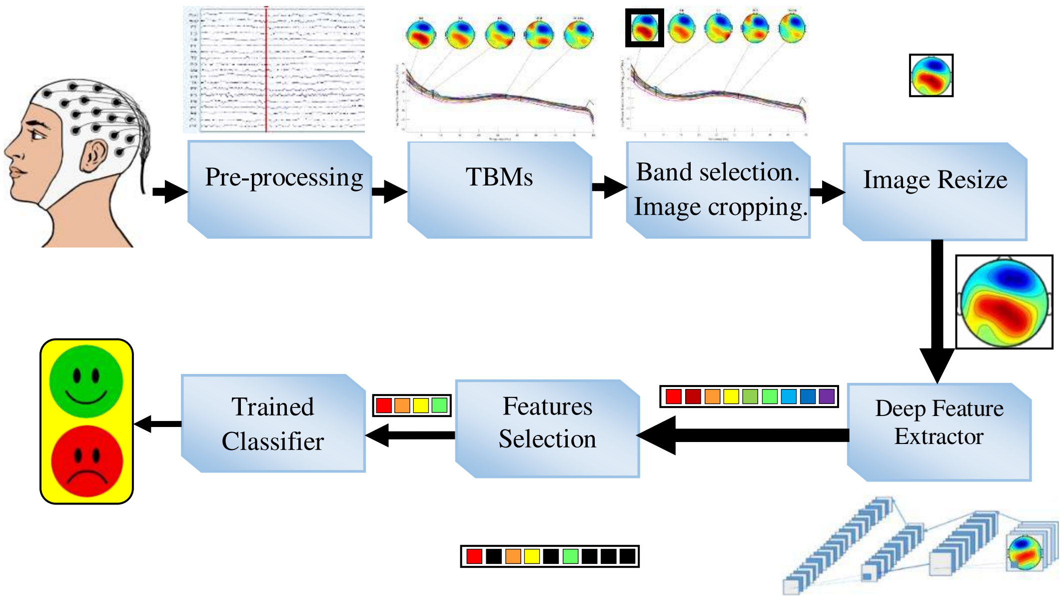

Figure 3.33. The workflow of the proposed Method (2) for ASD detection.

4. RESULTS AND DISCUSSIONS

4.1. Performance Analysis and Decision Support

The Thesis proposed two methods that were thoroughly evaluated during the performance analysis and decision support phase (A.J.Al-Sammarraie, 2024; Ting, 2007). These methods were compared with relevant ASD detection studies to assess their effectiveness. It is assumed that the system can undergo continuous training on an hourly, daily, weekly, or monthly basis, which would further enhance its robustness. The trained model is designed for online deployment, allowing for rapid detection when testing new data. The results will be promptly communicated to medical practitioners via a suitable cloud infrastructure, supporting precision medicine decision-making. Table 4.1 provides an example of a confusion matrix, with the results of each method summarized in the following subsections.

Table 4.1. An example of confusion matrix.

		Predicted class	
		TD	**ASD**
Actual class	**TD**	*TN*	*FP*
	ASD	*FN*	*TP*

Where, True Positive (TP): ASD correctly classified. True Negative (TN): TD correctly classified. False Positive (FP): TD classified ASD. False Negative (FN): ASD classified TD.

The experiments were conducted using MATLAB® + plugin EEGLAB on a Microsoft Windows 10 Pro (22H2) platform, running on an Intel® CoreTM i7-7500U CPU @ 2.70-2.90 GHz, RAM 12 GB computer. EEGLAB (A Delorme et al., 2004), was utilized to process the EEG data, employing the "Clean Raw Data" plugin for automated artifact rejection. This feature automatically flagged and excluded bad data channels and data segments unsuitable for analysis.

To enhance model accuracy and generalization, the ratio of the training set to the testing set is crucial in EEG data classification (A Delorme et al., 2004). A large training set helps in learning complex patterns, reduces overfitting risks, and improves parameter estimation. This approach also increases statistical sensitivity, essential for detecting differences in clinical scenarios. Additionally, it supports strict validation, enhancing the model's stability and accuracy.

The 1st method used 120 epochs with a 70% (36 samples) training set and 30% (16 samples) testing set and for second method 60:40 % for training and testing. The samples were randomly permuted before each epoch. To ensure reliability and validity, 5-fold cross-validation was applied to each epoch. Despite these measures, gender-specific patterns could still influence outcomes, as females with ASD often exhibit subtler social deficits and neural oscillation differences. This distribution provided accurate assessments, resulting in robust and dependable outcomes. The accuracy of the K-fold was calculated using Equation (4.1), and an example of the k-fold cross-validation is shown in Figure 4.1.

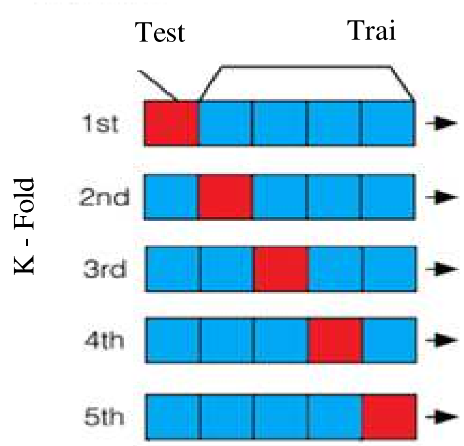

Figure 4.1. An example of k-folds in cross-validation (k = 5).

$$Accuracy = \frac{1}{K}\sum_{i=1}^{k} Acc_i \tag{4.1}$$

The confidence in the results was further increased by measuring the model's performance through various metrics, including Accuracy, Sensitivity, Specificity, Precision, and F1 measure. These metrics were calculated using a confusion matrix (Ting, 2007), as shown in Table 4.1, and their corresponding mathematical formulas are provided in Equations (4.2 to 4.6).

$$Accuracy\ (ACC.) = \frac{All\ correctly\ classified}{Total\ test\ samples} \tag{4.2}$$

$$Sensitivity\ (Sen.) = \frac{TP}{TP + FN} \tag{4.3}$$

$$Specificity\ (Spec.) = \frac{TN}{TN + FP} \tag{4.4}$$

$$Precision\ (Prec.) = \frac{TP}{TP + FP} \tag{4.5}$$

$$F1\ measure = \frac{2\ \times\ Prec. \times Sen.}{Prec. + Sen.} \tag{4.6}$$

4.2. Result of Method (1)

The confusion matrix determined the number of true positive, true negative, false positive, and false negative predictions. Subsequently, the precision achieved using the θ band was compared with that of the other bands (δ, α, β, and γ). Table 4.2 and Figure 4.2 illustrate the comparison.

The analysis in Tables 4.3, 4.4, and 4.5 compares the performance of different SVM classifiers (Linear, RBF, and Quadratic) across various configurations of energy windows (max, mean, and min) for EEG-based classification.

The study evaluates these configurations using five EEG frequency bands (γ, β, α, θ, and δ) with overlap ratios varying from 87.5% to 12.5%, corresponding to strides of 250 to 1750 samples:

- **Theta Band Superiority:** The θ band consistently delivers the best classification results, particularly with the SVM-Linear classifier. Using a maximum energy window with a stride of 250 samples (87.5% overlap), the mean accuracy reaches 91.73% with an SD of 7%, the highest among all configurations. This highlights the effectiveness of the θ band for early ASD detection.
- **Delta Band Performance:** The δ band demonstrates strong results, particularly with mean energy windows. For instance, using the SVM-Linear classifier, the δ band achieves a mean accuracy of 84.3% with an SD of 8.7% with a mean energy window at a stride of 250 samples. Similarly, with the SVM-Quadratic classifier, the δ band achieves a mean accuracy of 85% with an SD of 9.2% under the same conditions. Despite these strong results, the δ band does not surpass the superior performance of the θ band.
- **Impact of Overlap and Energy Window Settings:** Higher overlap ratios and the maximum energy window generally enhance classification accuracy, particularly for the θ band, by capturing more details in the EEG signals. The δ band remains relatively stable across configurations, indicating its robustness and usefulness. However, the θ band consistently delivers the highest accuracy.
- **Non-Linear SVM Kernels:** Using non-linear kernels such as RBF and Quadratic improves classification accuracy across frequency bands. The δ band performs reasonably well with the SVM-RBF kernel, achieving up to 82.7% accuracy in the mean energy window at a stride of 1000 samples (50% overlap). The γ band, however, shows lower overall performance, with its best accuracy of 73.3% achieved using SVM-Quadratic at a stride of 500 samples (75% overlap) in the minimum energy window.
- **Optimal Configuration for ASD Detection:** The highest accuracy for early ASD detection is achieved with the θ band, the maximum energy window, a stride of 250 samples, and a window size of 2000 samples (selected experimentally), classified using SVM-Linear. This configuration yields a mean accuracy of 91.7% with an SD of 7%,

Sensitivity of 91.4% with an SD of 9.7%, and a lower standard deviation (SD) compared to other EEG bands, as shown in Table 4.2.

To this end, θ band is the most accurate in distinguishing between ASD and TD groups, outperforming other bands such as δ, β and γ, which have lower accuracy and sensitivity. While the α band is effective, it does not match the superior performance of the θ band.

Table 4.2. Results for each decomposed EEG band using maximum energy windows with an 87.5% overlap ratio and SVM-L, presented as mean% (SD%).

	Delta	**Theta**	**Alpha**	**Beta**	**Gamma**
Acc.	70.1 (10.1)	91.7 (7.0)	82.7 (9.8)	64.6 (11.8)	58.4 (12.3)
Sen.	73.2 (18.4)	91.4 (9.7)	79.7 (13.1)	52.5 (18.2)	38.6 (13.7)
Spec.	67.1 (15.5)	92.1 (8.6)	85.8 (12.2)	77 (15.0)	78.2 (18.0)
Prec.	70.8 (12.1)	92 (9)	86 (11.6)	70.2 (18.3)	68.8 (20)
F1 measure	70.1 (12.3)	91.6 (6.4)	81.8 (11.3)	58.3 (16.5)	49.5 (13.8)

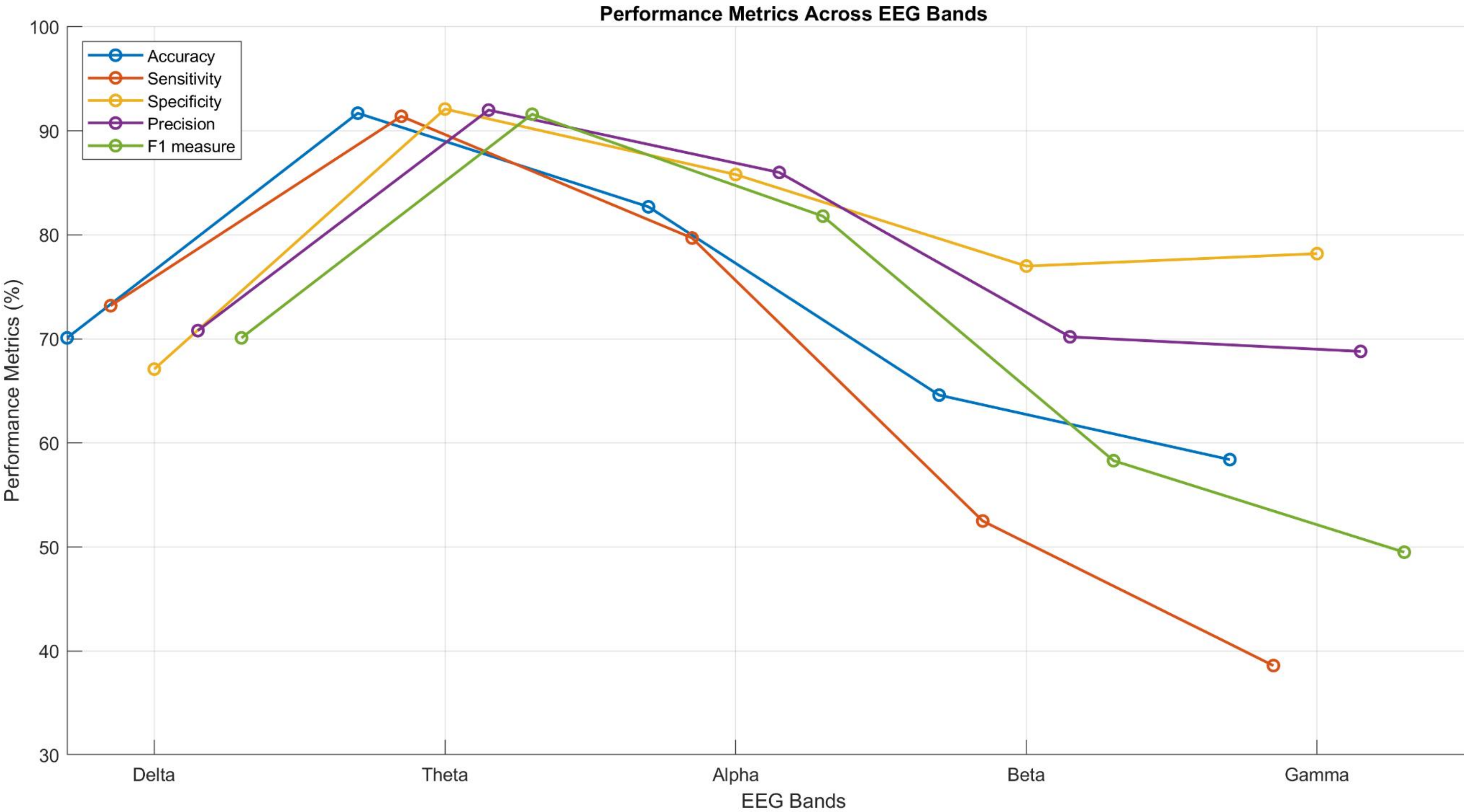

Figure 4.2. Classification results for each decomposed EEG band using maximum energy windows with 87.5% overlap ratio and SVM-Linear, reported as mean values.

Table 4.3. Results of each decomposed EEG band, for maximum window of energy.

Parameters		**Accuracy of SVM-L mean % (SD%)**					**Accuracy of SVM-RBF mean % (SD%)**					**Accuracy of SVM- Quadratic mean % (SD%)**				
Strid	**Overlap%**	**γ**	**β**	**α**	**θ**	**δ**	**γ**	**β**	**α**	**θ**	**δ**	**γ**	**β**	**α**	**θ**	**δ**
250	**87.5**	58.4 (12.3)	64.6 (11.8)	82.7 (9.8)	**91.7 (7)**	70.1 (10.1)	51.9 (10.6)	58.5 (11.2)	78 (8.4)	84 (8.2)	66.6 (9.6)	46.7 (11.7)	61.2 (12)	81.4 (9.4)	84.2 (10.1)	63.7 (9.7)
500	**75**	47.5 (3.4)	63.75 (7.6)	78.9 (11.7)	90.7 (7.3)	67.6 (9)	86.5 (8)	56 (10.5)	78.2 (9.9)	83.9 (8.6)	65.5 (10.8)	82 (9.8)	60.6 (12)	83 (10.5)	82.5 (10.2)	63.5 (9.9)
750	**62.5**	57.4 (11.6)	65.4 (11)	81.1 (10)	88.1 (7.6)	69.7 (10.1)	48.7 (10.1)	59.2 (9.9)	77.7 (9.1)	86.4 (9.2)	67.2 (10.1)	45.3 (11.7)	62.5 (11.8)	80.4 (9.7)	87.1 (5.9)	64.4 (9.5)
1000	**50**	57.3 (7.3)	65.6 (7.5)	72.2 (11.5)	87.9 (9.1)	66.7 (9.1)	52.7 (9.7)	58.4 (10.7)	78.5 (9.8)	83.4 (7.9)	66.6 (9.9)	48.7 (10.2)	62.7 (10.9)	81.6 (10.6)	82 (10.3)	60.9 (10.2)
1250	**37.5**	58.9 (11.2)	62.9 (12)	85.5 (9)	86.4 (6.9)	65.2 (10)	53.5 (9.6)	57.8 (11.2)	79.2 (10)	80 (8.8)	65.3 (8.9)	47.8 (11.5)	62.2 (12.4)	81.7 (9.1)	77.5 (10)	62.9 (9.4)
1500	**25**	50.7 (9.9)	58.2 (10.1)	79.6 (11.1)	85.6 (9.6)	74 (10.7)	55.9 (11.7)	64 (11.3)	83.4 (10.8)	86.1 (9.8)	73.6 (9.9)	44.8 (10.8)	61.6 (10.9)	84 (11.3)	86.2 (9.9)	69.9 (11.3)
1750	**12.5**	57 (6.5)	61.6 (6.6)	75 (11.9)	86.5 (7.3)	67.9 (9)	54.4 (9.4)	56.9 (10.3)	80.3 (8.9)	82.5 (9.2)	62 (11)	48.4 (10.6)	61.9 (11.1)	80.6 (8.8)	83.4 (9.1)	64.9 (10.3)

Table 4.4. Results of each decomposed EEG band, for mean of windows energy.

Parameters		**Accuracy of SVM-L mean % (SD%)**					**Accuracy of SVM-RBF mean % (SD%)**					**Accuracy of SVM- Quadratic mean % (SD%)**				
Strid	**Overlap (%)**	**γ**	**β**	**α**	**θ**	**δ**	**γ**	**β**	**α**	**θ**	**δ**	**γ**	**β**	**α**	**θ**	**δ**
250	**87.5**	56.3 (9.7)	65 (9.7)	76.6 (11.1)	81.7 (8.4)	84.3 (8.7)	65.4 (10.1)	63.5 (8.9)	66.1 (11.1)	78.2 (9.9)	81.8 (9.5)	57 (9.7)	60 (9.1)	75.8 (12.7)	78.8 (9.9)	85 (9.2)
500	**75**	54.9 (12.4)	62.5 (10.5)	77.6 (11.3)	80.6 (9.1)	82.6 (9.5)	66.1 (10.8)	61 (9.9)	66.8 (10.6)	78 (10.3)	81.6 (9.2)	55.9 (10.8)	60.5 (9.1)	77.2 (11.7)	80.8 (9.1)	84.8 (10.5)
750	**62.5**	54.4 (11.1)	62.1 (10)	75.4 (12.4)	82 (7.8)	83.5 (4.7)	65 (10.7)	63.4 (10.6)	64.1 (11.2)	79.7 (9.3)	81.5 (8.5)	56.6 (9.9)	59.7 (9.1)	73 (12.7)	80.8 (9.3)	83.5 (9.7)
1000	**50**	52.1 (11.1)	64.7 (10.5)	78 (11.3)	79.6 (10.5)	82.1 (9.3)	62.5 (10.2)	64.5 (9.2)	67.3 (12)	77.3 (11.9)	82.7 (9.2)	55.1 (9.7)	60.2 (9.8)	76.6 (12.3)	79.8 (10.3)	83.9 (10.8)
1250	**37.5**	55.2 (10.2)	64.1 (11.6)	77.2 (10.2)	79.2 (10.1)	84.4 (8.7)	65.5 (9.8)	63.5 (10.2)	66.4 (10.6)	75.5 (11.1)	81.3 (9.36)	56.3 (9.7)	63.5 (10.2)	76.3 (11.9)	78.8 (9.7)	83.9 (11.1)
1500	**25**	53.5 (11.3)	62.6 (9.2)	77.3 (11.7)	80.1 (8.5)	84.2 (9.3)	64.8 (10.8)	61.5 (9.4)	65.1 (10.4)	78.1 (9.7)	80.7 (10.5)	57 (10.3)	58.9 (9.8)	73.4 (13.3)	80.3 (9)	83.5 (10.7)
1750	**12.5**	53.9 (10.2)	63.9 (10.9)	78.3 (10.6)	80.5 (7.9)	82.4 (11.3)	64.7 (11)	62.3 (9.4)	66.4 (11.4)	80.1 (8.8)	81.1 (8.8)	57.2 (9.9)	62.4 (9.5)	75 (12.7)	81 (8.3)	82.4 (11.3)

Table 4.5. Results of each decomposed EEG band, for minimum window of energy.

Parameters		**Accuracy of SVM-L mean % (SD%)**					**Accuracy of SVM-RBF mean % (SD%)**					**Accuracy of SVM- Quadratic mean % (SD%)**				
Strid	**Overlap%**	**γ**	**β**	**α**	**θ**	**δ**	**γ**	**β**	**α**	**θ**	**δ**	**γ**	**β**	**α**	**θ**	**δ**
250	**87.5**	45.3 (7.4)	45.3 (8.1)	57 (9.1)	52 (8.4)	57.5 (13.2)	81 (8.7)	68.5 (6.7)	75.7 (10.2)	76.4 (6.6)	67.8 (9.1)	73.2 (10.3)	65.7 (9.9)	72.1 (9.8)	79.6 (7.7)	69.6 (10.5)
500	**75**	45.8 (7.3)	48.3 (8.4)	58.6 (9.8)	57.9 (10.5)	59 (9.4)	79.5 (8.9)	70.9 (9)	76.9 (8.6)	77.3 (9)	68.3 (8.7)	73.3 (10.5)	66. (10.3)	67.5 (11.6)	79.7 (8.2)	68.6 (9.5)
750	**62.5**	46.5 (8)	49.2 (8.9)	58.5 (9.6)	60.8 (10.1)	66 (11.3)	77.8 (9.8)	68.1 (9.8)	72.5 (9.6)	76.3 (8.5)	67.6 (9.1)	73.3 (9.2)	64.9 (10.6)	64.4 (10)	78.2 (10.1)	74.1 (9.9)
1000	**50**	46.2 (9.2)	48.6 (9.2)	55.4 (9.9)	59.9 (9.4)	61.7 (9.9)	76.2 (9.4)	71.4 (9.5)	72.8 (10.9)	76.8 (9.6)	63.8 (10.2)	46.7 (11.7)	61.2 (12)	81.4 (9.4)	84.2 (10.1)	63.7 (9.7)
1250	**37.5**	64.4 (7.4)	49.8 (10.3)	57.3 (11.4)	56.9 (9.3)	57.5 (12)	75.8 (8.7)	68.5 (9)	70.3 (9.5)	73.4 (8.4)	68.4 (9.4)	82 (9.8)	60.6 (12)	83 (10.5)	82.5 (10.2)	63.5 (9.9)
1500	**25**	47.2 (8)	49.3 (9.7)	57.1 (10.1)	57.3 (9.5)	62.5 (11.1)	74.8 (9.5)	68.8 (9.3)	69.7 (8.7)	74.5 (8.9)	65.3 (11.8)	45.3 (11.7)	62.5 (11.8)	80.4 (9.7)	87.1 (5.9)	64.4 (9.5)
1750	**12.5**	45.7 (8.3)	49.6 (8.6)	55 (10.2)	57 (8.7)	63 (8.5)	72.1 (8.5)	67.8 (8.5)	72.2 (10.2)	73.9 (9.3)	73.1 (10.9)	48.7 (10.2)	62.7 (10.9)	81.6 (10.6)	82 (10.3)	60.9 (10.2)

Compared to this study, previous EEG-based ASD detection classification studies involved diverse participant groups and employed various classifiers and feature selection techniques. An examination of recent publications, as summarized in Table 4.6, reveals that many studies included groups with wide age ranges or showed significant disparities between TD and ASD individuals.

Table 4.6. Comparison of the performance of the proposed method (1) with that of other studies.

Source	**Test method**	**Male (No.) Female (No.)**	**Age years**	**Method**	**Accuracy Mean % (SD) %**
Current study method 1	GARS CARS DSM-5-TR Medical History	ASD: M (18); F (4) TD: M (18); F (12)	ASD: 4.85 ± 1.5 TD: 5.9 ± 3.5	Energies Windowing SVM	91.7 (7)
(Singh et al., 2024)	Not available	ASD: 28 TD: 28	ASD:18–68 TD: 18–68	Statistical and spectral features+CSTO-DRN	88.6
(Rogala et al., 2023)	PANS DSM-V Medical history Professional Clinical	ASD: M (12); F (6) TD: M (12); F (6)	ASD: 3.92 ± 1.38 TD: 3.84 ± 1.24	Statistical and spectral brain connectivity	83 (14) to 86 (18)
(Husna et al., 2021)	Two datasets (ABIDE I and ABIDE II)–images/5–64 years			FMRI+CNN VGG16, ResNet50	63.4 –87.0
(Grossi et al., 2017)	DSM-V ADOS scale	ASD: M (13); F (2) TD: M (4); F (6)	ASD: 10.4 TD: 9.2	MS-ROM/I-FAST, TWIST + ANN	84–92.8

4.3. Results of Method (2).

Results are presented in Table 4.7 and Table 4.8, which illustrate that the alpha band consistently yields the highest values for performance metrics-accuracy, sensitivity, specificity, precision, and F1 measure for all CNN feature extractors (AlexNet-FC6, AlexNet-FC7, AlexNet-FC8, and GoogLeNet) combined with feature selection (ANOVA) and classifier (LDA and SVM-L). The use of ANOVA further augmented the results, improving the accuracy in all bands for both datasets and reducing the classification time, as shown in Figure 4.3.

The configuration of GoogleNet+ANOVA+SVM-L for the classification of TBMs images in the alpha band showed the highest performance on Iraq datasets. It achieved a mean accuracy of 98 with an SD of 2.3% with a mean F1 measure of 97.9 with an SD of 2.9%. The second-best performing interconnection AlexNet-FC6+ANOVA+SVM-L achieved a mean accuracy of 97.8 with an SD of 2.8% and a mean F1 measure of 97.3 with an SD of 3.6%.

Similarly, for the Poland dataset, the most optimal combination of CNN and classifier in the Alpha band is the interconnection approach of AlexNet-FC6+ANOVA+SVM-L achieved a mean accuracy of 96.5% with an SD of 3.6% and a mean F1 measure of 96.4% with an SD of 3.8%, representing the highest accuracy and overall performance metrics from Table 4.8. Despite reasonable performance in some cases, LDA is far from achieving high performance, as with the case of AlexNet-FC7+ANOVA+SVM-L for the γ band.

The performance difference between the two models is minor, which made the GoogleNet interconnection more time-consuming than the model with AlexNet-FC6. This is reflected in Figure 4.3, which presents a comparison of time consumption.

Additionally, the study tested the exclusion of ASR during Pre-processing and ANOVA from the analysis; the model attained an accuracy of 59.5%. The resulting lower accuracy basically proved the efficiency of ASR and ANOVA.

Second, feature selection using ANOVA clearly improved the model performance in finding relevant patterns, especially in the Alpha bands; see Figure 4.4.

These results confirm that the Alpha band is the most informative within the Iraq and Poland datasets, with SVM-linear showing notably high results. This also points to the fact that previous research findings have shown Alpha band activity to be highly informative in the detection of ASD (Edgar et al., 2015), and the model is effectively capturing this information. In (Han et al., 2023), it has been shown that alpha-band activity in the posterior brain area was significantly suppressed in the TD group after looming stimuli, while no changes were present in the ASD group. Overall, the findings demonstrate that using ANOVA further improves performance while reducing time consumption spatially with SVM-L as depicted in Figure 4.3 and Figure 4.4.

This approach presented ASR in the Pre-processing stage along with AlexNet-FC6+ANOVA+SVM-L classifiers combined, which gives the maximum accuracy with reduced SD in both datasets for alpha band.

The main differences in the performance and interconnection model in Iraq and Poland datasets are explained by different Pre-processing methods; thus, device differences contributed to the differing results between the datasets, for example (Wei et al., 2023).

ANOVA works best on linear or approximately linear data. Since our study uses linear classifiers, namely SVM-L and LDA, ANOVA is in line with the basic assumption of these methods. For non-linear relationships, one might consider other means of feature selection, but ANOVA often provides a great trade-off between simplicity and interpretability versus performance for linear data.

Figure 4.3 presents the time efficiency of various interconnection models. Indeed, the most important insights provided by the heatmaps are: first, SVM-L always outperforms LDA, taking less time per image, regardless of which feature set is employed. After applying feature selection-choosing the best 50 features-processing time decreases for both classifiers, but the relative reduction is higher for SVM-L. Among the feature sets, GoogleNet (144 layers) requires the most time, suggesting higher computational complexity compared to AlexNet (25 layers) (e.g., FC6, FC7, and FC8). The latter three feature sets exhibit similar time consumption with only minor differences, indicating comparable computational loads.

Table 4.7. The results of the proposed method obtained by Iraq dataset (mean ± SD)%.

CNN Name	I/P size	Fc name	O/P length	ANOVA		ML - Classifier Name									
						SVM-linear					**LDA**				
						Delta	Theta	Alpha	Beta	Gamma	Delta	Theta	Alpha	Beta	Gamma
AlexNet	227 × 227 × 3	FC6	4096	Select best 50 features	**Accuracy**	95.2±3.4	96.9±3.1	97.8±2.8	93.8±4.1	90.9±3.4	87.3±5.1	92.1±5.4	92.2±4.7	86.4±8	77.6±11.4
					Sensitivity	88.8±8	93.3±7.5	95.5±6.6	85.5±9.6	89.4±9.1	79.4±10.9	91.1±6.8	92.8±10.4	87.2±13.1	78.3±16.7
					Specificity	100±0	99.5±1.8	99.5±1.8	100±0	92±5.7	93.3±5.7	92.9±10.2	91.8±8.1	85.8±11.5	77±13.7
					Precision	100±0	99.5±2.2	99.5±2.2	100±0	90.2±6.6	90.6±7.5	92.2±10.7	90.7±8.5	83.6±12.1	73.1±13
					F1 measure	93.9±4.7	96.1±4	97.3±3.6	91.9±5.5	89.3±4.3	84±7.2	91±5.4	91±5.6	84.5±9.6	74.7±12.8
		FC7	4096		**Accuracy**	95.7±3	97.3±2.8	97.7±3.6	93.5±4.7	93.5±4.7	81.9±8.8	95.7±3	96.1±3.4	84.5±7.5	73.5±9.3
					Sensitivity	91.1±7.7	93.8±6.7	94.7±8.5	86.1±9.4	91.1±7.7	77.2±11.6	91.6±7	93.1±6.3	85.5±14.9	72.2±15.9
					Specificity	99.1±2.5	100±0	100±0	99.1±2.5	95.4±6.3	85.4±11.7	98.7±3	98.5±4.3	83.7±10.6	74.5±13.6
					Precision	99±3	100±0	100±0	98.7±3.8	94.3±7.6	81.2±12.9	98.4±3.8	98.2±4.9	81.2±10.4	69.2±12.2
					F1 measure	94.6±3.9	96.7±3.6	97.1±4.7	91.7±6.1	92.3±5.4	78.6±10.1	94.7±3.8	95.4±4	82.1±9.7	69.7±11.3
		FC8	1000		**Accuracy**	94±4.8	96.4±3.4	97.1±2.7	90.4±3.4	86.6±7.8	86.6±9.7	94.2±4.7	94.5±4.4	80.4±7.5	81.6±8.6
					Sensitivity	86.1±11.3	91.6±7.9	93.4±6.5	87.2±6.5	79.4±15.4	84.4±13.6	92.7±8.2	93.1±7.05	76.6±9.4	80±14.6
					Specificity	100±0	100±0	99.9±0.8	92.9±4.8	92±7.8	88.3±12.2	95.4±5	95.6±7.5	83.3±14.8	82.9±11.6
					Precision	100±0	100±0	99.9±1	90.6±6	89±10.2	85.7±13.7	94.1±6.5	95.1±8	80.5±14.3	79.4±12.2
					F1 measure	92.1±6.6	95.4±4.4	96.4±3.5	88.6±4.2	83±10.8	84.4±11.4	93.2±5.7	93.7±4.9	77.4±7.2	78.6±10
GoogleNet	224 × 224 × 3	loss3-classifier	1000		**Accuracy**	92.6±4.2	95.7±3.4	**98 ±2.3**	92.3±3.2	73.3±8	77.8±5.8	86.1±8.1	90±5.5	81.6±7.1	55.7±8.8
					Sensitivity	86.6±11.1	92.2±7.2	**95.5±5.5**	91.1±6.8	68.3±15.8	72.2±15.9	79.4±17.3	90.6±8.5	83.3±9.1	53.3±19.6
					Specificity	97±4.8	98.3±3.4	**100±0**	93.3±6.3	77±11.1	82±10.2	91.2±5.7	89.5±9.3	80.4±11.2	57.5±16.1
					Precision	96.4±5.8	97.8±4.3	**100±0**	91.9±7.3	70±9.5	76.8±10.3	87.1±8.4	87.8±9.2	77.2±9.9	48.6±12.2
					F1 measure	90.6±5.7	94.7±4.2	**97.6±2.9**	91.1±3.6	68.1±10	72.9±9.3	82.2±12.1	88.6±5.9	79.7±7.2	49.5±13.3

Table 4.8. The results of the proposed method obtained by Poland dataset (mean ± SD)%.

CNN Name	I/P size	Fc name	O/P length	ANOVA		ML - Classifier Name									
						SVM-linear					**LDA**				
						Delta	Theta	Alpha	Beta	Gamma	Delta	Theta	Alpha	Beta	Gamma
AlexNet	227 × 227 × 3	FC6	4096	Select best 50 features	**Accuracy**	87.5±8.2	93.5±5.8	**96.5±3.6**	90.5±6.2	90.7±4.4	79.5±8.75	80.5±8.8	90±5.5	81.8±6.2	88.1±6.8
					Sensitivity	92±13.4	93.5±6.3	**97±6.5**	95±6.2	94±6.3	76.5±14.1	81.5±12	94.7±8.7	77.5±12.9	93.7±6.5
					Specificity	83±13.4	93.5±8.9	**96±5.9**	86±11.5	87.5±8	82.5±14.8	79.5±11.3	85.2±10.6	86.2±9.2	82.5±10.5
					Precision	85.7±9.7	94±7.9	**96.4±5.2**	88.1±9.6	88.8±6.6	83.1±11.8	80.4±9	87.5±8.2	85.8±8.3	84.8±8.1
					F1 measure	87.7±9.4	93.5±5.6	**96.4±3.8**	91±5.7	91±4.2	78.5±9.6	80.5±8.8	90.4±5.2	80.6±7.4	88.8±6.2
		FC7	4096		**Accuracy**	87.2±7.7	94.7±4.6	94.8±4.6	85.7±6.3	89.5±5.6	76.5±9	82.7±7.5	83.7±6.9	70±11.2	88.2±9.2
					Sensitivity	97±5.4	98.5±4.1	97.5±6.2	86±9.7	89±7.5	83±11.3	82±14.4	84±13.7	70.5±21.6	85.5±14.2
					Specificity	77.5±14.8	91±9.2	92±7.9	85.5±11.2	90±10.2	70±15.7	83.5±12.3	83.5±12.8	69.5±19.4	91±9.2
					Precision	82.410.3	92.3±7.5	92.9±6.7	86.6±9.1	90.8±8.7	74.7±10.5	84.6±9.5	85±8.7	71.5±15.8	90.89.8
					F1 measure	88.6±6.3	95±4.2	94.9±4.6	85.7±6.4	89.5±5.3	77.9±8.1	82.2±8.2	83.4±7.16	68.9±14.6	87.5±10.3
		FC8	1000		**Accuracy**	84.2±6.7	87.7±7.7	91.5±5.6	80.7±7.6	74.5±9	71.2±10	76±7.7	82±9	61.5±10.4	62.5±11.1
					Sensitivity	95.5±7.1	85±11.9	88±8.4	79±13.3	70.5±14.3	72±17	79±14.7	81±17.3	56±14.9	57±20.4
					Specificity	73±14.7	90.5±9.7	95±8.8	82.5±12.5	78.5±14.2	70.5±19	73±15.5	83±11.9	67±20.6	68±17.7
					Precision	79.2±9.5	90.6±9.1	95.3±7.7	83.3±10.7	78.2±13	73.3±13	76.1±10.8	83.8±9.9	65.2±16.6	65.2±12.1
					F1 measure	86±5.5	87.1±8.3	91.1±5.8	80.1±8.3	73±10.6	70.8±11.7	76.4±8.2	80.9±12.3	58.6±13	58.9±13.9
GoogleNet	224 × 224 × 3	loss3-classifier	1000		**Accuracy**	77.5±5.7	87.5±5.9	89.2±6.1	80±8.4	87.2±7.5	60.7±10.7	72.2±8.4	89.7±8.4	63±11.3	69.2±11.5
					Sensitivity	86.5±12.9	93.5±7.3	95±7.2	86.5±12.9	90±11.4	54±20	74±13.9	92±9.4	65±18.7	72±19.8
					Specificity	68.5±10.8	81.5±13	83.5±12.8	73.5±15.8	84.5±12.1	67.5±18.3	70.5±17.2	87.5±12.5	61±16.6	66.5±17.9
					Precision	73.9±5.8	84.7±9.6	86.4±9.7	77.9±9.9	86.4±10.1	63.3±11.9	73.5±12.1	88.9±10.2	62.8±12.3	69.5±13.2
					F1 measure	79±6.4	88.3±5.1	90±5.3	81.1±7.9	87.5±7.6	56.4±14.7	72.5±8.3	90±8	62.7±14	69.1±13.3

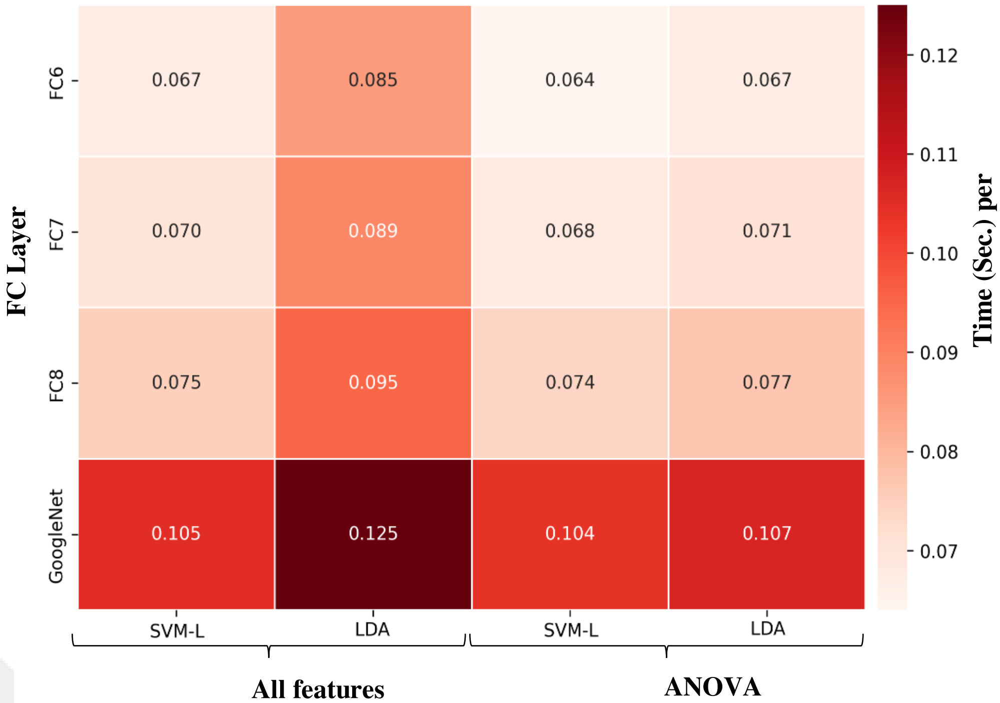

Figure 4.3. Illustrates the time (Sec.) consuming of each interconnection model with and without ANOVA / TBM sample.

The primary enhancements achieved through ANOVA and ASR of both datasets classified alpha band TBMs with proposed interconnection. Figure 4.4 illustrates the significant effects of ANOVA enhanced the mean value of the accuracy by 0.9% and reduced the SD by 0.1% of the alpha band using GoogleNet+SVM-L. Similarly, for the Poland dataset, ANOVA enhanced the mean value of the accuracy by 6.5% and reduced the SD by 4.3% of the alpha band using AlexNet-FC6+SVM-L and this connection is faster than another interconnection model.

The accuracy of ASD detection using the Poland dataset demonstrated a notable mean improvement of approximately 10.4% and the SD reduced by 14.4% compared to (Rogala et al., 2023). These accuracy enhancement rates highlight the success of the method and suggest its potential for early ASD diagnostics. The diagnostic evaluation of ASD levels may be prone to errors; several problems in connecting the EEG electrodes and sleepless nights of the participant are certain disadvantages.

A comparison of the results based on the Iraqi dataset showed that the second proposed method outperformed the first (See Figure 4.4), with an average increase in accuracy of 6.3% and a reduction in standard deviation by 4.7%. These findings highlight the effectiveness of the second method.

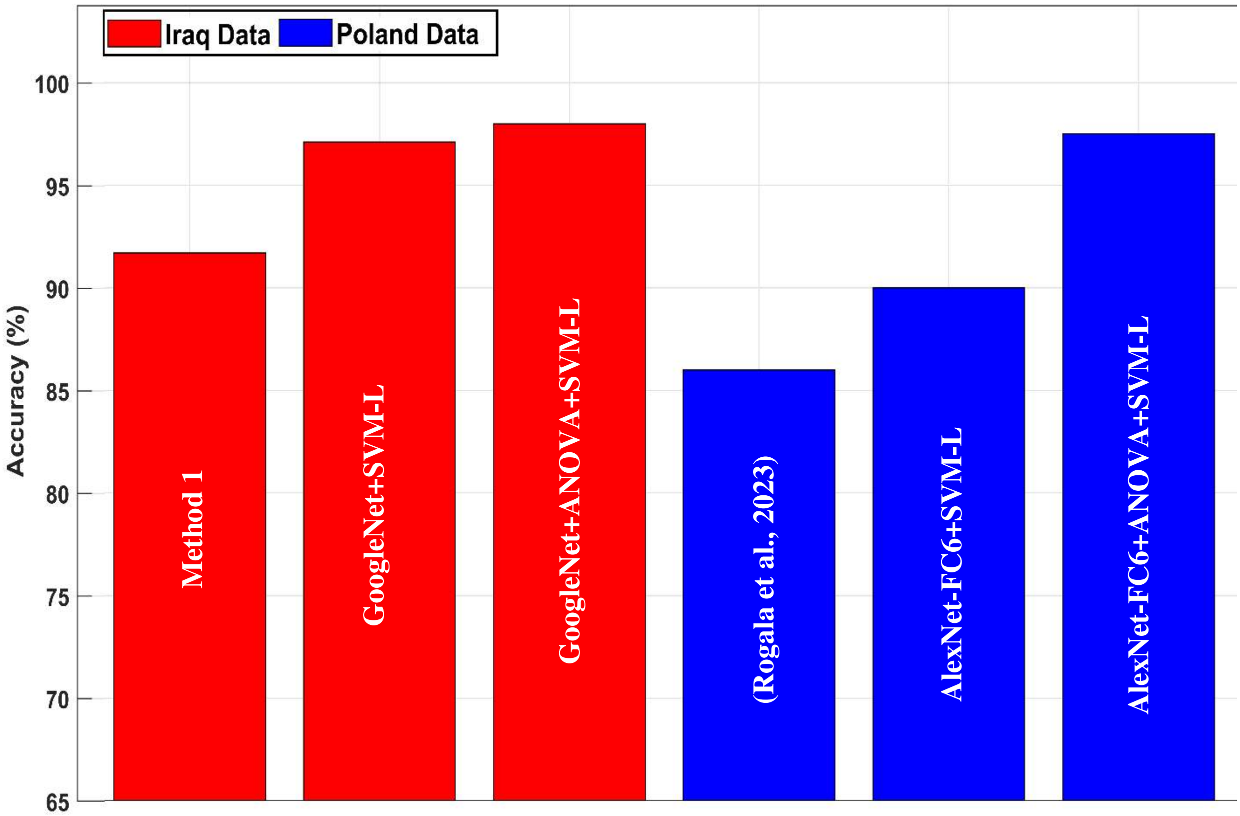

Figure 4.4 The performance of the proposed interconnection models shows the impact of ANOVA.

However, the proposed approach has some merits: it is efficient and simple. Accuracy scores were computed based on real data and an artifact/noise type. The results confirmed that the proposed approach was effective in the detection of autism in sleeping individuals.

This methodology was followed to ensure that the classification of alpha bands was done in a realistic and practical manner for TBM. The proposed method fully automated ASD detection using real EEG data that usually suffered from challenges involving artifacts, which include blinking and muscle activity, and different recording times.

Our results also indicated that the maximum feature separation for the TD children and the children with ASD was at the alpha frequency. This agrees with recent publications where it is reported that alpha frequency can be considered as discriminatory between ASD and TD. Here are a few studies that support (Lefebvre, A. et al., 2018; Dickinson et al., 2018).

Table 4.9 compares the obtained performance outcomes of our proposed method (2) with the accuracy of the ten, compared to other works. The results highlight the superior performance of our proposed method.

The differences in dataset quality, network architecture, feature representation, and classifier interaction led to AlexNet-FC7+ANOVA+SVM-L performing best for Poland, while GoogLeNet+ANOVA+SVM-L excelled with the Iraq dataset

Table 4.9. Comparison of the accuracy's Method 2 with different studies.

Source Date	Method of test	Dataset size	Average age years	Method	Accuracy (SD) %
(Grossi et al., 2017)	DSM-V ADOS	ASD: boys (13) + girls (2) TD: boys (4) + girls (6)	ASD: 10.4 years TD: 9.2 years	MS-ROM/I-FAST, TWIST + ANN	92.8
(Husna et al., 2021)	Two Dataset ABIDE (I&II)– images		ASD: 5-64 years TD: 5-64 years	FMRI + CNN (ResNet-50, VGG-16)	63.4 To 87
(Singh et al., 2024)	Not available		ASD: 18- 68 years TD: 18- 68 years	Spectral features + CSTO-DRN + Statistical	88.6
(Alhassan et al., 2023)	Clinical psychologists diagnostic criteria	ASD: total (15) TD: total (15)	ASD: 31±6 months TD: 29±4 months	Energy efficient ML	96
(Rogala et al., 2023)	DSM-V PANS medical history professionals clinical	ASD: boys (12) + girls (6) TD: boys (12) + girls (6)	ASD: 3.92±1.38 years TD: 3.84±1.24 years	Statistical and spectral brain connectivity + ciPLV+PLV+ML	83 (14) To 86 (18)
(Kang et al., 2020)	Not available	ASD: total (58) TD: total (50)	ASD: 3-6 years TD: 3-6 years	PSD + AOI +mRMR + SVM	91.43
(Sheikhani, 2008)	IQ Exam DSMIV-TR	ASD: boys (13) + girls (2) TD: boys (7) + girls (4)	ASD: 6-11 years TD: 6-11 years	Spectrogram (STFT) + QEEG Statistical analysis + classification	92.3
(Wadhera, 2024)	Not available	ASD: total (30) TD: total (30)	ASD: 8-20 years TD: 7-20 years	Kernel-based discriminant correlation analysis +mRMR + SVM	92

Source Date	Method of test	Dataset size	Average age years	Method	Accuracy (SD) %
(Sriramakrishnan et al., 2024)	ABIDE dataset Not available	ASD: total (1000) TD: total (1000)	ASD: 2-25 years TD: 2-25 years	Pelican Remora Optimization Algorithm + Deep Convolutional Neural Network	95.8
(Ghoreishi et al., 2021)	Not available	ASD: total (34) TD: total (23)	ASD: 4 to 8 years TD: 4 to 8 years	EEG-2 Channels C3 and C4 Polar features of delayed phase space (mean,variance,mode) SVM	81.9
Our	medical history professionals clinical DSM-5-TR GARS CARS	ASD: boys (18) + girls (4) TD: boys (18) + girls (12)	ASD: 4.85 ± 1.5 years TD: 5.9 ± 3.5 years	Pre-processing + GoogLeNet + ANOVA + SVM-L	98 (2.3)
Our	dataset in (Rogala et al., 2023), (Poland dataset) “ALLEEG.data”-2 sec-Clean data			Pre-processing + AlexNet-FC6 + ANOVA + SVM-L	96.4 (3.6)

This comparison of method 2 to prior ASD classification studies based on EEG data showed that the groups compared were highly varied, as were the classifiers and feature selection methods. A survey of recent publications indicated that most studies had groups with wide age ranges, or otherwise showed differences between TD and ASD subjects. All experiments were carried out in a closely monitored laboratory environment while the participants were at rest to minimize the effects of artifacts. The results indicated that the accuracy of the proposed method was better compared to the results of other methods.

The study (Al-Saffar et al., 2022) shows that standard CNNs usually need a large amount of data during training to obtain reasonable accuracy, as illustrated in Figure 4.5. On the other hand, Artificial Neural Networks (ANNs) and SVMs are more effective when used with a small number of samples. As it is widely understood, neural networks such as CNNs are voracious consumers of data. Nevertheless, these models can be improved by methods such as data augmentation and transfer learning, which allow to get the maximum out of a small dataset (Brigato et al., 2020). On the other hand, SVMs and ANNs are usually more effective with small datasets because of their simplicity and do not need large data sets to develop good models (Alzubaidi et al., 2021; IBM, 2023). Finally, it is possible to train CNN architectures even with limited data but in general, traditional ML architectures are more suitable for such scenarios because they are less complex and need less data for training (Brownlee, 2019). To build on these strengths, the proposed method is CNN + ANOVA + ML to deliver high performance with limited data. The standard AlexNet model yielded a maximum accuracy of 93.6% on the Iraq dataset, and our proposed approach enhanced this accuracy, thus proving the efficiency of these techniques.

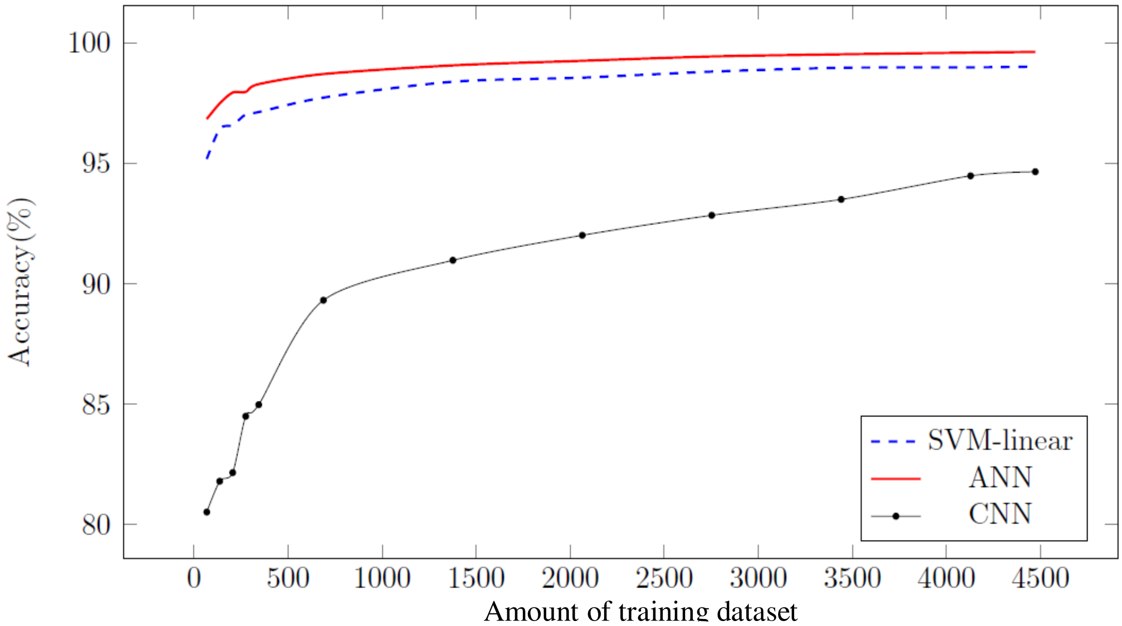

Figure 4 5. The Accuracy of ANN, SVM, and CNN models as a function of the training dataset size (Al-Saffar et al., 2022).

4.4. General Findings and Comparison

The overall outcomes of the two methods in your study demonstrate the efficiency of the EEG-based automated ASD detection, but they also show that each of the methods has its advantages depending on the band under consideration. The first method, Brain Hemisphere Energy Analysis, was most accurate in the Theta band while the second method, EEG TBMs and DL, was most accurate in the Alpha band. These results can be explained by the properties of each frequency band and the information they convey about brain activity, as well as by the differences in the methodological approaches. In this thesis, we achieved the highest accuracy for detecting ASD using the Alpha and Theta bands with Methods 1 and 2, respectively. This aligns with (Larrain-Valenzuela et al., 2017), used group differences were found in alpha power in the occipital cortex and theta power in the left premotor and right prefrontal cortex. Reduced theta power was related to autistic symptoms, which indicates that the oscillatory activity during working memory may be recruited abnormally in ASD, which may be related to the physiopathology of the disorder.

Method 1: Brain Hemisphere Energy Analysis and the Theta Band. Theta band (4–8 Hz) is connected with memory function, affect regulation and attentional modulation, functions that have been reported to be impaired in individuals with ASD. The first of these, which concerns the distribution of energy across the left and right hemispheres, is well represented by these methods. The method compares energy metrics (maximum, mean, minimum) with different overlapping sliding window ratios and reveals asymmetric patterns in the Theta band.

Theta Band Activity in ASD, this study has shown that ASD participants had different theta band responses during social cognition and emotion processes. For instance, a study comparing in children with ASD and normal children in a reward processing task obtained significantly lower theta activity during reward anticipation in children with ASD than in normal children (Stavropoulos et al., 2018). Right Hemisphere Involvement, brain and cognitive science has discovered that the right hemisphere is involved in social cognition and specifically emotions; for instance, the right inferior frontal gyrus (RIFG). The enhancement of social cognition after intermittent theta burst stimulation over the RIFG in participants diagnosed with ASD underlines the role of this region in social cognitive processes (Ni et al., 2024). Hemispheric Energy Asymmetry, hemispheric energy asymmetry is a concept that compares energy values in the left and right hemispheres. The analysis of the recorded EEG demonstrated changes in the patterns of hemispheric asymmetry in ASD subjects, with some reports suggesting that ASD subjects have greater power in the left hemisphere than in the right in a broad frequency range (Jun Wang et al., 2013). This could explain why the first method which is based on the concept of hemispheric energy asymmetry yields the best results in this Theta band.

The Alpha band which ranges between 8-12 Hz is believed to have connection with sensory; information processing, executive working towards control of thought process and being the resting state of the brain. The second method involves using TBMs as inputs to CNN architectures such as AlexNet, GoogLeNet and addresses spatial patterns of brain activity. TBMs can show regional differences in Alpha activity that have been described as biomarkers in ASD (Prany et al., 2022). The Alpha band is especially useful in identifying the disruptions in the connectivity of the default-mode network (DMN) that is impaired in people with ASD. The fact that TBMs can depict spatial brain activity over the scalp may be the reason why the second method performs well in the Alpha band.

The first method, based on the identification of left and right channels, is focused on the differentiation of the brain's activity in the two hemispheres. This approach is particularly useful for detecting asymmetries, which are present in ASD and most evident in the Theta band. For instance, neuroimaging investigations have suggested that in ASD there is increased right hemisphere activation which is or social, language delay and emotional processing (Floris et al., 2021). This focus on left-right hemispheric energy metrics is in harmony with these findings.

The second method, using TBMs, offers a more extensive spatial distribution of brain activity. TBMs coordinate activity across channels to construct a global map of neural activity. Although this approach is not as specific to hemispheric differences, it is superior at detecting spatial features that are associated with ASD, especially in the Alpha band. The Alpha band is important for the analysis of aberrant Sensory Integration (SI) and DMN connectivity which TBMs can reveal with the help of spatial mapping.

While the methods are based on different characteristics of the EEG signals (hemispheric asymmetry vs spatial distribution), the two are related. Differences in energy between the two hemispheres in the Theta band (Method 1) may be associated with specific spatial patterns in TBMs

(Method 2). For instance, areas with increased activity in the right hemisphere may be associated with the hot spots on TBMs in the same frequency range.

4.5. Discussion

The results of this thesis show that both EEG-based methodologies have the potential for the early identification of ASD and reveal the advantages and differences of the two methods. Both methods demonstrated high classification accuracy, which utilized the characteristics of EEG signals, indicating that spatial and temporal analysis can complement each other in the study of neural activity in ASD.

Method 1: The results demonstrate that the selection of the energy window, stride, and SVM kernel significantly impacts classification performance. The θ band emerges as the most effective for differentiating between ASD and TD groups, particularly with shorter strides (greater overlap), suggesting its ability to capture neural oscillations most closely associated with ASD.

SVM with a linear kernel outperforms non-linear kernels (RBF and Quadratic) under conditions with small strides and maximum energy windows. This highlights the effectiveness of the linear kernel in well-defined feature spaces, such as the θ band.

However, non-linear kernels, such as RBF and Quadratic, provide valuable insights across various frequency bands. While the θ band remains the most informative, the δ band also shows potential, particularly with non-linear kernels. This suggests that more complex decision boundaries are better suited to capturing the EEG patterns associated with ASD.

As shown in Table 4.8, comparisons indicate that higher levels of windowing improve classification performance across all SVM kernels. Greater overlap (smaller strides) enhances feature extraction, resulting in better ASD detection. Conversely, less overlap (larger strides) significantly decreases performance across nearly all frequency bands.

When compared to existing studies, our results are competitive. For instance, the current study's mean accuracy of 91.7% with an SD of 7% is higher than the accuracy reported in (Singh et al., 2024) (88.6%) and comparable to the range reported in (Rogala et al., 2023) (83–86% with SD of 14–18). The use of SVM with energy features, combined with windowing techniques, has proven to be an effective approach for differentiating between ASD and TD.

Our classification performance also surpasses previous studies, such as those using statistical and spectral features combined with methods like CSTO-DRN, which reported accuracies ranging from 83% to 86% in (Rogala et al., 2023). Furthermore, studies employing fMRI and CNN-based architectures, such as VGG16 and ResNet50, achieved accuracies between 63.4% and 87% in (Husna et al., 2021). These comparisons highlight the effectiveness of the proposed method, particularly the application of SVM with energy features, windowing strategies, and high overlap ratios for early ASD detection.

Method 2: This study focuses on the possibility of improving the early detection of ASD by using EEG-based methods integrated with ML and DL. In particular, the presented findings revealed that the alpha band reflects the differences between ASD and TD groups in a most significant manner. This is in accordance with previous studies that have established that alpha band activity is essential in neural connectivity and cognition. The significant increase in the accuracy observed in both datasets, Iraq, and Poland demonstrates the efficiency of the proposed approach and pipeline consisting of preprocessing step, a feature extraction step, and the ML classification step. In preprocessing using ASR, the quality of data was enhanced with the removal of noise and artifacts to greatly improve feature extraction. The combination of CNN-based feature extractors like AlexNet and GoogLeNet with feature selection methods like ANOVA improved the classification accuracy. The highest accuracies were obtained in the alpha band, where GoogleNet + ANOVA + SVM-L provided 98% for the Iraq dataset, and AlexNet-FC6 + ANOVA + SVM-L provided 96.5% for the Poland dataset. These results support the use of the alpha band as a discriminative feature for ASD diagnosis.

Finally, in EEG Topographic Mapping and DL, the spatial properties of EEG signal were further explored using TBMs as inputs to state-of-art DL networks including AlexNet and GoogLeNet. The emphasis on the Alpha band was especially beneficial because this frequency is associated with sensory processing and DMN coupling. Alpha band perturbations are established in ASD, indicating variations in cortical connection and sensory input. Extension of the analysis of variance to the feature selection process, followed by the use of SVM-L classifiers allowed for the reduction of the dimension space while improving classification efficiency. The spatial representation offered by TBMs was essential for the detection of cortical abnormalities, and therefore, this approach is ideal for the identification of neural alterations linked to ASD. However, its computational requirements especially when using GoogLeNet make it unsuitable for real-time or low operations environments. The author also found that the specific configurations of AlexNet were less computationally intensive while maintaining the same level of accuracy.

Surprisingly, the alpha band was stable in terms of performance across every dataset highlighting its utility in identifying neural patterns corresponding to ASD. The ability of ANOVA in identifying the most important features underlines its significance in the elimination of computational costs without much impact on the classification performance. Furthermore, the study showed that the SVM-L classifier was more accurate and computationally efficient than LDA, which is why it is more suitable for use in practice.

However, the presented study demonstrates several restrictions that have to be discussed. The calculation of methods is limited with the relatively small sample size and induced-sleep EEG recordings. Further, the analysis of two data sets used in the present study might not reflect the full range of the ASD phenomenology in other populations. Further studies should examine these methods on a larger sample of participants and of different age and gender, and future research should also compare the diagnostic accuracy of awake-state EEG in ASD.

This study offers good support for the use of alpha band activity in EEG-based ASD identification. Altogether, the identification of the CNN-based feature extractor, the application of the ANOVA statistical tool for selecting the most discriminative features, and the SVM-L classifier make it possible to provide an efficient early diagnostic method for ASD. Possible developments in this area in the future include data collection with bigger sample sizes, other DL structures, as well as utilization of real-time systems for constant tracking and use in clinical practice.

This study demonstrates the potential of EEG-based methodologies for the early identification of ASD by leveraging the spatial and temporal characteristics of neural activity. Both proposed methods yielded high classification accuracies, showcasing their value in enhancing diagnostic processes. Each method had unique strengths, offering insights into complementary aspects of ASD-related neural patterns.

Both methods demonstrated high potential for early ASD detection, with Method 1 excelling in temporal analysis and Method 2 providing spatial insights through deep learning. The combination of CNN-based feature extraction, ANOVA feature selection, and SVM classifiers proved effective in creating robust diagnostic tools. These methodologies lay a strong foundation for the development of automated, cost-effective, and non-invasive diagnostic systems for ASD.

5 CONCLUSIONS

Assessing small datasets using confusion metrics presents a common challenge in clinical and research settings. The limited size of the dataset (52 samples) may pose challenges for training a robust ML model, particularly in medical signal analysis. However, this dataset is comparable to those used in similar research studies.

Method 1: This study identifies the best parameters for classifying ASD versus TD groups as the θ band with a maximum energy window, small stride, and high overlap, achieving a mean accuracy of 91.7% with an SD of 7% with the SVM-Linear classifier. While the δ band shows good performance in mean energy windows, it does not surpass the performance of the θ band.

The highest overlap ratios, combined with the maximum energy window, produce the best outcomes for early ASD detection, particularly when using the θ band, which delivers the highest accuracy and sensitivity in this study. The use of non-linear SVM kernels further enhances classification performance, and the δ band also shows promise under certain conditions. However, the θ band remains the most accurate across all decomposed EEG bands. These results indicate that energy features from both the left and right hemispheres of the brain can be used to detect ASD, which holds significant potential for future medical applications.

The main contribution of this study is the development of a novel EEG-based method for diagnosing ASD by analyzing energy differences between the left and right brain hemispheres. It demonstrates that the θ band, combined with a maximum energy window and high overlap, achieves the highest classification accuracy (91.7%) using a linear SVM. The study underscores the importance of windowing parameters and kernel selection, offering a reliable and cost-effective approach for early ASD detection. This method also provides a foundation for future advancements using more sophisticated ML techniques.

Method 2: The approach frequently results in inconsistent, unstable, and less generalizable outcomes due to dataset scarcity. Integrating CNN with classical ML to classify low-volume datasets is vital to address this issue, especially when supplemented with explanation methods. The proposed method leveraged two datasets and efficiently identified ASD by combining diverse methodologies, which enhanced the reliability of the results (A.J.Al-Sammarraie, 2024.; Al-Saffar et al., 2023).

The Pre-processing aimed to down-sample raw EEG data and reject unwanted frequencies. The ASR was crucial in automatically rejecting large artifacts, such as movements and muscle activity. This study used SVM-L classifiers integrated with a CNN model (AlexNet) and extracted a deep features from FC6 and reduced dimensionality to 50-D using ANOVA combining SVM-L yielded the best accuracy and stability, specifically in the alpha band, and achieved > 96% accuracy in both datasets. ANOVA feature selection combined with SVM-L emerges as the fastest approach, particularly when using FC6 features, becoming the most efficient option in terms of the consumption of time. The study itself showed the effectiveness of fusing DL with ML techniques for screening ASD in children.

This thesis highlights the potential of EEG-based methodologies for the early detection of ASD. Two complementary approaches were explored, each addressing unique aspects of EEG signal processing and analysis. The first method focused on energy differences between the left and right hemispheres of the brain, leveraging the theta band as a key discriminator for ASD. The second method utilized TBMs processed through deep learning architectures, particularly AlexNet and GoogLeNet, with the alpha band emerging as the most informative frequency range. Both methods demonstrated high classification accuracy and highlighted the importance of robust preprocessing techniques like ASR and advanced feature extraction strategies. Together, these methodologies offer a reliable foundation for the development of non-invasive, cost-effective diagnostic tools, potentially bridging the gap between research and clinical application.

Future work in this field should focus on addressing the limitations identified in this study to improve the applicability and effectiveness of EEG-based ASD diagnostic systems. A key priority is the collection of larger and more diverse datasets, encompassing different age groups, genders, and cultural contexts, to enhance model generalizability and reliability. The development of real-time diagnostic systems for clinical and educational settings could enable immediate ASD screening and intervention planning, bridging the gap between research advancements and practical applications. Integrating EEG data with other physiological signals, such as heart rate, may provide a more holistic assessment of ASD. Additionally, optimizing DL models to create lightweight and computationally efficient architectures will facilitate deployment in resource-constrained environments. Exploring less commonly studied frequency bands may uncover further insights into ASD-related neural activity, while longitudinal studies could establish links between EEG patterns, developmental trajectories, and intervention outcomes. Tailoring diagnostic tools to specific age groups, cultural contexts, and clinical requirements will maximize their accessibility and effectiveness. Furthermore, enhancing model interpretability should be a priority, ensuring that diagnostic outputs are both accurate and comprehensible for clinicians. These future directions will help to advance the field, creating robust, efficient, and widely applicable diagnostic tools for ASD detection.

A major weakness of this study is the relatively small dataset size; however, it is acceptable when compared to other studies. This could affect the generalization of the findings especially with regard to the differences in the EEG recording devices in the Poland dataset, participants' characteristics and data preprocessing methods between the Iraq and Poland datasets. 120 epoch were performed on both the training and testing datasets. The training and testing samples were shuffled for each epoch, additionally, the LDA and SVM-L model was trained with 5-fold cross-validation per epoch to ensure the robustness and generalization of the results were collected. We then averaged the results and calculated the means and the SD to achieve more accurate outcomes.

A primary limitation of this study is the relatively small dataset size, although it remains comparable to other studies in the field. This limitation may affect the generalizability of the findings. A total of 120 epochs were conducted on both the training and testing datasets, with samples shuffled for each epoch. Additionally, three different SVM kernels were trained using 5-fold cross-validation per epoch to ensure robustness and generalizability. The results were averaged, and the means and SD were calculated to enhance accuracy. This rigorous approach strengthens the practical relevance and reliability of our findings.

Another limitation involves the use of sedation in a pediatric population. Chloral hydrate, used as a sedative, introduces variables that can confound EEG interpretation. Many sedative agents can alter EEG patterns, potentially affecting signal analysis. For example, sedation may induce low-frequency high-amplitude activity, which can obscure or mimic some EEG characteristics (Samra et al., 1995).

REFERENCES

Akin, M., Kiymik, M. K., Arserim, M. A., & Turkoglu, I. (2000). Separation of brain signals using FFT and neural networks. *Proc. of Biyomut*, 161–164.

Al-Qazzaz, N. K., Sabir, M. K., Ali, S. H. B. M., Ahmad, S. A., & Grammer, K. (2021). Multichannel Optimization with Hybrid Spectral- Entropy Markers for Gender Identification Enhancement of Emotional-Based EEGs. *IEEE Access*, *9*, 107059–107078. doi: 10.1109/ACCESS.2021.3096430

Al-Qazzaz, N., Sabir, M., Ali, S., Ahmad, S. A., & Grammer, K. (2021). Electroencephalogram Brain Mapping for revealing the emotional changes over the brain regions using Entropy biomarker. *MDPI*, 9834. doi: 10.3390/entropy2021-09834

Al-Saffar, B., Al-Abbas, A. R., & Özel, S. A. (2023). A Comparative Study on the Recognition of English and Arabic Handwritten Digits Based on the Combination of Transfer Learning and Classifier. *Lecture Notes in Networks and Systems*, *573 LNNS*, 95–107. doi: 10.1007/978-3-031-20429-6_10

Al-Saffar, B., Arica, S., & Tangolar, S. (2022). Automatic counting of grapes from vineyard images. *Pakistan Journal of Agricultural Sciences*, *59*(3), 347–355. doi: 10.21162/PAKJAS/22.644

Alhassan, S., Soudani, A., & Almusallam, M. (2023). Energy-Efficient EEG-Based Scheme for Autism Spectrum Disorder Detection Using Wearable Sensors. *Sensors*, *23*(4). doi: 10.3390/s23042228

Alzubaidi, L., Zhang, J., Humaidi, A. J., Al-Dujaili, A., Duan, Y., Al-Shamma, O., Santamaría, J., Fadhel, M. A., Al-Amidie, M., & Farhan, L. (2021). Review of deep learning: concepts, CNN architectures, challenges, applications, future directions. *Journal of Big Data*, *8*(1). doi: 10.1186/s40537-021-00444-8

Autism Speaks. (2022). New Study Shows Increase in Global Prevalence of Autism. *Autism Speaks*. Retrieved from https://www.autismspeaks.org/science-news/new-study-shows-increase-global-prevalence-autism

Autism Spectrum Australia. (2024). At least 1 in 40 Australians are Autistic: New estimate by Aspect on World Autism. *ASA*. Retrieved from https://www.aspect.org.au/news/at-least-1-in-40-australians-are-autistic

Bah, A. O., & Arica, S. (2023). Classification of attempted hand movements from EEG signals using the Hadamard basis matching movement-related cortical potential. *2023 5th International Congress on Human-Computer Interaction, Optimization and Robotic Applications (HORA)*. doi: 10.1109/HORA58378.2023.10156763

Baio, J. (2014). Prevalence of autism spectrum disorder among children aged 8 years - Autism And Developmental Disabilities Monitoring network, 11 sites, United States, 2010. *MMWR Surveillance Summaries*, *63*(2). Retrieved from http://www.cdc.gov/mmwr/preview/mmwrhtml/ss6302a1

Balakrishnama, S., & Ganapathiraju, A. (n.d.). Linear Discriminant Analysis - a Brief Tutorial. *Compute*.

Banos, O., Galvez, J. M., Damas, M., Pomares, H., & Rojas, I. (2014). Window size impact in human activity recognition. *Sensors (Switzerland)*, *14*(4), 6474–6499. doi: 10.3390/s140406474

Baygin, M., Dogan, S., Tuncer, T., Datta Barua, P., Faust, O., Arunkumar, N., Abdulhay, E. W., Emma Palmer, E., & Rajendra Acharya, U. (2021). Automated ASD detection using hybrid deep lightweight features extracted from EEG signals. *Computers in Biology and Medicine*, *134*. doi: 10.1016/j.compbiomed.2021.104548

Bell, A. J., & Sejnowski, T. J. (1995). An information-maximization approach to blind separation and blind deconvolution. *Neural Computation*, *7*(6), 1129–1159. doi: 10.1162/neco.1995.7.6.1129

Bigdely-Shamlo, N., Mullen, T., Kothe, C., Su, K. M., & Robbins, K. A. (2015). The PREP pipeline: Standardized preprocessing for large-scale EEG analysis. *Frontiers in Neuroinformatics*, *9*(JUNE), 1–19. doi: 10.3389/fninf.2015.00016

Blum, S., Jacobsen, N. S. J., Bleichner, M. G., & Debener, S. (2019). A riemannian modification of artifact subspace reconstruction for EEG artifact handling. *Frontiers in Human Neuroscience*, *13*. doi: 10.3389/fnhum.2019.00141

Blume, J., Kahathuduwa, C., & Mastergeorge, A. (2023). Intrinsic Structural Connectivity of the Default Mode Network and Behavioral Correlates of Executive Function and Social Skills in Youth with Autism Spectrum Disorders. *Journal of Autism and Developmental Disorders*, *53*(5), 1930–1941. doi: 10.1007/s10803-022-05460-y

Brigato, L., & Iocchi, L. (2020). A close look at deep learning with small data. *Proceedings - International Conference on Pattern Recognition*, 2490–2497. doi: 10.1109/ICPR48806.2021.9412492

Bronzino, J. D. (1984). Quantitative Analysis of the EEG—General Concepts and Animal Studies. *IEEE Transactions on Biomedical Engineering*, *BME-31*(12), 850–856. doi: 10.1109/TBME.1984.325247

Brownlee, J. (2019). Impact of Dataset Size on Deep Learning Model Skill And Performance Estimates. *Machinelearningmastery.Com*, 1. Retrieved from https://machinelearningmastery.com/impact-of-dataset-size-on-deep-learning-model-skill-and-performance-estimates/%0A(accessed%0Aon%0A8%0AAugust%0A2019)

Cancer Research UK. (2015). Why is early diagnosis important? *Cancer Res. UK*, 3–5. Retrieved from http://www.cancerresearchuk.org/about-cancer/cancer-symptoms/why-is-early-diagnosis-important

Cao, J., Li, G., Shen, J., & Dai, C. (2024). IFBCLNet: Spatio-temporal frequency feature extraction-based MI-EEG classification convolutional network. *Biomedical Signal Processing and*

Control, *92*. doi: 10.1016/j.bspc.2024.106092

Castellanos, N. P., & Makarov, V. A. (2006). Recovering EEG brain signals: Artifact suppression with wavelet enhanced independent component analysis. *Journal of Neuroscience Methods*, *158*(2), 300–312. doi: 10.1016/j.jneumeth.2006.05.033

Chang, C. Y., Hsu, S. H., Pion-Tonachini, L., & Jung, T. P. (2020). Evaluation of Artifact Subspace Reconstruction for Automatic Artifact Components Removal in Multi-Channel EEG Recordings. *IEEE Transactions on Biomedical Engineering*, *67*(4), 1114–1121. doi: 10.1109/TBME.2019.2930186

Cheng, R., Zhao, Z., Hou, W. W., Zhou, G., Liao, H. T., Zhang, X., & Li, J. (2024). Machine learning algorithms for identifying autism spectrum disorder through eye-tracking in different intention videos. *Chinese Journal of Contemporary Pediatrics*, *26*(2), 151–157. doi: 10.7499/j.issn.1008-8830.2309073

Cristianini, N., & Shawe-Taylor, J. (2000). An Introduction to Support Vector Machines and Other Kernel-based Learning Methods. *An Introduction to Support Vector Machines and Other Kernel-Based Learning Methods*. doi: 10.1017/cbo9780511801389

De Cheveigné, A., & Arzounian, D. (2018). Robust detrending, rereferencing, outlier detection, and inpainting for multichannel data. *NeuroImage*, *172*, 903–912. doi: 10.1016/j.neuroimage.2018.01.035

De Melo, G. C., Castellano, G., & Forner-Cordero, A. (2024). A procedure to minimize EEG variability for BCI applications. *Biomedical Signal Processing and Control*, *89*. doi: 10.1016/j.bspc.2023.105745

Dehghani, A., Sarbishei, O., Glatard, T., & Shihab, E. (2019). A quantitative comparison of overlapping and non-overlapping sliding windows for human activity recognition using inertial sensors. *Sensors (Switzerland)*, *19*(22). doi: 10.3390/s19225026

Delorme, A, & Makeig, S. (2004). *EEGLAB - Open Source Matlab Toolbox for Electrophysiological Research*. Retrieved from http://sccn.ucsd.edu/eeglab/

Delorme, Arnaud, & Makeig, S. (2004). EEGLAB: An open source toolbox for analysis of single-trial EEG dynamics including independent component analysis. *Journal of Neuroscience Methods*, *134*(1), 9–21. doi: 10.1016/j.jneumeth.2003.10.009

Dickinson, A., DiStefano, C., Lin, Y. Y., Scheffler, A. W., Senturk, D., & Jeste, S. S. (2018). Interhemispheric alpha-band hypoconnectivity in children with autism spectrum disorder. *Behavioural Brain Research*, *348*, 227–234. doi: 10.1016/j.bbr.2018.04.026

Ding, H., Feng, P. M., Chen, W., & Lin, H. (2014). Identification of bacteriophage virion proteins by the ANOVA feature selection and analysis. *Molecular BioSystems*, *10*(8), 2229–2235. doi: 10.1039/c4mb00316k

Dong, H., Chen, D., Zhang, L., Ke, H., & Li, X. (2021). Subject sensitive EEG discrimination with fast reconstructable CNN driven by reinforcement learning: A case study of ASD evaluation.

Neurocomputing, *449*, 136–145. doi: 10.1016/j.neucom.2021.04.009

Dumont, R., & Willis, J. O. (2008). Gilliam Autism Rating Scale. *Encyclopedia of Special Education*, 975–976. doi: 10.1002/9780470373699.speced0926

Edgar, J. C., Heiken, K., Chen, Y. H., Herrington, J. D., Chow, V., Liu, S., Bloy, L., Huang, M., Pandey, J., Cannon, K. M., Qasmieh, S., Levy, S. E., Schultz, R. T., & Roberts, T. P. L. (2015). Resting-State Alpha in Autism Spectrum Disorder and Alpha Associations with Thalamic Volume. *Journal of Autism and Developmental Disorders*, *45*(3), 795–804. doi: 10.1007/s10803-014-2236-1

Faja, S., & Dawson, G. (2006). Early Intervention for Autism. *Handbook of Preschool Mental Health: Development, Disorders, and Treatment*, 388–416. Retrieved from http://ovidsp.ovid.com/ovidweb.cgi?T=JS&CSC=Y&NEWS=N&PAGE=fulltext&D=psyc5&AN=2006-10334-018 http://digitaal.uba.uva.nl:9003/uva-linker?sid=OVID:psycdb&id=pmid:&id=doi:&issn=&isbn=1593853130&volume=&issue=&spage=388&pages=388-416&date=2006&title=Handbook+

Falih, B. S., Gierz, Ł., & Al-Sammarraie, M. A. J. (2024). Fruit Classification By Assessing Slice Hardness Based on Rgb Imaging. Case Study: Apple Slices. *Journal of Applied Mathematics and Computational Mechanics*, *23*(3), 7–18. doi: 10.17512/jamcm.2024.3.01

Fan, C., Xie, H., Tao, J., Li, Y., Pei, G., Li, T., & Lv, Z. (2024). ICaps-ResLSTM: Improved capsule network and residual LSTM for EEG emotion recognition. *Biomedical Signal Processing and Control*, *87*. doi: 10.1016/j.bspc.2023.105422

Firat Ince, N., Arica, S., & Tewfik, A. (2006). Classification of single trial motor imagery EEG recordings with subject adapted non-dyadic arbitrary time-frequency tilings. *Journal of Neural Engineering*, *3*(3), 235–244. doi: 10.1088/1741-2560/3/3/006

Floris, D. L., Wolfers, T., Zabihi, M., Holz, N. E., Zwiers, M. P., Charman, T., Tillmann, J., Ecker, C., Dell'Acqua, F., Banaschewski, T., Moessnang, C., Baron-Cohen, S., Holt, R., Durston, S., Loth, E., Murphy, D. G. M., Marquand, A., Buitelaar, J. K., Beckmann, C. F., … Wooldridge, C. (2021). Atypical Brain Asymmetry in Autism—A Candidate for Clinically Meaningful Stratification. *Biological Psychiatry: Cognitive Neuroscience and Neuroimaging*, *6*(8), 802–812. doi: 10.1016/j.bpsc.2020.08.008

Fu, R., Cai, M., Wang, S., Wang, Y., & Jia, C. (2024). Exploring non-Euclidean relationships in EEG emotion recognition: A dynamic graph attention network. *Biomedical Signal Processing and Control*, *94*. doi: 10.1016/j.bspc.2024.106276

Fu, R., Tian, Y., Bao, T., Meng, Z., & Shi, P. (2019). Improvement Motor Imagery EEG Classification Based on Regularized Linear Discriminant Analysis. *Journal of Medical Systems*, *43*(6). doi: 10.1007/s10916-019-1270-0

Gaur, P., McCreadie, K., Pachori, R. B., Wang, H., & Prasad, G. (2021). An automatic subject specific channel selection method for enhancing motor imagery classification in EEG-BCI using correlation. *Biomedical Signal Processing and Control*, *68*. doi: 10.1016/j.bspc.2021.102574

Ghoreishi, N., Goshvarpour, A., Zare-Molekabad, S., Khorshidi, N., & Baratzade, S. (2021). Classification of autistic children using polar-based lagged state-space indices of EEG signals. *Signal, Image and Video Processing*, *15*(8), 1805–1812. doi: 10.1007/s11760-021-01928-z

Grossi, E., Olivieri, C., & Buscema, M. (2017). Diagnosis of autism through EEG processed by advanced computational algorithms: A pilot study. *Computer Methods and Programs in Biomedicine*, *142*, 73–79. doi: 10.1016/j.cmpb.2017.02.002

Haghighat, H. (2023). A sex-dependent functional-effective connectivity model for diagnostic classification of Autism Spectrum Disorder using resting-state fMRI. *Biomedical Signal Processing and Control*, *85*. doi: 10.1016/j.bspc.2023.104837

Hajjej, F., Ayouni, S., Alohali, M. A., & Maddeh, M. (2024). Novel Framework for Autism Spectrum Disorder Identification and Tailored Education With Effective Data Mining and Ensemble Learning Techniques. *IEEE Access*, *12*, 35448–35461. doi: 10.1109/ACCESS.2024.3349988

Halaki, M., & Gi, K. (2012). Normalization of EMG Signals: To Normalize or Not to Normalize and What to Normalize to? *Computational Intelligence in Electromyography Analysis - A Perspective on Current Applications and Future Challenges*. doi: 10.5772/49957

Han, C., Guo, M., Ke, X., Zeng, L., Li, M., Haihambo, N., Lu, J., Wang, L., & Wei, P. (2023). Oscillatory biomarkers of autism: evidence from the innate visual fear evoking paradigm. *Cognitive Neurodynamics*, *17*(2), 459–466. doi: 10.1007/s11571-022-09839-6

Hasan, M. R., Ibrahimy, M. I., Motakabber, S. M. A., & Shahid, S. (2015). Classification of Multichannel EEG Signal by Linear Discriminant Analysis. *Advances in Intelligent Systems and Computing*, *1089*, 279–282. doi: 10.1007/978-3-319-08422-0_42

Hazim Hammed, S., & Albahri, A. S. (2023). Unlocking the Potential of Autism Detection: Integrating Traditional Feature Selection and Machine Learning Techniques. *Applied Data Science and Analysis*, 42–58. doi: 10.58496/adsa/2023/003

Herman, P., Prasad, G., McGinnity, T. M., & Coyle, D. (2008). Comparative analysis of spectral approaches to feature extraction for EEG-based motor imagery classification. *IEEE Transactions on Neural Systems and Rehabilitation Engineering*, *16*(4), 317–326. doi: 10.1109/TNSRE.2008.926694

Houston, M. C. (1942). Some Aspects of a College Health Service. *The American Journal of Nursing*, *42*(10), 1183. doi: 10.2307/3415737

Huang, S., Nianguang, C. A. I., Penzuti Pacheco, P., Narandes, S., Wang, Y., & Wayne, X. U. (2018). Applications of support vector machine (SVM) learning in cancer genomics. *Cancer Genomics and Proteomics*, *15*(1), 41–51. doi: 10.21873/cgp.20063

Husna, R. N. S., Syafeeza, A. R., Hamid, N. A., Wong, Y. C., & Raihan, R. A. (2021). Functional magnetic resonance imaging for autism spectrum disorder detection using deep learning. *Jurnal*

Teknologi, *83*(3), 45–52. doi: 10.11113/JURNALTEKNOLOGI.V83.16389

IBM. (2023). AI vs. Machine Learning vs. Deep Learning vs. Neural Networks: What's the Difference? *Ibm*, *May*, 7. Retrieved from https://www.ibm.com/blog/ai-vs-machine-learning-vs-deep-learning-vs-neural-networks/%0Ahttps://www.ibm.com/cloud/blog/ai-vs-machine-learning-vs-deep-learning-vs-neural-networks

Iragui, V. (2014). *Removing electroencephalographic artifacts by blind source separation*. *2000*, 163–178.

Janidarmian, M., Fekr, A. R., Radecka, K., & Zilic, Z. (2017). A comprehensive analysis on wearable acceleration sensors in human activity recognition. *Sensors (Switzerland)*, *17*(3). doi: 10.3390/s17030529

Jas, M., Engemann, D. A., Bekhti, Y., Raimondo, F., & Gramfort, A. (2017). Autoreject: Automated artifact rejection for MEG and EEG data. *NeuroImage*, *159*, 417–429. doi: 10.1016/j.neuroimage.2017.06.030

Jung, M., Tu, Y., Lang, C. A., Ortiz, A., Park, J., Jorgenson, K., Kong, X. J., & Kong, J. (2019). Decreased structural connectivity and resting-state brain activity in the lateral occipital cortex is associated with social communication deficits in boys with autism spectrum disorder. *NeuroImage*, *190*, 205–212. doi: 10.1016/j.neuroimage.2017.09.031

Kang, J., Han, X., Song, J., Niu, Z., & Li, X. (2020). The identification of children with autism spectrum disorder by SVM approach on EEG and eye-tracking data. *Computers in Biology and Medicine*, *120*. doi: 10.1016/j.compbiomed.2020.103722

Kbah, S. N. S., Al-Qazzaz, N. K., Jaafer, S. H., & Sabir, M. K. (2022). Epileptic EEG activity detection for children using entropy-based biomarkers. *Neuroscience Informatics*, *2*(4), 100101. doi: 10.1016/j.neuri.2022.100101

Khalid, B., Majid, M., Nizami, I. F., Anwar, S. M., & Alnowami, M. (2020). EEG Compression Using Motion Compensated Temporal Filtering and Wavelet Based Subband Coding. *IEEE Access*, *8*, 102502–102511. doi: 10.1109/ACCESS.2020.2999091

Kim, H., Yoshimura, N., & Koike, Y. (2019). Characteristics of Kinematic Parameters in Decoding Intended Reaching Movements Using Electroencephalography (EEG). *Frontiers in Neuroscience*, *13*. doi: 10.3389/fnins.2019.01148

Krizhevsky, A., Sutskever, I., & Hinton, G. E. (2012). ImageNet classification with deep convolutional neural networks. *Advances in Neural Information Processing Systems*, *2*, 1097–1105.

Lalawat, R. S., & Bajaj, V. (2024). An Automatic Framework For Detecting Autism Spectrum Disorder From EEG Signals Using TFD. *IEEE Sensors Journal*. doi: 10.1109/JSEN.2024.3362341

Lara, Ó. D., & Labrador, M. A. (2013). A survey on human activity recognition using wearable sensors. *IEEE Communications Surveys and Tutorials*, *15*(3), 1192–1209. doi:

10.1109/SURV.2012.110112.00192

Larrain-Valenzuela, J., Zamorano, F., Soto-Icaza, P., Carrasco, X., Herrera, C., Daiber, F., Aboitiz, F., & Billeke, P. (2017). Theta and Alpha Oscillation Impairments in Autistic Spectrum Disorder Reflect Working Memory Deficit. *Scientific Reports*, *7*(1). doi: 10.1038/s41598-017-14744-8

Lefebvre, A., Delorme, R., Delanoë, C., Amsellem, F., Beggiato, A., Germanaud, D., Bourgeron, T., Toro, R., & Dumas, G. (2018). Alpha waves as a neuromarker of autism spectrum disorder: The challenge of reproducibility and heterogeneity. Frontiers in Neuroscience, 12, 662. https://doi.org/10.3389/fnins.2018.00662

Li, F., & Yang, Y. (2005). Analysis of recursive feature elimination methods. *SIGIR 2005 - Proceedings of the 28th Annual International ACM SIGIR Conference on Research and Development in Information Retrieval*, 633–634. doi: 10.1145/1076034.1076164

Liang, Z., Zheng, Z., Chen, W., Pei, Z., Wang, J., & Chen, J. (2024). A novel deep transfer learning framework integrating general and domain-specific features for EEG-based brain–computer interface. *Biomedical Signal Processing and Control*, *95*. doi: 10.1016/j.bspc.2024.106311

Limpornpugdee S, Thanawirattananit P, Yimtae K, Chayaopas N, Priprem A, Soontornpas C, Uppala R, Wongswadiwat Y, L. S. (2021). Melatonin niosome gel vs Chloral hydrate for sedation in children undergoing auditory brainstem response: a randomized controlled trial. *Vajira Medical Journal: Journal of Urban Medicine*, *76*(4), 621–630. doi: https://www.cochranelibrary.com/central/doi/10.1002/central/CN-02352443/full

Maenner, M. J., Shaw, K. A., Bakian, A. V, Bilder, D. A., Durkin, M. S., Esler, A., & Cogswell, M. E. (2018). Prevalence and Characteristics of Autism Spectrum Disorder Among Children Aged 8 Years—Autism and Developmental Disabilities Monitoring Network, 11 Sites. *CDC United States*, *70*, 11–20.

Makeig, S., Bell, A. J., Jung, T. P., & Sejnowski, T. J. (1995). Independent Component Analysis of Electroencephalographic Data. *NIPS 1995: Proceedings of the 8th International Conference on Neural Information Processing Systems*, 145–151.

Melinda, M., Oktiana, M., Yunidar, Y., Nabila, N. H., & Enriko, I. K. A. (2023). Classification of EEG Signal using Independent Component Analysis and Discrete Wavelet Transform based on Linear Discriminant Analysis. *International Journal on Informatics Visualization*, *7*(3), 830–838. doi: 10.30630/joiv.7.3.1219

Menaka, R., Karthik, R., Saranya, S., Niranjan, M., & Kabilan, S. (2024). An Improved AlexNet Model and Cepstral Coefficient-Based Classification of Autism Using EEG. *Clinical EEG and Neuroscience*, *55*(1), 43–51. doi: 10.1177/15500594231178274

Ministry of Education. (2015). *About autism spectrum disorder (ASD)*. Retrieved from http://www.minedu.govt.nz/NZEducation/EducationPolicies/SpecialEducation/OurWorkProgramme/SupportingChildrenWithASD/AboutAutismSpectrumDisorder.aspx

Mohi-Ud-Din, Q., & Jayanthy, A. K. (2021). Detection of Autism Spectrum Disorder from EEG signals using pre-trained deep convolution neural networks. *Proceedings of 2021 IEEE 7th International Conference on Bio Signals, Images and Instrumentation, ICBSII 2021*. doi: 10.1109/ICBSII51839.2021.9445193

Morley, A., Hill, L., & Kaditis, A. G. (2016). 10-20 System EEG Placement. *European Respiratory Society*, 34. Retrieved from http://en.wikipedia.org/wiki/10-20_system_%28EEG%29

Mullen, T. R., Kothe, C. A. E., Chi, Y. M., Ojeda, A., Kerth, T., Makeig, S., Jung, T. P., & Cauwenberghs, G. (2015). Real-time neuroimaging and cognitive monitoring using wearable dry EEG. *IEEE Transactions on Biomedical Engineering*, *62*(11), 2553–2567. doi: 10.1109/TBME.2015.2481482

Ni, H. C., Chen, Y. L., Hsieh, M. Y., Wu, C. Te, Chen, R. S., Juan, C. H., Li, C. T., Gau, S. S. F., & Lin, H. Y. (2024). Improving social cognition following theta burst stimulation over the right inferior frontal gyrus in autism spectrum: An 8-week double-blind sham-controlled trial. *Psychological Medicine*. doi: 10.1017/S0033291724001387

Nunez, P. L. (1973). Representation of Evoked Potentials by Fourier-Bessel Expansions. *IEEE Transactions on Biomedical Engineering*, *BME-20*(5), 372–374. doi: 10.1109/TBME.1973.324232

Ohwovoriole, T. (2021). *Causes and Risk Factors of Autism Spectrum Disorder (ASD)*. Retrieved from https://www.verywellmind.com/autism-causes-and-risk-factors-5195311

Omar, N. (2024). EEG-Based Autism Detection Using Multi-Input 1D Convolutional Neural Networks. *Traitement Du Signal*, *41*(1), 333–341. doi: 10.18280/ts.410128

Ozonoff, S., Iosif, A.-M., & et al. (2010). a Prospective Study of the Emergence O Early Signs of Autism. *Changes*, *49*(3), 256–266.

Pahuja, S. K., Veer, K., & others. (2022). Recent approaches on classification and feature extraction of EEG signal: A review. *Robotica*, *40*(1), 77–101.

Platt, J., & others. (1999). Probabilistic outputs for support vector machines and comparisons to regularized likelihood methods. *Advances in Large Margin Classifiers*, *10*(3), 61–74.

Podder, P., Mehedi Hasan, M., Rafiqul Islam, M., & Sayeed, M. (2014). Design and Implementation of Butterworth, Chebyshev-I and Elliptic Filter for Speech Signal Analysis. *International Journal of Computer Applications*, *98*(7), 12–18. doi: 10.5120/17195-7390

Prany, W., Patrice, C., Franck, D., Fabrice, W., Mahdi, M., Pierre, D., Christian, M., Jean-Marc, G., Fabian, G., Francis, E., Jean-Marc, B., & Bérengère, G. G. (2022). EEG resting-state functional connectivity: evidence for an imbalance of external/internal information integration in autism. *Journal of Neurodevelopmental Disorders*, *14*(1). doi: 10.1186/s11689-022-09456-8

Prijono, B. (2018). *Student Notes: Convolutional Neural Networks (CNN) Introduction*. 7 March 2018. Retrieved from https://indoml.com/2018/03/07/student-notes-convolutional-neural-networks-cnn-introduction/

Quan, J., Li, Y., Wang, L., He, R., Yang, S., & Guo, L. (2023). EEG-based cross-subject emotion recognition using multi-source domain transfer learning. *Biomedical Signal Processing and Control*, *84*. doi: 10.1016/j.bspc.2023.104741

Qureshi, M. S., Qureshi, M. B., Asghar, J., Alam, F., & Aljarbouh, A. (2023). Prediction and Analysis of Autism Spectrum Disorder Using Machine Learning Techniques. *Journal of Healthcare Engineering*, *2023*. doi: 10.1155/2023/4853800

Rambabu, C., & Rama Murthy, B. (2014). EEG Signal with Feature Extraction using SVM and ICA Classifiers. *International Journal of Computer Applications*, *85*(3), 1–7. doi: 10.5120/14818-3046

Rashid, M., Sulaiman, N., P. P. Abdul Majeed, A., Musa, R. M., Ahmad, A. F., Bari, B. S., & Khatun, S. (2020). Current Status, Challenges, and Possible Solutions of EEG-Based Brain-Computer Interface: A Comprehensive Review. *Frontiers in Neurorobotics*, *14*. doi: 10.3389/fnbot.2020.00025

Robinson, N., Guan, C., Vinod, A. P., Keng Ang, K., & Peng Tee, K. (2013). Multi-class EEG classification of voluntary hand movement directions. *Journal of Neural Engineering*, *10*(5). doi: 10.1088/1741-2560/10/5/056018

Rogala, J., Żygierewicz, J., Malinowska, U., Cygan, H., Stawicka, E., Kobus, A., & Vanrumste, B. (2023). Enhancing autism spectrum disorder classification in children through the integration of traditional statistics and classical machine learning techniques in EEG analysis. *Scientific Reports*, *13*(1). doi: 10.1038/s41598-023-49048-7

Saffar, B. S. F. Al. (n.d.). *Implementation and performance evaluation of classifiers SVM, CNN and ANN in vineyard estimation*.

Samra, S. K., Sneyd, J. R., Ross, D. A., & Henry, T. R. (1995). Effects of propofol sedation on seizures and intracranially recorded epileptiform activity in patients with partial epilepsy. *Anesthesiology*, *82*(4), 843–851. doi: 10.1097/00000542-199504000-00005

Sanderson, A. C., Segen, J., & Richey, E. (1980). Hierarchical Modeling of Eeg Signals. *IEEE Transactions on Pattern Analysis and Machine Intelligence*, *PAMI-2*(5), 405–415. doi: 10.1109/TPAMI.1980.6592361

Scholkopf, B., Poggio, T., Sung, K. K., Burges, C. J. C., Girosi, F., Niyogi, P., & Vapnik, V. (1997). Comparing support vector machines with Gaussian kernels to radial basis function classifiers. *IEEE Transactions on Signal Processing*, *45*(11), 2758–2765. Retrieved from http://scholar.google.com/scholar?hl=en&btnG=Search&q=intitle:Comparing+Support+Vector+Machines+with+Gaussian+Kernels+to+Radial+Basis+Function+Classifiers#0

Schopler, E., Reichler, R. J., DeVellis, R. F., & Daly, K. (1980). Toward objective classification of childhood autism: Childhood Autism Rating Scale (CARS). *Journal of Autism and Developmental Disorders*, *10*(1), 91–103. doi: 10.1007/BF02408436

Seyed Fakhari, S. N., Ghaderi, F., Tehrani-Doost, M., & Moghadam Charkari, N. (2023). EEG-based brain connectivity analysis in autism spectrum disorder: Unraveling the effects of bumetanide treatment. *Biomedical Signal Processing and Control*, *86*. doi: 10.1016/j.bspc.2023.105054

Sharma, A. (2024). Computerised detection of autism spectrum disorder using EEG signals. *International Journal of Medical Engineering and Informatics*, *16*(1), 47–55. doi: 10.1504/IJMEI.2024.135680

Sheikhani, A. (2008). Evaluation of Quantitative Electroencephalography in Children with Autistic Disorders in Various Conditions Based on Spectrogram. *Iranian Journal Psychiatry*, 4–10.

Shivhare, S. N., & Kumar, N. (2021). Tumor bagging: a novel framework for brain tumor segmentation using metaheuristic optimization algorithms. *Multimedia Tools and Applications*, *80*(17), 26969–26995. doi: 10.1007/s11042-021-10969-y

Singh, J. K., & Kakkar, D. (2024). Chronological sewing training optimization enabled deep learning for autism spectrum disorder using EEG signal. *Multimedia Tools and Applications*. doi: 10.1007/s11042-024-18341-6

Sriramakrishnan, G. V., Rani, V. V., Thatavarti, S., & Maram, B. (2024). Chronological pelican remora optimization-enabled deep learning for detection of autism spectrum disorder. *Signal, Image and Video Processing*, *18*(1), 515–523. doi: 10.1007/s11760-023-02741-6

Statistics. (n.d.). Retrieved from https://www.statista.com/statistics/1250352/south-korea-number-of-registered-autism-cases/

Stavropoulos, K. K. M., & Carver, L. J. (2018). Oscillatory rhythm of reward: Anticipation and processing of rewards in children with and without autism. *Molecular Autism*, *9*(1). doi: 10.1186/s13229-018-0189-5

Steyrl, D., & Müller-Putz, G. R. (2019). Artifacts in EEG of simultaneous EEG-fMRI: Pulse artifact remainders in the gradient artifact template are a source of artifact residuals after average artifact subtraction. *Journal of Neural Engineering*, *16*(1). doi: 10.1088/1741-2552/aaec42

Subasi A. (2007). EEG signal classification using wavelet feature extraction and a mixture of expert model. *Expert Systems with Applications*, *32*, 1084 – 1093.

Sung, G., & Park, E. (2024). Aggregate and transfer knowledge of functional connectivity of brain for detecting autism spectrum disorder for multi-site research. *Biomedical Signal Processing and Control*, *93*. doi: 10.1016/j.bspc.2024.106068

Tang, P., Wang, H., & Kwong, S. (2017). G-MS2F: GoogLeNet based multi-stage feature fusion of deep CNN for scene recognition. *Neurocomputing*, *225*, 188–197. doi: 10.1016/j.neucom.2016.11.023

Tanguay, P. E. (2011). Autism in DSM-5. *American Journal of Psychiatry*, *168*(11), 1142–1144. doi: 10.1176/appi.ajp.2011.11071024

Tawhid, M. N.A., Siuly, S., & Wang, H. (2020). Diagnosis of autism spectrum disorder from EEG using a time-frequency spectrogram image-based approach. *Electronics Letters*, *56*(25), 1372–1375. doi: 10.1049/el.2020.2646

Tawhid, Md Nurul Ahad, Siuly, S., Wang, H., Whittaker, F., Wang, K., & Zhang, Y. (2021). A spectrogram image based intelligent technique for automatic detection of autism spectrum disorder from EEG. *PLoS ONE*, *16*(6 June). doi: 10.1371/journal.pone.0253094

Ting, K. M. (2007). Confusion matrix. *Encyclopedia of Machine Learning and Data Mining*, *2*, 4–6. doi: https://doi.org/10.1007/978-1-4899-7687-1_50

Tsuchimoto, S., Shibusawa, S., Iwama, S., Hayashi, M., Okuyama, K., Mizuguchi, N., Kato, K., & Ushiba, J. (2021). Use of common average reference and large-Laplacian spatial-filters enhances EEG signal-to-noise ratios in intrinsic sensorimotor activity. *Journal of Neuroscience Methods*, *353*. doi: 10.1016/j.jneumeth.2021.109089

Urbach, T. P., & Kutas, M. (2006). Interpreting event-related brain potential (ERP) distributions: Implications of baseline potentials and variability with application to amplitude normalization by vector scaling. *Biological Psychology*, *72*(3), 333–343. doi: 10.1016/j.biopsycho.2005.11.012

Wadhera, T. (2024). Multimodal Kernel-based discriminant correlation analysis data-fusion approach: an automated autism spectrum disorder diagnostic system. *Physical and Engineering Sciences in Medicine*, *47*(1), 361–369. doi: 10.1007/s13246-023-01350-4

Wang, Jingjing, Gao, J., Ren, J., Luan, Z., Yu, Z., Zhao, Y., & Zhao, Y. (2021). DFP-ResUNet:Convolutional Neural Network with a Dilated Convolutional Feature Pyramid for Multimodal Brain Tumor Segmentation. *Computer Methods and Programs in Biomedicine*, *208*. doi: 10.1016/j.cmpb.2021.106208

Wang, Jun, Barstein, J., Ethridge, L. E., Mosconi, M. W., Takarae, Y., & Sweeney, J. A. (2013). Resting state EEG abnormalities in autism spectrum disorders. *Journal of Neurodevelopmental Disorders*, *5*(1). doi: 10.1186/1866-1955-5-24

Wei, X., Adamson, H., Schwendemann, M., Goucha, T., Friederici, A. D., & Anwander, A. (2023). Native language differences in the structural connectome of the human brain. *NeuroImage*, *270*. doi: 10.1016/j.neuroimage.2023.119955

World Health Organisation (WOH*) autism spectrum disorders (ASD)*. (n.d.). WOH. Retrieved from https://www.who.int/news-room/fact-sheets/detail/autism-spectrum-disorders

Yang, Y. (2017). A Signal Theoretic Approach for Envelope Analysis of Real-Valued Signals. *IEEE Access*, *5*, 5623–5630. doi: 10.1109/ACCESS.2017.2688467

Zwaigenbaum, L., Bauman, M. L., Stone, W. L., Yirmiya, N., Estes, A., Hansen, R. L., McPartland, J. C., Natowicz, M. R., Choueiri, R., Fein, D., Kasari, C., Pierce, K., Buie, T., Carter, A., Davis, P. A., Granpeesheh, D., Mailloux, Z., Newschaffer, C., Robins, D., … Wetherby, A. (2015). Early identification of autism spectrum disorder: Recommendations for practice and research. *Pediatrics*, *136*, S10–S40. doi: 10.1542/peds.2014-3667C

CURRICULUM VITAE

BASHAR SAAD FALIH AL-SAFFAR. He received his B.Sc. in Electrical Engineering from the University of Technology, Baghdad, Iraq, in 2014, and his M.Sc. in Electrical and Electronic Engineering from Cukurova University, Turkey, in 2019. He served as an external lecturer at the University of Baghdad, Al-Khwarizmi College – Biomedical Engineering Department. Since 2021, he has been a lecturer at Al-Salam University in the Computer Techniques Engineering Department, Baghdad, Iraq, and is currently a Ph.D. student in Electrical and Electronic Engineering at Cukurova University, Turkey. His areas of expertise include AI, Digital Image Processing, Digital Signal Processing, Computer Vision, and Biomedical Signal and Image Processing.

APPENDICES

applied sciences

an Open Access Journal by MDPI

IMPACT FACTOR 2.5

CITESCORE 5.3

CERTIFICATE OF ACCEPTANCE

The certificate of acceptance for the manuscript (**applsci-3329017**) titled:

Impact of Sliding Window Overlapping Ratio on EEG-Based ASD Diagnosis Using Brain Hemisphere Energy and Machine Learning

Authored by:

BASHAR S. Falih; Mohannad K Sabir; Ahmet AYDIN

was accepted in *Appl. Sci.* (ISSN 2076-3417) on 12 December 2024

MDPI

Basel, December 2024

Stefan Tochev
Chief Executive Officer

applied sciences

an Open Access Journal by MDPI

IMPACT FACTOR 2.5

CITESCORE 5.3

CERTIFICATE OF PUBLICATION

The certificate of publication for the article titled:

Impact of Sliding Window Overlap Ratio on EEG-Based ASD Diagnosis Using Brain Hemisphere Energy and Machine Learning

Authored by:

Bashar S. Falih; Mohannad K. Sabir; Ahmet Aydın

Published in:

Appl. Sci. **2024**, Volume 14, Issue 24, 11702

MDPI

Basel, December 2024

Stefan Tochev
Chief Executive Officer

Bashar Saad <bashar.saad@kecbu.uobaghdad.edu.iq>

Folder shared with you: "Autism_EEG_files"

1 message

Jacek Rogala (via Google Drive) <drive-shares-dm-noreply@google.com> Thu, Jan 25, 2024 at 9:29 PM
Reply-To: Jacek Rogala <j.rogala3@uw.edu.pl>
To: bashar.saad@kecbu.uobaghdad.edu.iq

Jacek Rogala shared a folder

Jacek Rogala (j.rogala3@uw.edu.pl) has invited you to **contribute to** the following shared folder:

There are files in EEGLab format. Please let me know if files were copied correctly.
Best,
Jacek Rogala

Autism_EEG_files

Jacek Rogala is outside your organization.

Open

If you don't want to receive files from this person, block the sender from Drive

Republic of Iraq
Ministry of Higher Education
and Scientific Research
University of Baghdad
Alkhwarizmi College of Engineering
Scientific Affairs Unit

جمهورية العراق
وزارة التعليم العالي والبحث العلمي
جامعة بغداد
كلية الهندسة الخوارزمي
وحدة الشؤون العلمية

No.: العدد: م ع ش / ١٨٤
Date: التاريخ: ٩ / ١ / ٢٠٢٤

"استثمار الطاقة النظيفة طريقنا نحو التنمية المستدامة "

وزارة الصحة
دائرة مدينة الطب
الواردة
العدد ١٥٠٨
التاريخ ١٠/ ١ / ٢٠٢

الى/ دائرة مدينة الطب

م / ابداء مساعدة

تحية طيبة .....

يرجى تفضلكم بإبداء المساعدة الممكنة للتدريسي ((أ.م.د.مهند كاظم صابر)) / قسم هندسة الطب الحياتي في كليتنا ، لغرض الحصول على إشارات تخطيط الدماغ لمرضى التوحد ، وذلك للحاجة الماسة لإتمام المشاريع البحثية في هذا المجال .

...تقبلوا وافر التقدير والاحترام

كلية الهندسة الخوارزمي - جامعة بغداد - الجادرية - حي الكرادة - الهاتف المباشر: 7788509
Alkhwarizmi College of Engineering - University of Baghdad - Al-jadriyah - Karrada District - Phone No.:7788509
E-mail: sci_af@kecbu.uobaghdad.edu.iq

Subject / Healthy & Autistic (EEG dataset)

To whom it may concern

Following a request from the University of Baghdad / Al-Khwarizmi College, Department of Biomedical Engineering, the Children's Welfare Teaching Hospital (Autism Division and EEG Division) in Medical City, Baghdad, Iraq, facilitated the collection of data on autism signals under the authorization of Assist. Prof. Dr. Muhannad K. Saber (Authorization No. M.A.S. 184, dated 01-09-2024). Collaboration ensued, and EEG data were collected. The patient with pure autism spectrum disorder (ASD) labeling was conducted by Dr. Ali H. Ali, with EEG recording undertaken by Dr. Noor H. Al-Janabi. 22 samples from individuals with ASD and 30 samples from typically developing (TD) individuals were gathered. All data were anonymized, and names and other HIPAA identifiers were removed from all manuscript sections, including supplementary information.

Mohannad K Sabir
Department of Biomedical Engineering, Al-Khwarizmi College of Engineering, University of Baghdad, Baghdad, Iraq.
dr.mohaned@kecbu.uobaghdad.edu.iq

Ali H. Ali
National Autism Centre, Child and Adolescent Psychiatrist, Children's Welfare Teaching Hospital, Medical City, Baghdad, Iraq.
Ali_idris95@gmail.com

Noor H. Al-Janabi
EEG Unit, Clinical Neurophysiologist, Children's Welfare Teaching Hospital, Medical City, Baghdad, Iraq.
Noor.Hamaza64@gmail.com